



**NATIONAL REPORT
REPUBLIC OF KOREA**

Korean National Committee for COSPAR



**NATIONAL REPORT
REPUBLIC OF KOREA**

Korean National Committee for COSPAR



Preface

As the chair of Korean National Committee for COSPAR (KNCC), it is my great honor to announce the publication of the 2020 COSPAR National Report of Republic of Korea.

In last few years, Korea had achieved the remarkable progress in space missions and expanded the research activities in various space research area. The next generation small satellite-1 (NEXTSat-1) for space astronomy and space physics was successfully launched by Falcon-9 in December, 2018. The Geostationary Korea Multi-Purpose Satellite (Geo-KOMPSAT) 2A and 2B were also launched in 2018 and 2020 respectively for weather forecasting, space weather, oceanography, and atmospheric environment.

In addition, the other space programs including the Korea Pathfinder Lunar Orbiter (KPLO), KOMPSAT-6 (SAR mission), and Small scale Magnetospheric and Ionospheric Plasma Experiment (SNIPE, cubesats mission for space weather), have been well developing with the participation of enthusiastic expertise in governments, research institutes, universities and industries. All these missions will be launched in next two years.

The international collaboration is the one of the key strategies for expanding our activities in space research area and several interesting collaborations are undertaking in the organization and personal level. The co-work with NASA in the Next Generation Coronagraph on ISS, CLPS, SPHERE-x and KPLO missions might be the outstanding case of the international collaboration as the government level.

In this report, we summarized the latest information of the space missions and the scientific results for space research in Korea to share the knowledge and experiences with all the scientists and engineers in the world.

I hope that the publication of National Report 2020 can provide the chance to understand the endeavor of Korea in space research and contribute to the promotion of not only KNCC's but also COSPAR's activities.

Jong Uk (James) Park, Ph.D.
Chair
Korean National Committee for COSPAR
December 2020

Table of Contents

SC-A The Earth’s Surface, Meteorology, and Climate

<i>GEO-KOMPSAT-2 (Cheollian-2/GK2) Program</i>	8
<i>Geostationary Environment Monitoring Spectrometer (GEMS) on GK2B</i>	20
<i>KOMPSAT-6 Mission</i>	25

SC-B The Earth-Moon System, Planets, and Small Bodies of the Solar System

<i>Korea Pathfinder Lunar Orbiter (KPLLO) Mission</i>	30
<i>CLPS Korea Project – Opening the Door of the Lunar Surface Science</i>	34
<i>Optical Properties of NEA Phaethon</i>	35
<i>Space Geodetic Infrastructures and Researches</i>	36

SC-C The Upper Atmospheres of the Earth and Planets including Reference Atmospheres

<i>Upper Atmospheric Research Activities</i>	40
<i>Ionospheric Observations from Space</i>	44

SC-D Space Plasma in the Solar System, Including Planetary Magnetosphere

<i>The Chromospheric Instrument Development Plans</i>	50
<i>Toward Next Generation Coronagraph: DICE, BITSE, and CODEX</i>	54
<i>Solar wind researches based on new space missions</i>	57
<i>SNiPE Mission for Space Weather Research</i>	60
<i>Korean Space Environment Monitor (KSEM) on GK2A</i>	62



SC-E Astrophysics from Space

Infrared Imaging Spectroscopic Survey Missions 68

SC-F Life Sciences as Related to Space

What the egg diversity of Antarctic tardigrades tells us 72

Lithic niches acting as reservoirs of microbial life in a high Arctic polar desert 74

Genetics, development and physiology of animal models in altered gravity 77

Hormetic effects of hypergravity on the immune system and its mechanism 80

Impairment of cerebellar motor coordination and object recognition in the hypergravity-exposed rats 82

SC-G Materials Science in Space

Levitation Technology for Ground Based Experiments 88

SC-H Fundamental Physics in Space

Combustion Science and Fire Safety Research for Manned Space Exploration 92

SC-A

The Earth's Surface, Meteorology, and Climate

GEO-KOMPSAT-2 (Cheollian-2/GK2) Program

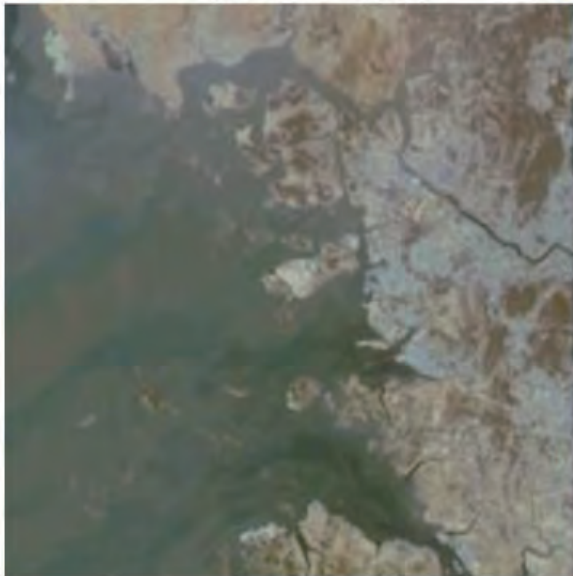
Geostationary Environment Monitoring Spectrometer (GEMS) on GK2B

KOMPSAT-6 Mission



(image credit: KARI)

[GOCI-I image]



[GOCI-II Image]



(image credit: MSIT/KHOA)

GEO-KOMPSAT-2 (Cheollian-2/GK2) Program

Jaedong Choi, Korea Aerospace Research Institute

The GEO-KOMPSAT-2 program, more widely known as the Cheollian-2 in Korea, has been approved in September 2010, and was kicked off in July 2011. The Ministry of Science and ICT (MSIT), Korea Meteorological Administration (KMA), Ministry of Oceans and Fisheries (MOF), and Ministry of Environment (MOE) of Korea started the follow-on satellites of COMS program for continuous monitoring of meteorological, ocean and atmospheric environment around East Asia, including the Korean Peninsula.

The Cheollian-2(GK2) program comprises two satellites for multi-purpose applications: Cheollian-2A (GK2A) for meteorological and space weather missions and Cheollian-2B(GK2B) for ocean and environmental monitoring missions. KARI (Korea Aerospace Research Institute) of

Daejeon, Korea, is responsible for the development of the Cheollian-2(GK2) space segment while KMA/MOF/MOE implement the ground segment for image-receiving data processing [1, 2].

KARI is currently operating COMS (Cheollian-1), which is Korea's first geostationary communications, ocean, and meteorological satellite. KARI started also a meteorological service of Cheollian-2A(GK2A) in July 2019, and the Cheollian-2B(GK2B) will begin marine and environmental services in early 2021. The Cheollian-2 satellites inherit the mission of COMS (Cheollian-1) to observe the weather and ocean environment, and also strengthen the national capability to monitor the environment pollution around the Korean Peninsula and East Asia (Fig. SC-A-1).

- GK2 program is a follow-on program to the successful COMS Program with upgraded performance for spacecraft bus and mission payload.
- GK2 satellites are being developed under KARI responsibility which is a medium sized geostationary satellite platform with the launch mass of around 3.5ton.

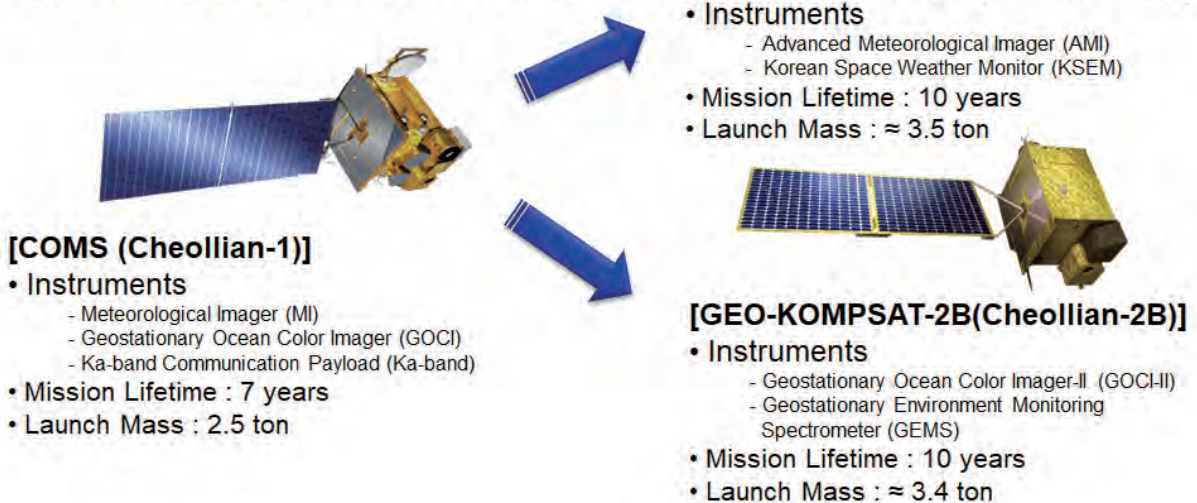


Fig. SC-A-1. Follow-on Satellites of COMS(Cheollian-1) (image credit: KARI)

Cheollian-2A(GK2A) is for the meteorological mission and the space weather monitoring mission, so it is equipped with the instruments: AMI (Advanced Meteorological Imager) and KSEM (Korean Space wEather Monitor Monitor).

Specific mission of Cheollian-2A(GK2A) are as follows:

Meteorological Mission

- Maintaining of COMS mission continuity and quality in environmental observations in the GK2A timeframe
- Monitoring of weather and climate phenomena with enhanced measurement cycle
- Monitoring more accurately high-impact weather events with high spatial resolution

Space Weather Monitoring Mission

- Measuring of energetic particle flux and magnetic field in the Geo-orbit
- Monitoring of spacecraft charging due to space weather phenomena
- Monitoring of space weather phenomena

Cheollian-2B(GK2B) is the twin satellite of Cheollian-2A for meteorological observations launched in December 2018. It is equipped with the world's first geostationary environment payload and a marine payload with significantly enhanced performance compared to Cheollian-1.

Since the observation range of Cheollian-2B(GK2B) GEMS Payload covers East Asia, from Japan in the east to Northern Indonesia in the west and Southern Mongolia in the north, it will contribute to the international community by providing information on the atmospheric environment of each region.

Continuous monitoring of atmospheric pollutants, such as fine dust generated and migrated in East Asia and the Korean Peninsula, and analysis of the impact of flows out of the region are expected to secure the reference data in preparation for international disputes regarding the atmospheric environment. Geostationary Ocean Color Imager-II (GOCI-II) is a marine payload that can observe in real time the migration of red/green tide and oil spills in the seas around the Korean Peninsula.

Specific mission of Cheollian-2B(GK2B) are as follows:

Environment Monitoring Mission

- Measurements of atmospheric chemistry, precursors of aerosols and ozone with high temporal and spatial resolution over Asia

- Monitoring of regional transport events (trans-boundary pollution and Asian dust)
- Monitoring of air quality for long-term trends

Ocean Color Monitoring Mission

- Maintaining of COMS mission continuity and quality in ocean color observations in the GK2 timeframe
- Improved monitoring of ocean biophysical phenomena and maritime disasters with enhanced spatial resolution and increased spectral bands

1. GEO-KOMPSAT-2 Spacecrafts

All areas of Chollian-2(GK2) satellite development, including the development of satellite control systems, were developed under the responsibility of the Korea Aerospace Research Institute (KARI).

The platforms of the Chollian-2A(GK2A) and Chollian-2B(GK2B) are approximately the same, and are equipped with different payloads only depending on the satellite's mission. The platform has been developed and validated by KARI. Some units are manufactured and qualified by Korean industries with KARI's involvement and qualified units are procured from qualified manufacturers.

For the verification of the Chollian-2(GK2) platform, the structural and thermal subsystem were validated through Structure and Thermal Model(STM), the electrical performance was verified through Electrical Test Bed(ETB), and the flight software was validated through Software Test Bed(STB), respectively.



Fig. SC-A-2. STM Final Configuration of Cheollian-2 (image credit: KARI)

Cheollian-2A Spacecraft (GK2A)

The Cheollian-2A(GK2A) was launched on December 4, 2018 (20:37 UTC) on an Ariane-5 ECA vehicle from the Guiana Space Center in Kourou. The flight is designated VA246 in Arianespace terminology [3, 4].

Cheollian-2A, owned and operated by KARI, provides meteorological and space weather monitoring over the

Asia-Pacific region including the Korean Peninsula. The satellite has a design life of more than 10 years.

The main characteristics, mechanical configuration, electrical architecture, and test activities of the Cheollian-2A satellite are as follows (Table SC-A-1, Fig. SC-A-3~SC-A-6).

Table SC-A-1. Cheollian-2A(GK2A) Key Characteristics

Contents	Cheollian-2A (GK2A)
Payload	<ul style="list-style-type: none"> ▪ Advanced Meteorological Imager ▪ Korean Space Environment Monitor
Orbit Determination and Prediction Accuracy	▪ < 3km (using 2 ground stations)
Mission Life Time	▪ 10 years
Mass	<ul style="list-style-type: none"> ▪ 3.2 ton @ mission life ▪ 3.5 ton @ maximum allowable
Pointing Accuracy	<ul style="list-style-type: none"> ▪ Normal Mode (AMI) - 0.075°(3σ) for roll/pitch axes - 0.108°(3σ) for yaw axis
S/A Power	2,550W @ EOL, AEX
Volume	<ul style="list-style-type: none"> ▪ Launch : 2.9 ´ 2.4 ´ 4.6 (m) ▪ On-Orbit : 3.8 ´ 8.9 ´ 4.6 (m)

Mechanical Configuration

- Single Solar Array Wing
- Short Yoke + 2 Panels
- Bi-Propellant Propulsion System with Central Tube
- Active and passive PS thermal control
- Asymmetric configuration
 - Box Shape with Cylindrical Core Structure
 - 1194 mm Clamp Band LV interface
 - Mass: 3.5 ton @ maximum allowable
 - Volume: 3.8 ´ 8.9 ´ 4.6 (m) @ On-orbit

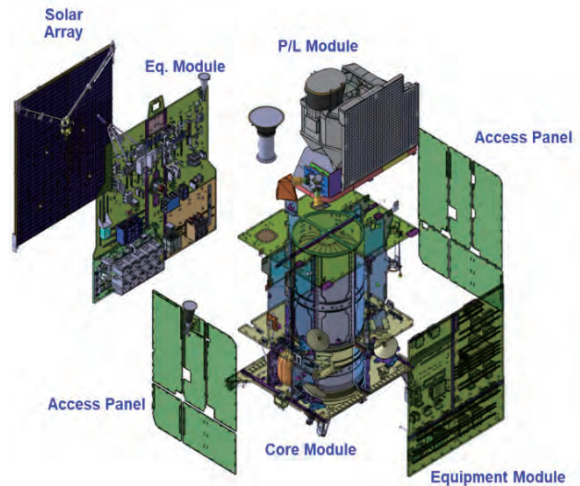


Figure SC-A-3. Mechanical Configuration of Cheollian-2A (image credit: KARI)

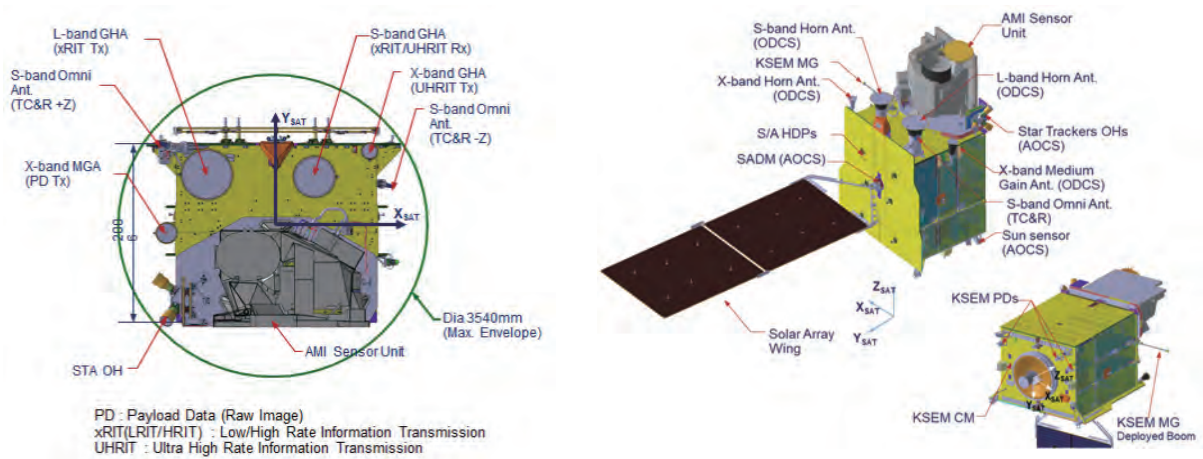


Fig. SC-A-4. Top/Bottom Floor Equipment Layout of the Cheollian-2A spacecraft (image credit: KARI)

Electrical Architecture

- S/A Power Requirements: 2,550W @ EOL
- Power Capability: 2,620W @ AEX, EOL
 - Battery Capacity: 225Ah @ BOL
- Electrical IF:
 - Spacewire for Payload Data
 - RS422 & RS48
 - 1553B Data Bus
 - Command/Telemetry
 - Power Bus(+50V) etc.



Fig. SC-A-5. Electrical Test Bed Cheollian-2 (image credit: KARI)

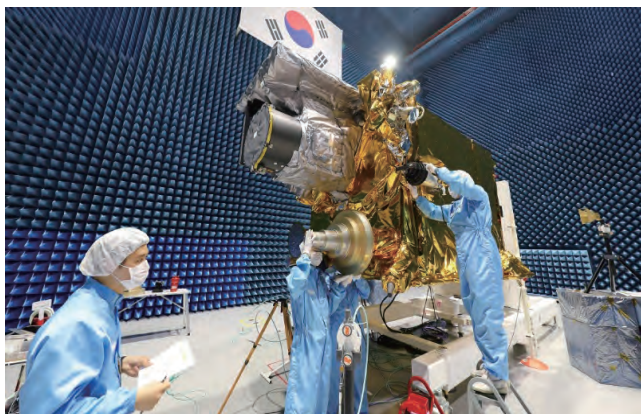


Fig. SC-A-6. Photo of Cheollian-2A Environment Test (image credit: KARI)

Cheollian-2B Spacecraft (GK2B)

The Cheollian-2B was launched on February 18, 2020 (22:18 UTC) on an Ariane-5 ECA vehicle from the Guiana Space Center in Kourou. The flight is designated VA252 in Arianespace terminology.

Cheollian-2B(GK2B) provides environmental monitoring over Asia-Pacific region and Ocean monitoring around the Korea Peninsula. The satellite has a design life of more than 10 years.

The main characteristics mechanical configuration, electrical architecture, and test activities of the Cheollian-

2B satellite are as follows(Table SC-A-2, Fig. SC-A-3~SC-A-10).

The Chollian-2B bus platform is almost the same as the Chollian-2A bus platform, but the difference is that there is no Observation Data Communication Subsystem (ODCS) that redistributes observational image data. The overall volume of the Chollian-2B satellite varies somewhat from the Chollian-2A depending on the size and shape of the payload module.

Table SC-A-2. Cheollian-2B (GK2B) Key Characteristics

Contents	Cheollian-2B (GK2B)
Payload	<ul style="list-style-type: none"> ▪ Geostationary Environment Monitoring Spectrometer ▪ Geostationary Ocean Color Imager-II
Orbit Determination and Prediction Accuracy	▪ < 3km (using 2 ground stations)
Mission Life Time	▪ 10 years
Mass	<ul style="list-style-type: none"> ▪ 3.2 ton @ mission life ▪ 3.4 ton @ maximum allowable
Pointing Accuracy	<ul style="list-style-type: none"> ▪ Normal Mode (AMI) <ul style="list-style-type: none"> - 0.075°(3σ) for roll/pitch axes - 0.108°(3σ) for yaw axis
S/A Power	2,550W @ EOL, AEX
Volume	<ul style="list-style-type: none"> ▪ Launch : 2.9 ´ 2.4 ´ 3.8 (m) ▪ On-Orbit : 2.9 ´ 8.8 ´ 3.8(m)

Mechanical Configuration

- Single Solar Array Wing
- Short Yoke + 2 Panels
- Bi-Propellant Propulsion System with Central Tube
- Active and passive PS thermal control
- Asymmetric configuration
 - Box Shape with Cylindrical Core Structure
 - 1194 mm Clamp Band LV interface
 - Mass: 3.5 ton @ maximum allowable
 - Volume: 2.9 ´ 8.8 ´ 3.8 (m) @ On-orbit

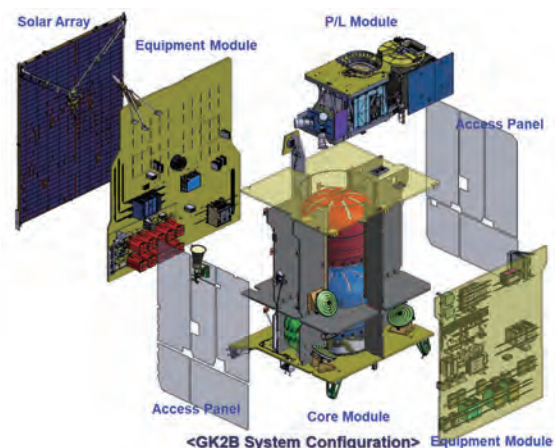


Fig. SC-A-7. Mechanical Configuration of Cheollian-2B (image credit: KARI)

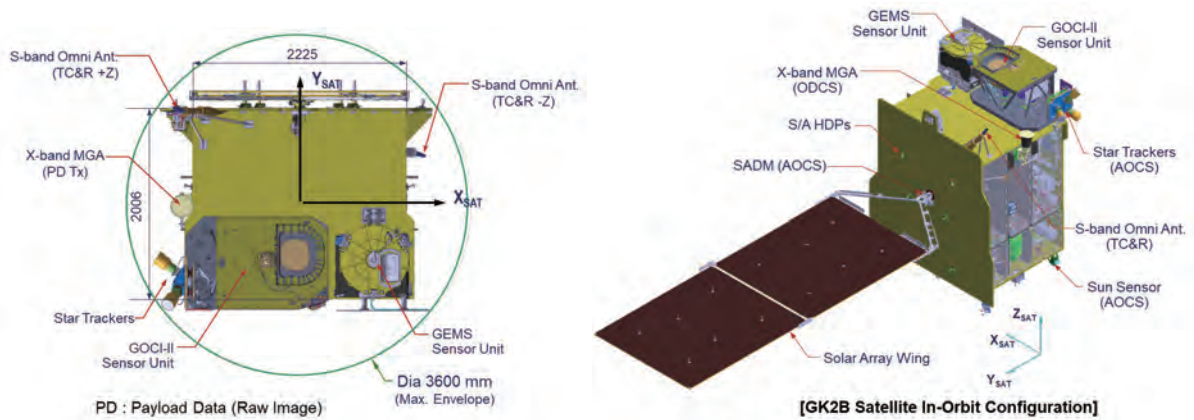


Fig. SC-A-8. Top/Bottom Floor Equipment Layout of the Cheollian-2B spacecraft (image credit: KARI)

Electrical Architecture

- S/A Power Requirements: 2,550W @ EOL
- Power Capability: 2,620W @ AEX, EOL
 - Battery Capacity: 225Ah @ BOL
- Electrical IF:
 - Spacewire (GRDDP) interface (TM/Science data)
 - RS422 & RS485
 - 1553B Data Bus
 - Command/Telemetry
 - Power Bus(+50V) etc.



Fig. SC-A-9. Cheollian-2 Electrical Functional Test @ Dummy Wall (image credit: KARI)

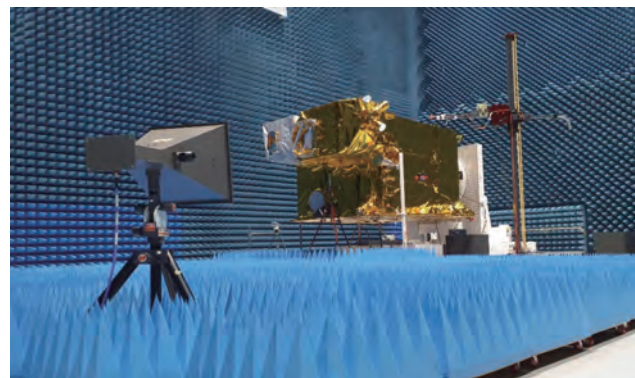


Fig. SC-A-10. Environment Test of Cheollian-2B (image credit: KARI)

2. GEO-KOMPSAT-2 Payloads

The Chollian-2(GK2) is a simultaneous development program for the Cheollian-2A(GK2A) satellite for meteorological and space weather observations and the Chollian-2B(GK2B) satellite for marine and environmental observations.

Thus, for the mission of each satellite, the Chollian-2A(GK2A) was equipped with meteorological and space weather observation sensors, while the Chollian-2B(GK2B) was equipped with the Ocean and environmental observation sensors.

Advanced Meteorological Imager (AMI) on GK2A

Cheollian-2A has four times the spatial resolution of Cheollian-1. Moreover, Cheollian-2A requires only 10 minutes to observe the entire sphere and 2 minutes to

observe the Korean Peninsula compared to the 3 hours and 15 minutes required by Cheollian-1 to observe the whole sphere and the Korean Peninsula, respectively, which means 18 times' faster observation. Therefore, it can detect local flooding at least two hours earlier than the previous satellite [5].

AMI Payload has 16 channels (4 visible, 2 near IR, and 10 IR) compared to 5 channels (1 visible and 4 IR) of Cheollian-1; thus, the serviced weather data increased by more than three times from 16 to 52. Moreover, the built-in space meteorological payload has enabled the study of the impact of the physical change of space on the geostationary satellite and meteorological condition and practical life on earth.

AMI Requirement Specification

A comparison table of requirements between GK2A AMI and COMS MI is as follows (Table SC-A-3).

Table SC-A-3. Comparison of GK2A AMI and COMS MI Requirement Specification

Parameter	GK2A AMI (Advanced Meteorological Imager)	COMS MI (Meteorological Imager)
Spectral bands	16 channels (4 VIS, 2 NIR, 10 IR)	5 channels ((1 VIS, 4 IR)
Spectral resolution	0.64 μm : 0.5 km Other VIS/NIR: 1.0 km IR: 2 km	0.675 μm : 1 km Other VIS/NIR: N/A IR: 4 km
Observation duration	Local Disk: ≤ 2 minutes Full disk: ≤ 10 minutes	Local Disk: ≤ 15 minutes Full disk: ≤ 3 hours
INR	$< 21\text{urad}$ (for Advanced Meteorological Imager)	$< 56\text{urad}$ (for Meteorological Imager)
Lifetime	10 years	7 years
On-board calibration	Visible: Solar Diffuser IR: Internal Blackbody Target	IR: Internal Blackbody Target

AMI Payload Configuration

AMI payload consists of Sensor Unit (SU) for collect scene radiance & convert to counts, Cryocooler Control Electronics(CCE) for operation of active cooler, Electronics Unit(EU) for command & control and data handling, and Power Converter(PC) for converting from 50V to 28V (Fig. SC-A-11).

AMI Observation Image

The observed images in Fig. SC-A-12 were obtained from Chollian-1 and Chollian-2A. The Chollian-2A shows a color image that has four times the resolution compared to the Chollian-1.

Korean Space Weather Monitor (KSEM) on GK2A

KSEM is the first Korean space weather instrument suite aboard a GEO satellite. The sensors are used to monitor the space environment the severe space weather information of high-impact space storms, the radiation environment hazardous to spacecraft, aircraft and radio communication for 24 hours/7 days during 10 years mission life time.

Detailed information on KSEM can be found in the end of SC-D section in this report.

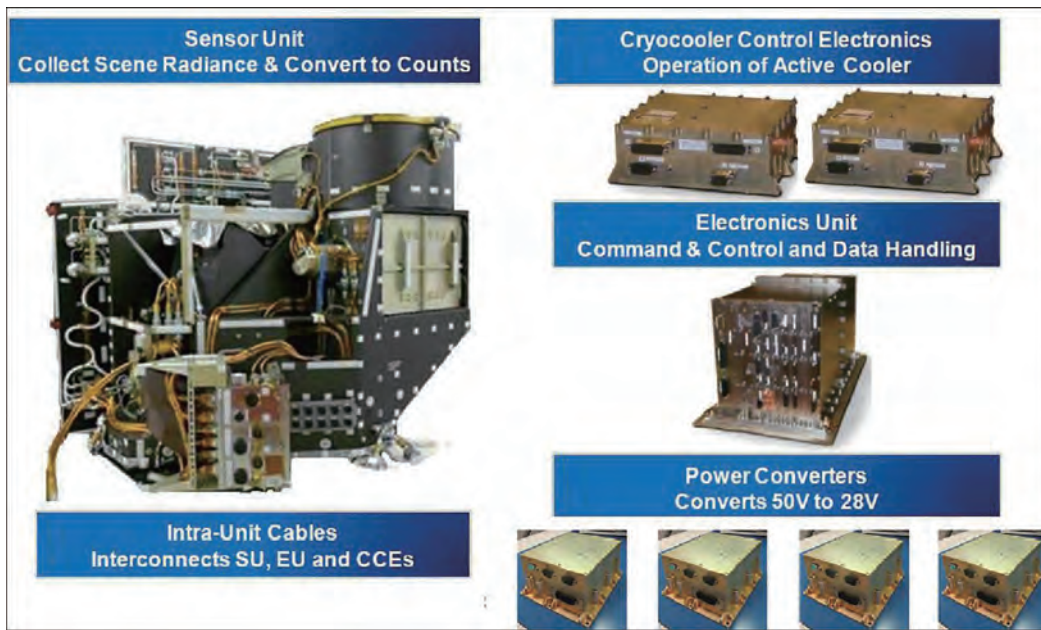


Fig. SC-A-11: Illustration of the AMI configuration (image credit: Harris Corporation)

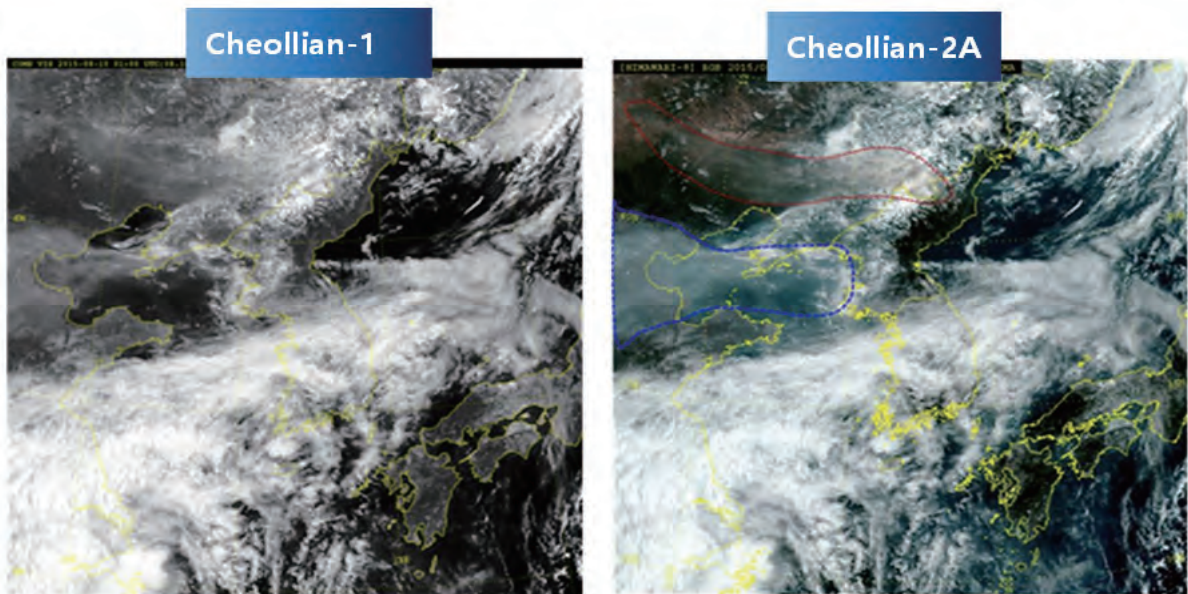


Fig. SC-A-12. Comparison of observed image processing results (image credit; MSIT/KMA)

Geostationary Ocean Color Imager II (GOCI-II) on GK2B

GOCI-II is the second-generation instrument of GOCI, one of the payloads on Cheollian-1 (COMS), the 1st ocean color imager in the world operating in the geostationary orbit.

GOCI had been developed to provide a monitoring of ocean color around the Korean Peninsula to detect, monitor, quantify, and predict short term changes of coastal ocean environment for marine science research and application purposes.

As such, GOCI acquired only LA (Local Area) mode observations in an area of size 2500 x 2500 km. The requirements of GOCI-II call for two coverage modes: LA (Local Area) and FD (Full Disk) as illustrated in Fig. SC-A-13.

In July 2013, KARI awarded a contract to Airbus Defence and Space (former EADS Astrium) to jointly design and manufacture the GOCI-II instrument for the future Korean mission Cheollian-2B (GK2B), launched in early 2020.

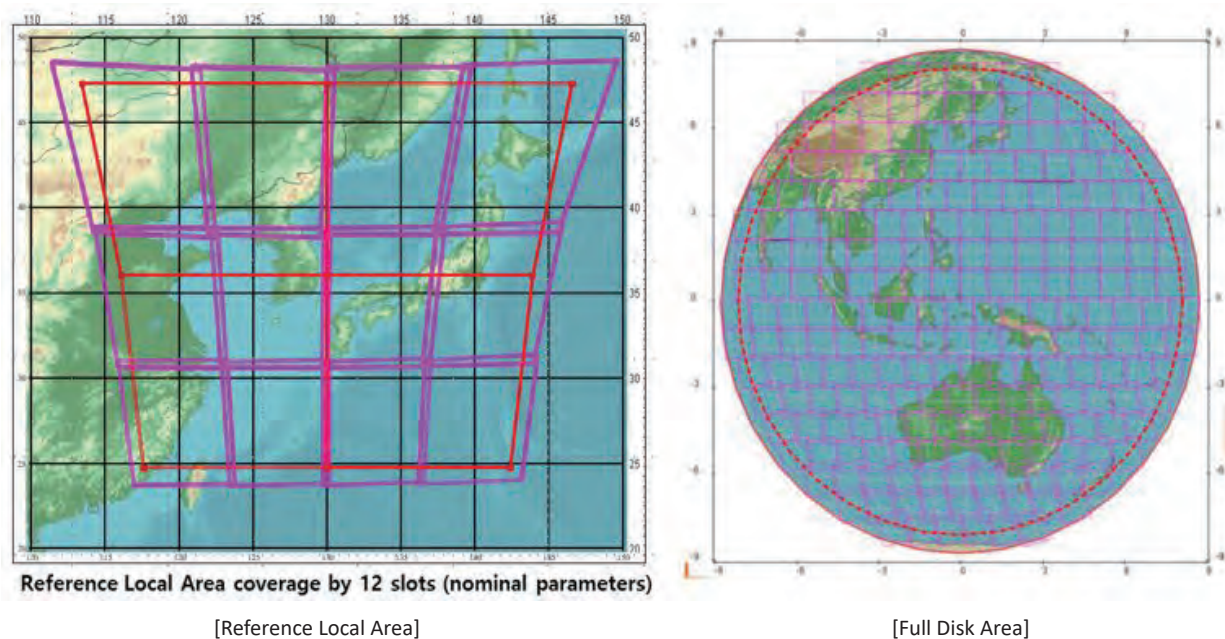


Fig. SC-A-13. LA mode and the FD mode of GOCI-II (image credit: KARI/KORDI)

GOCI-II Requirement Specification

GOCI-II is focused on the coastal and global ocean environment monitoring with better spatial resolution and spectral performance for the succession and expansion of the mission of GOCI (Table SC-A-4).

The main difference between GOCI-II and GOCI is the addition of the FD (Full Disk) mode, four times' higher

resolution and more observation bands (8 -> 13), as illustrated in Table SC-A-5).

It enables the systematic management and use of marine territory by precisely monitoring the marine environments such as marine dumping areas and tsunami areas [6, 7].

Table SC-A-4. Summary of GOCI-II performance requirements

Observation Area	Observation duration	Spatial Resolution	No of Channel/Spectral Band	SNR	Weight	Power
<ul style="list-style-type: none"> Local Disk (2500x2500km²) Full Disk 	<ul style="list-style-type: none"> Local Disk: 10times/1day Full Disk: 1times/1day 	250 x 250 m ² (@ 130E, 0N)	13channel/370~885nm	> 1000	150kg	250watt

Table SC-A-5. Comparison of GOCI and GOCI-II performance requirements

Item	GOCI Specification	GOCI-II Specification
Mission lifetime	7 years	10 years
Duty Cycle (Local Area : LA)	8 times / day	10 times / day (for 12 spectral channels)
Observation Time	≤30 minutes for LA	≤30 minutes for LA, ≤240 minutes for FD
Spatial resolution (GSD)	≤500 m @ center of Ref. LA (130°E, 36°N)	≤250 m @ (130°E, 0°N) (Min. Coverage of Ref. LA : 2.500 km x 2.500 km)
Number of bands	8 bands (VIS/NIR)	12 bands (VIS/NIR)+1 wideband

GOCI-II Payload Configuration

The GOCI-II instrument designed using the latest generation technologies developed by Airbus DS (former Astrium) for space applications, including a 7 Mpixel CMOS sensor, a silicon carbide telescope and a high-precision pointing mechanism. GOCI-II offers significant advances in comparison to GOCI: enhanced resolution (250 m), 12 spectral bands and daily coverage of full disk Earth data.

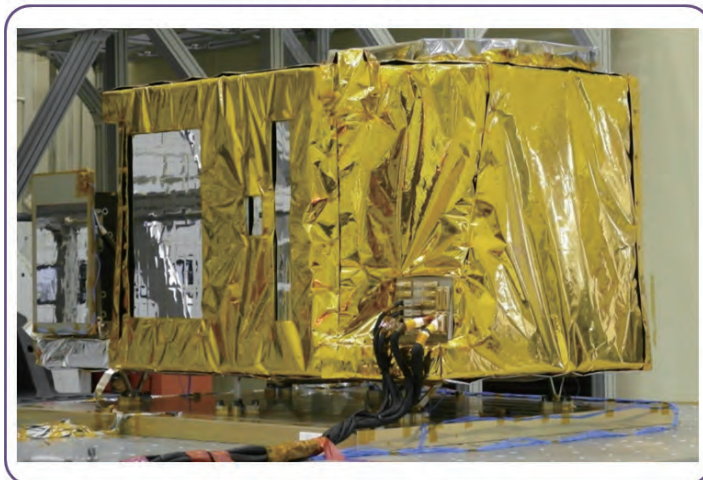
The GOCI-II instrument consists of a SU (Sensor Unit) and one IEU (Instrument Electronic Unit) integrated inside the Cheollian-2B platform(Fig. SC-A-14 and 15). The total mass of GOCI-II payload is about 150 kg. The 12 narrow band spectral channels are obtained by means

of a filter wheel. A 13th wideband spectral channel is implemented for star imaging.

A PIP (Payload Interface Plate) supports a highly stable full SiC (Silicon Carbide) telescope, the two-dimensional FPA (Focal Plane Array) and a FEE (Front End Electronics), the pointing mirror mechanism, the filter wheel mechanism and also the shutter / calibration wheel mechanism.

GOCI-II was developed by the Joint Development Team, KARI, KIOST and Airbus DS. In addition, final performance/functional test and environment test including on-ground calibration were performed by Joint Development Team at KARI's Daejeon site in Korea.

Sensor Unit



Electronics Unit



Fig. SC-A-14. Photo of the GOCI-II instrument on a ground supporting structure, with electronics (image credit: Airbus DS/KARI)

GOCI-II Functional Test and Environment Test @ KARI

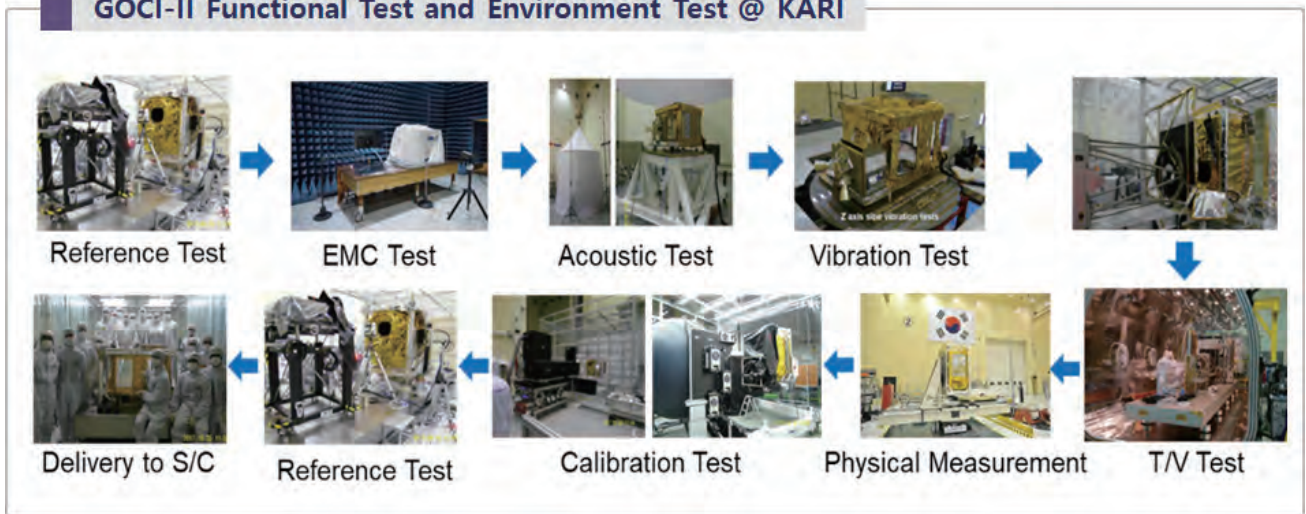


Fig. SC-A-15. Photo of the GOCI-II instrument on a ground test at KARI (image credit: KARI)

GOCI-II Observation Image

The ocean observation system with greatly enhanced performance will provide 26 types of information including red tide, floating algae, sea fog, and sea ice. The marine observation data provided in various formats are expected to be utilized by a wide range of fields, such as

marine environment protection, fisheries resource management, marine safety, and marine defense. The public can receive marine image data (pre-processing standard data) from the Cheollian-2B satellite free of charge through the KHOA website (www.khoa.go.kr).

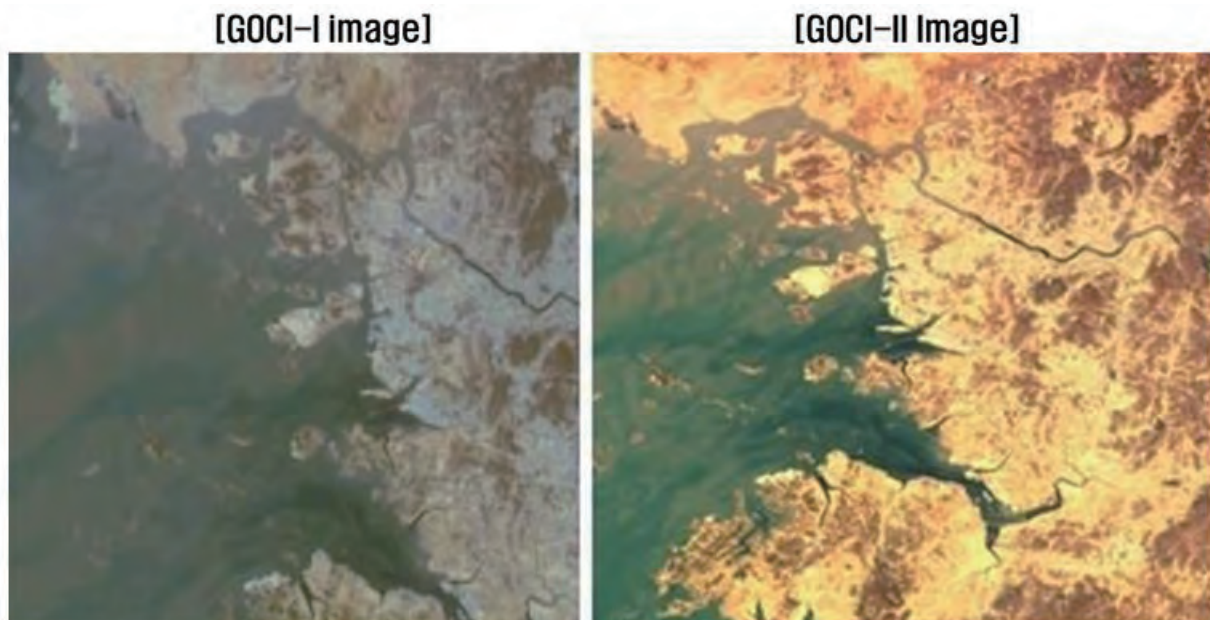


Fig. SC-A-16. Comparison of observed image between GOCI-I and GOCI-II @ Incheon of South Korea (image credit; MSIT/KHOA)

References

- [1] Jae-Dong Choi, "GEO-KOMPSAT-2(GK2) Satellite Development Status," International GOCI Symposium 2016, IGS 2016, Jeju, Korea.
- [2] "GEO-KOMPSAT-2 Program," KARI, https://www.kari.re.kr/eng/sub03_02_02.do
- [3] Herbert J. Kramer: <https://directory.eoportal.org/web/eoportal/satellite-missions/g/geo-kompsat-2>
- [4] Stephen Clark, "Ariane 5 • GSAT 11 & GEO-Kompsat 2A," Spaceflight Now, 25 October 2018, <https://spaceflightnow.com/launch-schedule/>
- [5] Koon-Ho Yang, "Advanced Meteorological Imager (AMI) Development for GEO-KOMPSAT-2A," The 1st KMA International Meteorological Satellite Conference, Seoul, Korea, November 16-18, 2015.
- [6] Pierre Coste, Franck Larnaudie, Philippe Luquet, Haengpal Heo, Junpyung Jung, Gmsil Kang, Sangyoun Shin, Sangsoon Yong, Young-Je Park, "Development of the new generation of geostationary ocean color image", International Conference on Space Optics, ICSSO 2016, 2016, Biarritz, France
- [7] Yu Hwan Ahn , Joo Hyung Ryu, Seong Ick Cho, Suk Hwan Kim, "Missions and User Requirements of the 2nd Geostationary Ocean Color Imager (GOCI-2)", The Korean Society of Remote Sensing, pp277-285, Vol.26 No. 2, April, 2010.

Geostationary Environment Monitoring Spectrometer (GEMS) on GK2B

Dong Won Lee, National Institute of Environmental Research (NIER)

Jhoon Kim, Yonsei University

Jaedong Choi, Korea Aerospace Research Institute

The First Air Quality Monitoring Mission from GEO

The first air quality monitoring mission, Geostationary Environment Monitoring Spectrometer (GEMS) was launched on Feb 19th KST 2020 and finished in orbit tests (IOTs) successfully (Fig. SC-A-17).

GEMS is a scanning, UV-visible spectrometers at an unprecedented spatial and temporal resolution. The spectral resolution is 0.6 nm over 300 – 500 nm, and spatial resolution is 7 km x 8 km for gases and 3.5 km x 8 km for

aerosols covering Asia (latitude: 5S – 45 N, longitude: 75 E – 145 E).

Since the first observation of the Sun and Earth, columnar concentrations of aerosol, ozone and their precursors are retrieved successfully from GEMS radiance spectra. Its first light images were released in November 2020, and operational service is to be continued from 2021.

GEMS is to revolutionize the air quality monitoring from space, which eventually contribute to top-down emission estimates and air quality forecast.



Fig. SC-A-17. Launch of GEMS onboard the GEO-KOMPSAT-2B (GK2B) spacecraft by Ariane 5 from Guiana Kourou on February 19th KST, 2020 (Image Credit: ESA CNES Arianespace)

GEMS Program

GEO-KOMPSAT(GK) series has been a key Geostationary Earth Orbit (GEO) program as listed in the National Space Program of Korea. GK1, known as the Communication, Oceanography and Meteorology Satellite (COMS) was launched in June, 2010 with Meteorological Imager (MI) and Geostationary Ocean Color Imager (GOCI).

The Ministry of Science, ICT and future Planning (MSIP) is the coordinating ministry for the development of the GK2, supported also by the Ministry of Oceans and Fisheries (MOF), Ministry of Environment (ME), and Korea Meteorological Administration (KMA). Under the auspices of MSIP, Korea Aerospace Research Institute (KARI) is the system integration organization for the GK mission including the launch.

GK2 consists of twin satellites, namely GK2A and GK2B, which was launched Dec., 2018 and Feb., 2020, respectively (See Fig. SC-A-17 for the launch scene of GK2B). GK2 hosts Geostationary Environment Monitoring Spectrometer (GEMS) in addition to Advanced Meteorological Imager (AMI) and GOCI-2.

Major specifications of these instruments are listed in Table SC-A-6. The National Institute of Environmental Research (NIER) of ME is responsible for the development and operation of GEMS for air quality monitoring in the Asia-Pacific region. The user requirements for the GEMS mission have been driven mainly by NIER and GEMS science team. Algorithm has been developed by GEMS science team.

Table SC-A-6. Specifications of Payload instruments for the GK-series satellite of Korea

Payload	GK 1 (COMS)		GK 2A	GK 2B	
	MI	GOCI		GOCI-2	GEMS
Channels	5	8	16	13	1000
Spatial Resolution (km)	1 (Vis) 4 (IR)	0.5 @ Seoul	0.5 / 1 (Vis) 2 (IR)	0.25 @ eq 1 (FD)	7 x 8 (gas) 3.5 x 8 (aerosol)
Spatial Coverage	FD /NH	East Asia	FD	East Asia / FD	Asia
Temporal resolution	15 min	1 hour	10 min	1 hour (FD 1/day)	1 hour
Wavelength	0.6–13 nm	412–860 nm	0.4–13 nm	375–860 nm	300–500 nm
FWHM (nm)	10–20	10–20	10–20	10–20	0.6(0.2)
Launch	Jun. 2010		Dec. 2018	Feb. 2020	
Lifetime	7 years		10 years		
Location	128.1 °E		128.2 °E		

GEMS Payload Configuration

The GEMS spectrometer is designed to monitor trans-boundary pollution events for the Korean peninsula and the Asia-Pacific region. The GEMS instrument consists of a SU (Sensor Unit), one ICE (Instrument Control Unit) and one FPE(Focal Plane Electronics) integrated inside the Cheollian-2B platform.

The total mass of GEMS payload is about 160 kg. The GEMS instrument has a 2-axis scan mirror and a 1 k x 2 k focal plane array using a CCD (Charge Coupled Device) to image the ultraviolet/visible spectrum. GEMS was developed by the Joint Development Team, KARI and BATC.

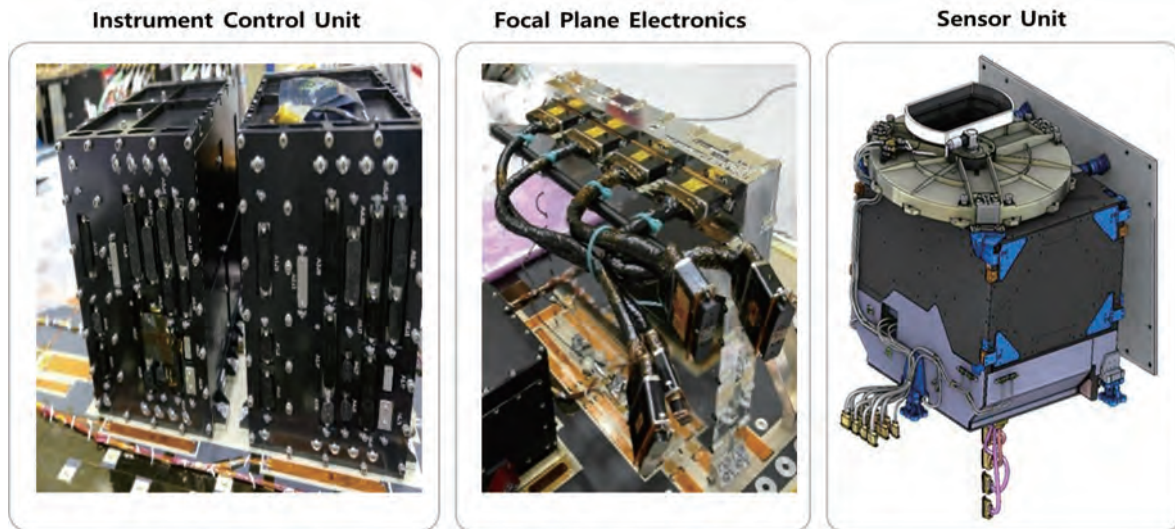


Fig. SC-A-18. Photo of the GEMS instrument (image credit: BATC/KARI)

GEMS Observation Image

Using a scanning UV-Visible spectrometer, its observations can contribute to provide a set of tropospheric column products over the Asia-Pacific region at spatial resolution of ~ 8 km and temporal resolution of 1 hour.

Other products include NO_2 , HCHO, SO_2 , and aerosol optical depth. GEMS scan a 5000 km East/ West area in less than 30 minutes with state-of-the-art calibration and high spatial and spectral resolution. In geostationary or

bit, GEMS collect images over an 8 to 12 hours period.

The Fig. SC-A-19 show four observations of nitrogen dioxide in East Asia from 10:45 a.m. to 2:45 p.m. on September 9. High concentrations of nitrogen dioxide were observed in large cities (Seoul, Pyongyang, Beijing, Shenyang, Osaka, Nagoya), industrial areas and thermal power plants.

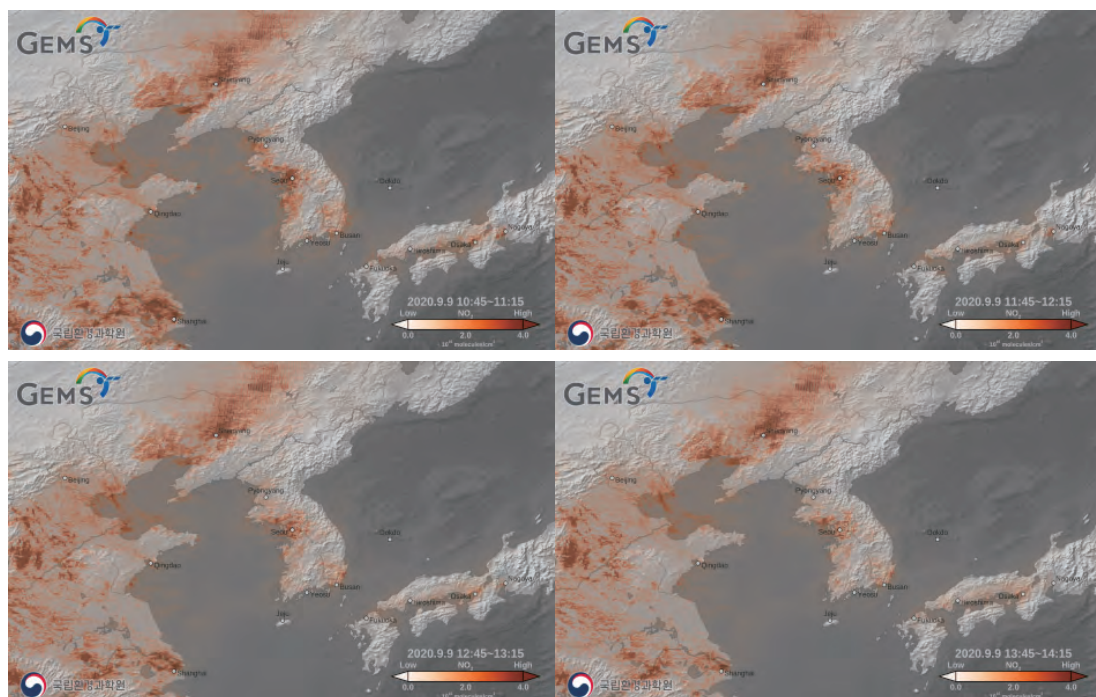
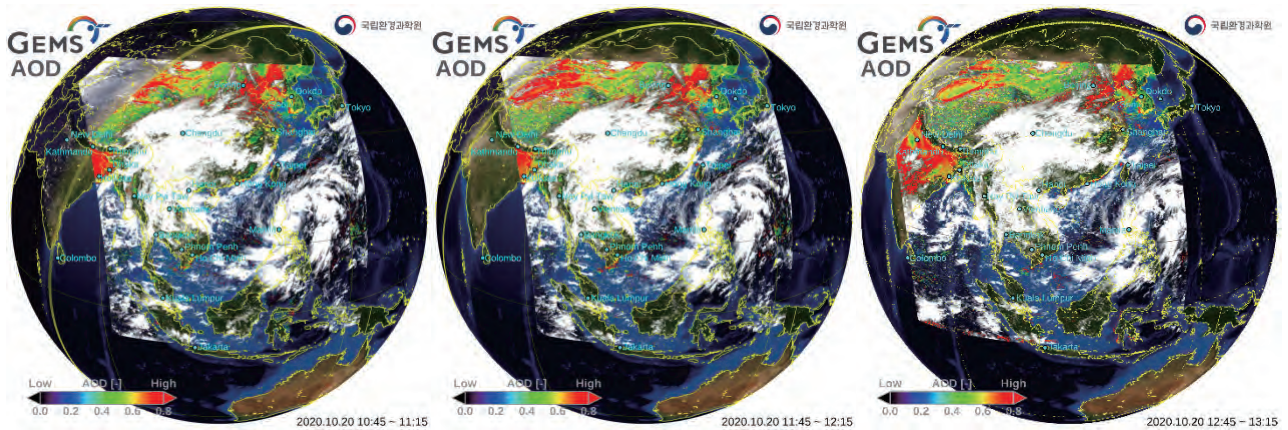


Fig. SC-A-19. Four observations of nitrogen dioxide in East Asia (image credit: NIER/MOE and MSIT)

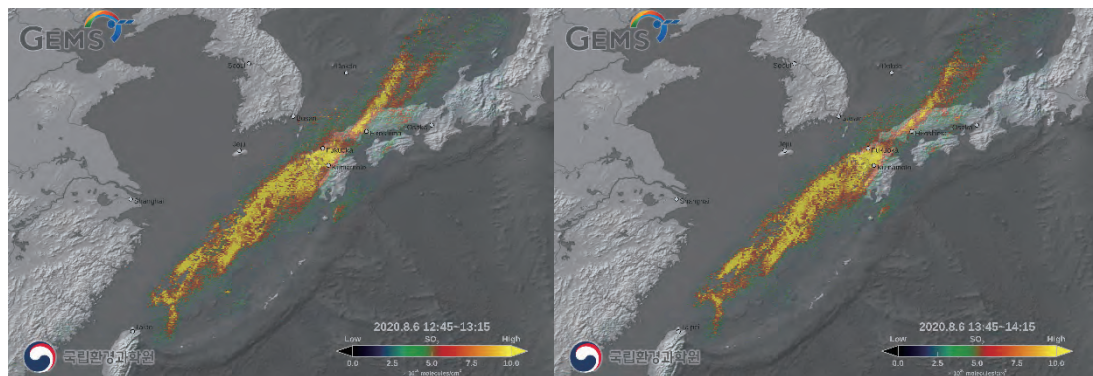
GEMS went through in orbit test (IOT) and its first light images were released in Nov., 2020 as shown in Fig. SC-A-20. Main products of GEMS include aerosol optical depth (AOD), ozone (O_3), nitrogen dioxide (NO_2), sulfur dioxide (SO_2), formaldehyde (HCHO), glyoxal (CHOCHO), UV indices of four different kind, cloud and surface properties

etc. Its potential future products include BrO, IO, photolysis rates, etc. after appropriate algorithm development and tests.

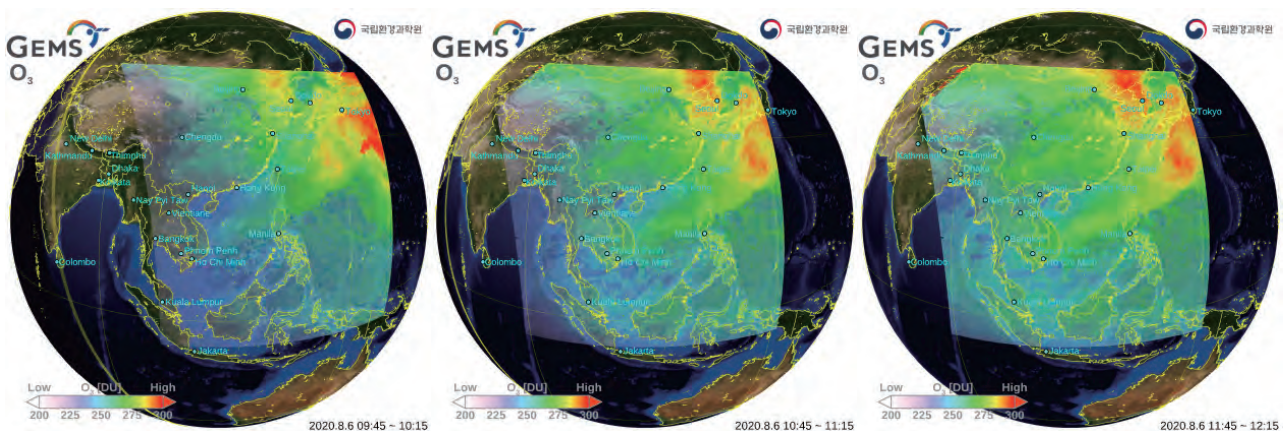
Ground-based networks are started to build up as essential components in the validation of the GEMS missions, where Pandora, a ground-based UV-visible



(a)



(b)



(c)

Fig. SC-A-20. The first light images of GEMS (a) aerosol optical depth (AOD), (b) sulfur dioxide from the Nishinoshima volcanic eruption in Japan, and (c) ozone (O_3) (image credit: NIER/MOE and MSIT).

spectrometer is a key instrument. Pandora Asia Network (PAN) is established to deploy tens of Pandora instrument to 13 countries within the GEMS field of Regard (FOR), with the support of Korea International Cooperation Agency (KOICA), United Nations Economic and Social Commission for Asia and the Pacific (UNESCAP) and Korea Environment Corporation(K-eco).

NIER has open data policy and is planning to distribute data to users through their network. Data distribution and capacity building is to be implemented through the Pan-Asia Partnership for Geospatial Air Quality information (PAPGAPI).

GEMS is about to revolutionize the air quality forecasting. GEMS data at high temporal and spatial resolution can be used widely in improving air quality forecasts and air pollutant emission statistics and providing air quality information services to public.

GEMS is to be followed up by NASA's TEMPO over North America in 2022 [4], and ESA's Sentinel-4 over Europe in 2023-2024 [5]. These three missions have similar observational capabilities to form GEO Air Quality (AQ) Constellation, as recognized by the Atmospheric Composition-Virtual Constellation of the Committee on Earth Observation Satellite (CEOS) [6]. The three GEO AQ missions together with environmental and meteorological measurements, will improve our understanding of transport, and chemical and physical processes by integrating multiplatform, cross-scale observational assets. The GEO AQ constellation will be the first of its kind to monitor global air quality in a coordinated manner.

References

- [1] Jhoon Kim, "Planned GEO Mission in Korea for Air Quality Measurements: GEMS(Geostationary Environmental Monitoring Spectrometer)," NASA-MEST (Ministry of Education Science and Technology of Korea) Technical Group for Geostationary Atmospheric Composition Measurements Meeting, Washington D.C., August 13, 2009
- [2] Choi, Won Jun, Kyung-Jung Moon, Jongmin Yoon, Ara Cho, Sang-kyun Kim, Seounghoon Lee, Daiho Ko, Jhoon Kim, Myung Hwan Ahn, Deok-Rae Kim, Sang-Min Kim, Ji-Young Kim, Dennis Nicks, Jeong-Su Kim, "Introducing the geostationary environment monitoring spectrometer," *J. Appl. Remote Sens.* 12(4), 044005 (2019), doi: 10.1117/1.JRS.12.044005
- [3] Kim, Jhoon, Ukkyo Jeong, Myoung-Hwan Ahn, Jae H. Kim, Rokjin J. Park, Hanlim Lee, Chul Han Song, Yong-Sang Choi, Kwon-Ho Lee, Jung-Moon Yoo, Myeong-Jae Jeong, Seon Ki Park, Kwang-Mog Lee, Chang-Keun Song, Sang-Woo Kim, Young-Joon Kim, Si-Wan Kim, Mijin Kim, Sujung Go, Xiong Liu, Kelly Chance, Christopher Chan Miller, Jay Al-Saadi, Ben Veihelmann, Pawan K. Bhartia, Omar Torres, Gonzalo González Abad, David P. Haffner, Dai Ho Ko, Seung Hoon Lee, Jung-Hun Woo, Heesung Chong, Sang Seo Park, Dennis Nicks, Won Jun Choi, Kyung-Jung Moon, Ara Cho, Jongmin Yoon, Sang-kyun Kim, Hyunkee Hong, Kyunghwa Lee, Hana Lee, Seoyoung Lee, Myungje Choi, Pepijn Veeffkind, Pieter Levelt, David P. Edwards, Mina Kang, Mijin Eo, Juseon Bak, Kanghyun Baek, Hyeong-Ahn Kwon, Jiwon Yang, Junsung Park, Kyung Man Han, Bo-Ram Kim, Hee-Woo Shin, Haklim Choi, Ebony Lee, Jihyo Chong, Yesol Cha, Ja-Ho Koo, Hitoshi Irie, Sachiko Hayashida, Yasko Kasai, Yugo Kanaya, Cheng Liu, Jintai Lin, James H. Crawford, Gregory R. Carmichael, Michael J. Newchurch, Barry L. Lefer, Jay R. Herman, Robert J. Swap, Alexis K H Lau, Thomas P. Kurosu, Glen Jaross, Berit Ahlers, Marcel Dobber, Tom McElroy, Yunsoo Choi (2020), *New Era of Air Quality Monitoring from Space: Geostationary Environment Monitoring Spectrometer (GEMS), BAMS*, 101, 1, doi:10.1175/BAMS-D-18-0013.1.
- [4] Zoogman, P, X. Liu, R.M. Suleiman, W.F. Pennington, D.E. Flittner, J.A. Al-Saadi, B.B. Hilton, D.K. Nicks, M.J. Newchurch, J.L. Carr, S.J. Janz, M.R. Andraschko, A. Arola, B.D. Baker, B.P. Canova, C. Chan Miller, R.C. Cohen, J.E. Davis, M.E. Dussault, D.P. Edwards, J. Fishman, A. Ghulam, G. González Abad, M. Grutter, J.R. Herman, J. Houck, D.J. Jacob, J. Joiner, B.J. Kerridge, J. Kim, N.A. Krotkov, L. Lamsal, C. Li, A. Lindfors, R.V. Martin, C.T. McElroy, C. McLinden, V. Natraj, D.O. Neil, C.R. Nowlan, E.J. O'Sullivan, P.I. Palmer, R.B. Pierce, M.R. Pippin, A. Saiz-Lopez, R.J.D. Spurr, J.J. Szykman, O. Torres, J.P. Veeffkindz, B. Veihelmann, H. Wang, J. Wang, K. Chance (2017), *Tropospheric Emissions: Monitoring of Pollution (TEMPO)*, *J. Quantitative Spectroscopy and Radiative Transfer*, 186, 17-39, doi: 10.1016/j.jqsrt.2016.05.008
- [5] Ingmann, P, B. Veihelmann, J. Langen, D. Lamarre, H. Stark, and G. B. Courrèges-Lacoste, 2012: Requirements for the GMES atmosphere service and ESA's implementation concept: Sentinels-4/-5 and -5p. *Remote Sens. Environ.*, 120, 58–69, doi: 10.1016/j.rse.2012.01.023.
- [6] CEOS (2011), *A Geostationary Satellite Constellation for Observing Global Air Quality: An International path Forward*, CEOS Atmospheric Composition Constellation White Paper

KOMPSAT-6 Mission

Seon-Ho Lee, Jae-Cheol Yoon, and Jin-Hee Kim, Korea Aerospace Research Institute

Korea Multi-Purpose Satellite (KOMPSAT) is the one of the key space programs in Korea for earth observation, which was started from 1994 to develop the KOMPSAT-1 satellite to provide the observation data for Geographical Information Systems (GIS) applications, oceanography and space physics.

The series of KOMPSAT satellite had been successfully launched from KOMPSAT-1 to KOMPSAT-5 in last two decades with various payloads such as the optical camera, infrared camera, space weather sensors, and laser retro-reflector.

The main mission objectives of KOMPSAT-6 satellite, follow-on program of KOMPSAT-5, are the expedite provision of the space-borne Synthetic Aperture Radar (SAR) standard images with sub-meter resolution required for the national demand in GIS, Ocean & Land management, Disaster monitoring, and Environment monitoring. The mission applications (“GOLDEN”) are described as follows:

- GIS: Acquisition of independent high-resolution images*
- Ocean & Land Management: Survey of natural resources*
- Disaster & ENvironment Monitoring: Surveillance of large-scale disasters and its countermeasure*

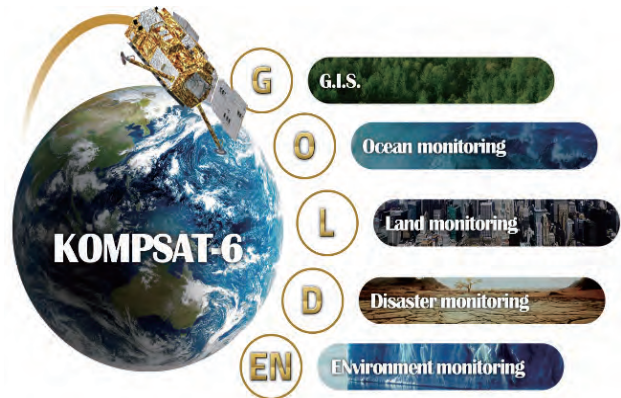


Fig.SC-A-21. KOMPSAT-6 Mission Application

The KOMPSAT-6 system consists of space segment, ground segment, launch segment, and various external interfaces including additional ground stations to support the payloads data reception during the Launch and Early Operation Phase (LEOP) and normal mission phase.

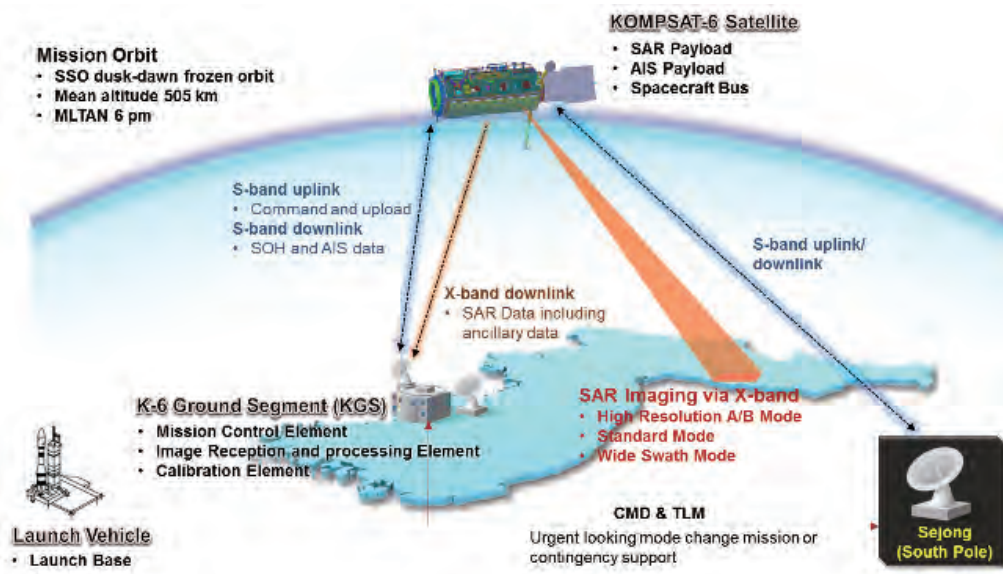


Fig. SC-A-22. KOMPSAT-6 System Architecture

The KOMPSAT-6 satellite will be delivered to low Earth orbit in 2022 for all-weather day-night monitoring of Korean peninsula. After achieving mission orbit and completing the in-orbit test, repetitive SAR observations for Earth’s land and ocean will be conducted for 5-year mission lifetime.

The primary mission of KOMPSAT-6 system is to provide the SAR image of 0.5 m and 1 m resolution for High Resolution mode, 3 m resolution for Standard mode, and 20 m resolution for Wide Swath mode at the incidence angle of 45 deg.

The KOMPSAT-6 satellite system is a single KOMPSAT-6 satellite flying in a repeat ground track frozen dusk-dawn orbit with 11 days repeat ground track period at mean altitude of 505 km.

The space segment which is also known as the satellite system is comprised of the SAR payload, AIS payload, and spacecraft bus. equipment, and launch services/operations required for delivery the satellite into mission orbit.

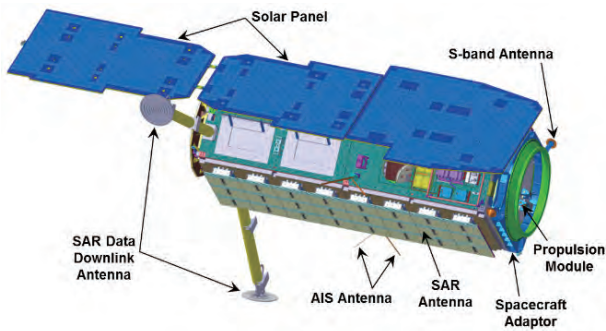


Fig. SC-A-23. KOMPSAT-6 In-orbit Configuration

Spacecraft Bus

The spacecraft bus provides a number of functions to support the system operations. These functions consist of providing a stable platform for SAR payload, AIS payload, the state of health telemetry data, satellite timing, power and thermal management, attitude pointing and determination, and orbit determination. The spacecraft bus also provides the orbit maneuver capability necessary to maintain the orbit required for the KOMPSAT-6 mission.

The spacecraft bus is comprised of seven subsystems such as Structures and Mechanisms Subsystem (SMS), Thermal Control Subsystem (TCS), Attitude and Orbit Control Subsystem (AOCS), Propulsion Subsystem (PS), Telemetry, Command, and Ranging Subsystem (TC&R), Electrical Power Subsystem (EPS), and Flight Software Subsystem (FSW). The key design features of KOMPSAT-6 spacecraft bus are described as follows.

- Integrated structure with hexagonal cross section
- Primary structure made out of CFRP
- Fixed SAR antenna on a panel
- Fixed solar array with one deployable wing
- Panel-mounted units covered with MLI tents
- 3-axis attitude control with zero momentum bias
- Dual frequency GPSR for POD generation
- Passive & processor-controlled thermal control
- 1N-thrusters for precise orbit correction
- Solar array capability: 2,250 Watts

For electrical interface of KOMPSAT-6 spacecraft bus, the MIL-STD-1553B data bus interfaces most of the spacecraft bus and payload to the IBMU. The dual frequency GPS receiver provides the time, satellite position and velocity for on-orbit ephemeris, and L1/L2 frequency GPS pseudo-range and carrier phase data for post-processed precision orbit determination on ground. TC&RS includes S-band antennas, a RF assembly and redundant S-band transponders. AOCS provides three-axis stabilization with off-pointing capability and yaw steering capability during imaging time.

In addition, the spacecraft bus provides the mechanical and electrical interface to the launch vehicle, and the necessary strength and stiffness to deliver the satellite to mission orbit during launch, ascent, and insertion. For the case where the launch vehicle has placed the satellite into orbit within nominal dispersions from the desired mission orbit, the spacecraft bus provides the capability to correct the orbit through a series of orbit maneuvers to the final mission orbit.

Table SC-A-7. KOMPSAT-6 Spacecraft Bus Characteristics

Characteristic	Values	Remarks
Lifetime	5 years	
Mass	1,750 kg	Satellite Wet Mass
Solar Array Power	2,250 W	
Repeat Ground Track Maintenance	250 m (3s)	
POD Accuracy	20 cm (1s)	Dual-Frequency GPS Receiver
Off-Pointing Angle	+/-37 deg	From the Nadir

SAR Payload

The primary payload of KOMPSAT-6, is space-borne SAR instrument for multi-mode operations to collect image data on a wide access area. The SAR payload is a multi-

mode X-band SAR that is capable of operating in four observation modes: High Resolution A/B Mode, Standard Mode, and Wide Swath Mode. Each mode will provide different characteristics in terms of geometric resolution and swath-width.

Table SC-A-8. SAR Payload Characteristics

Characteristic	Values
Lifetime	5 years
Operation Frequency	X-band
High Resolution-A	0.5 m (Res) 5 km (SW)
High Resolution-B	1 m (Res) 10 km (SW)
Standard	3 m (Res) 30 km (SW)
Wide Swath	20 m (Res) 100 km (SW)
Image Acquisition Time	150 sec per orbit
Multi-Polarization	Single (HH, HV, VV, VH)
	Dual (HH+HV, VV+VH)
	Quad (HH+HV+VV+VH)
Incidence Angle	20-60 deg
NESZ	-20 dB
Data Storage	1 Tbit
Downlink Rate	600 Mbps

The SAR payload consists of the SAR Sensor Subsystem (SSS) and the Data Link Subsystem (DLS). The SSS operates in X-band and it is equipped with an active phased array antenna, with electronic scanning capabilities in both the azimuth and the elevation planes. The DLS is in charge of the storage and transmission to ground of the SAR sensor scientific data and of the ancillary data.

The SSS operates a multi-mode X-band SAR with phase array antenna comprising the following functions.

- Transmit equipment for signal generation and distributed transmit signal high power amplification
- Receive equipment for distributed receive signal low noise amplification, coherent down-conversion and digitization
- Phased Array antenna assembly with real-time (PRI to PRI) beam forming capability in azimuth and elevation via phase and amplitude control incl. temperature compensation and providing single phase as well as dual phase center
- Quad linear polarization (HH, VV, VH, HV) with dual coherent HH/HV and VV/VH

- Internal calibration and diagnostics features
- Command and control functionality for agile and flexible operation

AIS Payload

Automatic Identification System (AIS) is a maritime wireless system designed to identify basic parameters relating to the position, heading, destination and cargo of larger vessels with the main purpose of collision avoidance. The AIS payload is the secondary payload of the KOMPSAT-6 satellite. The AIS payload receives and provides the AIS signal data for ship collision avoidance and traffic management.

The AIS payload for KOMPSAT-6 consist of AIS receivers and AIS antennas. Satellite AIS receivers are able to disentangle these collision signals and reconstruct the original messages. Satellite AIS receivers are able to operate in both frequency spectrum capture mode (Raw/OGP) and on-board processing (OBP) mode allowing simultaneous operation.

VHF band antennas are needed for the AIS signal reception. Multiple VHF antennas can be used for better AIS signal reception. Antenna deployment mechanism is applied for deploying antennas after satellite launch.

Table SC-A-9. AIS Payload Characteristics

Characteristic	Values
Lifetime	5 years
Mass	5 kg
Power	7 W
Operation Mode	OBP (On-board Processing)
	OGP (On-ground Processing)
Operation Frequency	VHF-band
Data Memory	4 GBytes

[1] Sang-Ryool Lee, Jin-Hee Kim, Jae-Cheol Yoon, "First SAR Satellite in Korea, KOMPSAT-5," Int. Conf. Space, Aeronautical & Navigational Electronics (ICSANE), 253-257, Oct. 2012.

[2] Sang-Ryool Lee, "Overview of KOMPSAT-5 Program, Mission, and System", IEEE Int. Geoscience and Remote Sensing Symposium (IGARSS), 797-800, 2010.

* This article is modified for the report from "KOMPSAT-6 Mission, Operation Concept, and System Design", which was presented in 11th European Conference on Synthetic Aperture Radar, Hamburg, Germany, 2016.

SC-B

The Earth-Moon System, Planets, and Small Bodies of the Solar System

Korea Pathfinder Lunar Orbiter (KPLLO) Mission

CLPS Korea Project – Opening the Door of the Lunar Surface Science

Optical Properties of NEA Phaethon

Space Geodetic Infrastructures and Researches



Korea Pathfinder Lunar Orbiter (KPLO) Mission

Eunhyeuk Kim, Haeng-Pal Heo, and Gm-Sil Kang, Korea Aerospace Research Institute

Minsup Jeong, Young-Jun Choi, and Bongkon Moon, Korea Astronomy and Space Science Institute

Sungsoo Kim, Ho Jin, and Khan Hyuk Kim, Kyung Hee University

Kyeong Ja Kim, Korea Institute of Geoscience and Mineral Resources

Kyung-In Kang, Korea Advanced Institute of Science and Technology

The Korea Pathfinder Lunar Orbiter (KPLO) mission is the first space exploration mission of the Republic of Korea beyond the Earth orbit. The Korea Aerospace Research Institute (KARI) has launched a series of Korea Multi-Purpose Satellite (KOMPSAT) and Geostationary KOMPSAT (GEO-KOMPSAT) satellites and aims to perform a safe moon landing by 2030.

KPLO is expected to be launched in the middle of 2022 using a Falcon-9 launch vehicle. After traveling to the Moon via a Ballistic Lunar Transfer (BLT) trajectory, KPLO will be inserted into mission orbit of approximately 100 km altitude circular orbit. KPLO will carry out its mission around the moon for one year, and there would be an extended mission depending on the amount of fuel.

The main goals of the KPLO mission are 1) to realize the first space exploration of Korea, 2) to develop and verify space technologies suitable for deep space exploration, and 3) to investigate the details of unknown physical characteristics of lunar surface for the future landing missions and human missions to the moon

To meet its mission goals, KPLO is equipped with five science instruments (LUTI, PolCam, KMAG, KGRS, and ShadowCam) and one technology demonstration instrument (DTNPL).

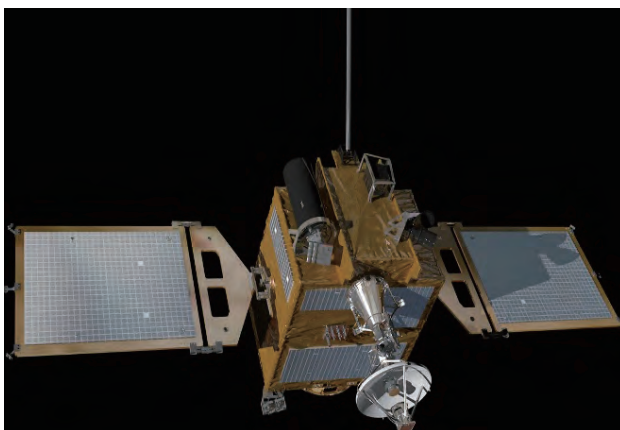


Fig. SC-B-1. The Korea Pathfinder Lunar Orbiter (KPLO)

The best time to launch KPLO would be around August 2022, when the required amount of fuel to be used to insert KPLO into the lunar orbits is expected to be small. However, the advantage of using a BLT trajectory is that it would provide a more plausible launch window. KPLO will travel to the moon for several months depending on the launch date and is expected to arrive by mid-December 2022.

Afterward, KPLO will enter the lunar orbit insertion (LOI) phase, where a large amount of fuel (about 70%) will be used to be captured by lunar gravity. After LOI, KPLO will have a polar orbit around the moon, and the inclination angle of the polar orbit will be around 90 degree and to be maintained for one year.

A one-month commissioning phase will follow LOI in which the spacecraft bus system and all the KPLO instruments will be activated for calibration and verification purposes before the nominal mission phase.

The orbit of spacecraft during the commissioning phase will be maintained within 100 ± 30 km, which corresponds to 2 hours of orbital period. KPLO will carry out its mission for 11 months after the termination of the commissioning phase, and would enter into an extended mission phase depending on the amount of fuel left after one-year mission in lunar orbit.

Fig. SC-B-2 displays the configuration of KPLO spacecraft (Bus and Payloads) at stowed position. It has two-wing, 1-axis solar panels directed to $\pm y$ -direction, and a propulsion system located at the bottom of the spacecraft in the $-x$ direction, where $+x$ direction denotes the flight direction of the spacecraft.

The KPLO instruments that will observe the surface of the moon are attached on $+x$ panel (KMAG, ShadowCam) or $+z$ panel (LUTI, PolCam, KGRS). The high gain antenna is located on the $-z$ direction for the communication with ground stations on earth.

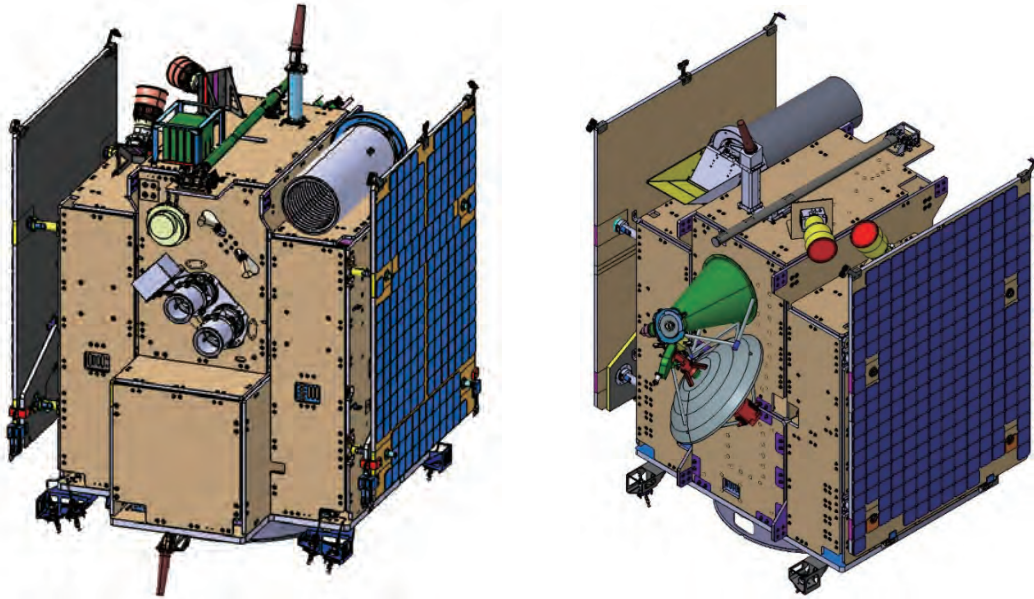


Fig. SC-B-2. Stowed configuration of KPO facing +Z (Left: Nadir) and -Z (Right: Zenith view)

The height of spacecraft bus is approximately 2.3 m, and the wing spans after the solar panel deployed is approximately 6.5 m wide. To generate the electric power from all instances of sunlight, the spacecraft will be operated by tilting 45 degrees, therefore all instruments except for KMAG, and DTNPL will be attached by compensating this spacecraft operation scenario.

According to the preliminary analysis, the electric power generated by the spacecraft is minimized at a Sun-beta angle of 45 degrees. Therefore, the operation of KPO is rather limited during those special cases.

Table SC-B-1 shows the overall configuration and measurements of the instruments on board KPO as well as a summary of exploration and scientific benefits. With the exception of DTNPL, our summarized introduction to the KPO science instruments are as follows.

Table SC-B-1. Overview of KPO Instruments

Instrument	Measurement	Exploration Benefit	Science Benefit
LUTI (KARI+)	2.5m/px resolution images of lunar surface (@100km altitude)	Future landing site for the next lunar mission	Geology, Topology of the lunar surface
PolCam (KASI+)	First polarimetric map of near- and far-side of the moon except for polar regions	Effect of lunar soil on electro-mechanical parts of landing module	Characteristics of lunar regolith, Space weathering process
KGRS (KIGAM+)	Mapping major elements (Mg, Ni, Cr, Ca, Al, Ti, Fe, Si, O, U, He-3, Water) distribution	Space Environment, Radiation environment for manned mission	Distribution of lunar resources, Water/mineral contents
KMAG (KHU+)	3D map of lunar magnetism, magnetic information of lunar swirls	Space Environment	Origin of the Moon, Lunar magnetic evolution
DTN (ETRI+)	First test of disruption tolerant network on lunar environment	Testing deep space communication	
ShadowCam (NASA)	Detailed imaging of permanently shadowed regions (PSRs) near lunar poles	Address NASA's lunar SKGs* on lunar volatiles, cold traps, and resources	Understanding of lunar polar volatiles, location, content, morphology

- **Lunar Terrain Imager (LUTI)** will take images of probable landing sites for the second stage lunar landing exploration mission and target sites of the lunar surfaces with a high spatial resolution.
- **Wide-Angle Polarimetric Camera (PolCam)** will perform polarimetric observations of the whole surface (except for the pole regions) of the Moon with a spatial resolution of <100 m.
- **KPO Gamma Ray Spectrometer (KGRS)** will investigate the characteristics of lunar resources including rare elements, minerals etc, and will map the surface distribution of key elements.
- **KPO MAGnetometer (KMAG)** will measure the magnetic strength of the lunar environment with ultra-sensitive magnetic sensors.
- **ShadowCam** will take the images of permanently shadowed regions (PSRs) near both north and south poles of the moon using TDI technology, and is expected to provide information about the resources and structures in these PSRs.

Lunar Terrain Imager (LUTI)

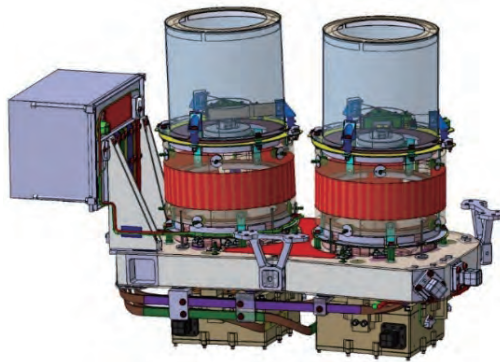
LUTI is an electro-optical instrument that will be mounted on KPO with the mission of capturing high resolution images of the candidate landing site on the Moon.

It will be operated in a push-broom manner and produce images with GSD of 2.5 m and swath width of 9.75 km at the nominal altitude of 100 km. LUTI consists of

two identical cameras mounted on the same bezel. It can provide a wide swath width and it can also be considered as redundancy. In addition, LUTI has been designed to have high dynamic range and can provide a minimum signal-to-noise ratio of 40 under the condition of radiance range from 5 to 300 W/m²/um/sr. This radiance range covers the lunar surface middle latitude.

High sensitive linear CCD has been used and the integration time can be controlled by command independently with the scan speed, i.e. line rate. Therefore, it can take images both in a very high or low phase angle.

Considering the low speed of communication link to the ground-station on Earth, LUTI has real-time image compression function. Radiometric and geometric characterization have been performed in the laboratory to be used for calibration and on-ground image correction.



Ground-Sample Distance	2.5m @100km altitude
Spectral Band	Panchromatic 450 to 850nm
Swath Width	9.75km @100km altitude
Signal to Noise Ratio	≥40 @phase angle of 30 to 60 degree
Modulation Transfer Function	≥10% @Nyquist frequency (payload level)
Radiometric Resolution	12bits
Mass	12kg

Fig. SC-B-3. Lunar Terrain Imager (LUTI) of KPL0 mission.

Wide-Angle Polarimetric Camera (PolCam)

Polarimetry is an effective tool to obtain physical properties of airless bodies, such as a grain size and the roughness of surface.

PolCam (Wide-Angle Polarimetric Camera) is the world's first lunar polarimetry instrument operated in a lunar orbit. To prepare PolCam, we conducted various polarimetric studies toward the Moon (Jeong et al. 2015; 2016; 2018; 2020, Sim et al. 2017; 2018; 2019; 2020; Kim et al. 2017).

The polarimetric data will be obtained at wavelengths of 430 nm and 750 nm with a spatial resolution of 100 m for phase angle ranges 0° - 135°. In addition, photometric data will be also obtained at a wavelength of 320 nm with a spatial resolution of 100 m. The phase angle coverage is the most important to obtain the maximum linear polarization degree which is correlated with grain sizes of regolith, and the grain size is correlated with space weathering.



Mass		3 kg
Dimensions	Electronics box	150 x 120 x 62 mm ³
	Optics box	250 x 150 x 100 mm ³
FOV		10°
Swath width		35 km (at 100 km)
Imaging pixels		512 x 6 channels
Input voltage		24 ~ 32.8 V
Power		15 W
Operating Temperature		-20° ~ 50°

Fig. SC-B-4. Optical unit (upper) and Specifications of PolCam.

Because the maximum linear polarization degree occurs around a phase angle of 100°, obtaining a large phase angle data is important for the polarimetry observation. To obtain a larger phase angle than 100° even at the equator, PolCam's each individual telescopes, Cam-L and Cam-R, are tilted ± 45° from the nadir direction to across track of the spacecraft motion. To obtain whole map of lunar surface, the field of view is 9.9°, which corresponds to the ground shift speed of the Moon.

Now, we are testing the performance of the flight model of PolCam system and it will be delivered in November 2020. It is widely anticipated that the data from PolCam can give new perspectives for lunar science because this is a new kind of information.

KPL0 Gamma-Ray Spectrometer (KGRS)

The KPL0 Gamma-Ray Spectrometer (KGRS) is a compact low-weight instrument for the elemental analysis of lunar surface materials within a gamma-ray energy range from ~30 keV to 12 MeV.

The major components of KGRS consist of a primary LaBr₃ gamma-ray detector with an anti-coincidence

counting module of 5% boron-loaded plastic scintillator to reduce both gamma-ray background from the spacecraft and housing materials, and cosmic ray background.

The science goals of KGRS are associated with investigations of both lunar geology and lunar resources down to a half-meter depth of the lunar surface. Both an Engineering Qualification Model (EQM) and a Flight Model (FM) of KGRS have been successfully developed at Korea Institute of Geoscience and Mineral Resources (KIGAM). KGRS data can be important to investigation of future lunar landing site for prospecting ISRU research activities on the Moon.



Fig. SC-B-5. Configurations of the KGRS sensor and electronics.

Table SC-B-2. Science goal and specification of the KPLO gamma-ray spectrometer (KGRS)

Science	Measure Gamma-rays from the Lunar surface for elemental mapping	
Performance	Energy range	~30 keV to 12 MeV (H.G.: 3 MeV, L.G.: 12 MeV)
	Energy resolution	< 5 % @ 662 keV
System	Mass	Total 7 kg (SU, EU)
	Detectors	LaBr3 (primary), BLPS (shielding)
	No. Energy channels	LaBr3 (8192,4096), BLPS (1024)
	Power	Input: +28 V Consumption: 8.5 W
Operation	Interface	RS-422, 115,200 bps
	Operating temperature	SU: Operation: -20 °C ~ +50 °C EU: Operation: -20 °C ~ +55 °C
	Life time	~ 1 year
Operation	Data collection / generation	10 sec / Max. 1.85Gbits / day (Duty 100%)
	Pointing	Nadir direction

KPLO Magnetometer

The KMAG is one of the scientific instruments of KPLO to measure the magnetic field of the Near Lunar space environment and the lunar surface. The scientific objectives focus on the lithospheric magnetism and investigation of wave properties near the Moon.

The KMAG instrument consists of two units as shown in Fig. SC-B-6. One is the MAG (MAGnetometer) unit, which consists of three magnetometers, a 1.2 m-long boom, and a deployment mechanism. The other unit is Fluxgate magnetometer Control Electronics (FCE), which consists of four electrical boards and its housing.



Fig. SC-B-6. KMAG configuration: MAG unit (left) and FCE unit (right). MAG unit consists of the CFRP boom, Actuator, and Hinge. Three fluxgate sensors are inside the boom, and the sensor at the end of the boom is the main magnetometer (MAG1). FCE unit consists of four electric boards and its housing. These electrical boards are stacked using PC104 connectors.

The instrument parameters are listed in Table SC-B-3 and the magnetometer performance is shown in Table SC-B-4.

Table SC-B-3. Main instrument parameters

Parameter	Performance
Magnetometer	3-axis fluxgate
Size	MAG unit: 1318 x 178 x 122 mm FCE unit: 150 x 135 x 82 mm
Mass	Total 3.5 kg
Power consumption	4.6 Watt
Operation temperature	MAG unit: -55°C ~ +70°C FCE unit: -20°C ~ +50°C
Interface	RS-422, 115,200 bps
Data generation	295.3 Mbit/dat (duty 100%)

Table SC-B-4. Specifications of KMAG magnetometer

Parameter	Performance
Magnetometer type	Fluxgate
Measurable range	± 1000 nT
Resolution	< 0.2 nT @ 10 Hz sampling rate
Noise level	50 pT / sqrt(Hz) at 1 Hz
Linearity	< 5 × 10 ⁻³ e
Temperature Coefficient	< 0.1 %/°C
Axis Alignment	< 1 deg.

The KMAG team also expected the new observation data set about a magnetic sounding of the lunar interior with other lunar missions such as ARTEMIS and CLPS (Commercial Lunar Payload Services).

CLPS Korea Project – Opening the Door of the Lunar Surface Science

Chae Kyung Sim, Young-Jun Choi, Minsup Jeong, Dukhang Lee, and Seul-Min Baek, Korea Astronomy and Space Science Institute
Sung-Joon Ye, Seoul National University
Ho Jin, Jongho Seon, and Sungsoo S. Kim, Kyung Hee University

Korean Payloads for the Lunar Surface Sciences

Korea Astronomy and Space Science Institute (KASI) is developing science payloads to make observations on the lunar surface in situ as a part of Commercial Lunar Payload Services (CLPS) of National Aeronautics and Space Administration (NASA), USA, based on the KASI-NASA Exploration Working Group. NASA is to pave the way toward the next generation space exploration sending various payloads to the lunar surface by commercial landers through the CLPS program in of step with Artemis mission.

KASI has selected four payloads to fly onboard one or more CLPS landers that will be developed by domestic universities and companies, as well as KASI. The Ministry of Science and ICT (MSIT), Korea is willing to support the development, mission operation, and data analysis processes of the payloads for 4.5 years in total at maximum.

GrainCams is consists of two light-field cameras, SurfCam and LevCam, for dust particles on and near the lunar surface. SurfCam will take 3D images of the hypothetical “fairy castle” structure of the upper regolith. LevCam will detect the motions of levitating and lofted regolith grains near the surface. The diurnal and time variations of the physical properties of the regolith and dust by the electric and magnetic fields will be also recorded by GrainCams. It will provide a unique and intact observations of the phenomena that are irreproducible on Earth, and cannot be preserved via a sample-return mission.

LVRad is a radiation dosimeter that consists of Lunar Radiation dosimeter and Spectrometer (LRDS) and Neutron Spectrometer (NS). LRDS will measure the radiation environment of the lunar surface and analyze its biological effects using a Tissue-Equivalent Proportional Counter

(TEPC). NS will measure the epithermal neutrons from the surface, which are potential evidence of subsurface water, and fast neutrons that are less frequently measured but have larger influences on a biological body.

LMAG is a fluxgate magnetometer to measure the magnetic field and its diurnal variation on the lunar magnetic anomalies in situ for the first time. Its measurements will be useful to estimate the magnetic field strength of the lunar paleo-dynamo using the magnetic field strength on the surface and corresponding direction and depth of the source.

LUSEM is a solid state telescope to detect high-energy particles of tens to hundreds keV such as solar wind, cosmic ray, solar energetic protons and secondary radiation, and geomagnetic material, including local effects that cannot be measured from the orbit. Its measurements will be helpful to study the space weathering on the Moon in terms of interactions between charged particles and micrometeoroids. It will be also useful to study the mechanism and influence of the transportation of the geomagnetic materials to the lunar surface.

Attributed largely to the heritages of previous space missions, experienced and passionate teams commenced to develop the payloads in the management of KASI’s CLPS Korea project. The scientific measurements of the payloads will provide valuable data to understand the nature of the Moon, our steadfast neighbor, when the payloads are landed and operated successfully on its surface. Based on the strengthened mutual trust, KASI and NASA will develop further collaboration in scientific research and space exploration. All of the science, technology, and experiences built up from this project will shed light on future lunar landing mission of Korea.

Optical Properties of NEA Phaethon

Myungjin Kim, Korea Astronomy and Space Science Institute

Near-Earth asteroid (3200) Phaethon, target of the DESTINY+ mission

We conducted the ground-based observation campaign of NEA Phaethon that is the target of JAXA's DESTINY+ mission. To cover the rotational phase of the asteroid during the 2017 apparition, a total of eight observatories with optical imagers in the Asian and American continents located in northern hemisphere were employed as shown in Table SC-B-5. We have analyzed the lightcurve of Phaethon and derived a synodic rotational period of 3.604 hr, with an axis ratio of $a/b = 1.07$.

Table SC-B-5. Observatories details

Tel.	Lon.	Lat.	Alt.	Date
SLT 0.4m	120:52:25	+23:28:07	2,879.0	15/12/2017
OWL 0.5m	249:12:38	+32:26:32	2,769.5	15-17/12/2017
SOAO 0.6m	128:27:27	+36:56:04	1,354.4	26-17/12/2017
CBNUO 0.6m	127:28:31	+36:46:53	87.0	07/12/2017
MAO 0.6m	66:53:44	+38:40:24	2,578.2	19-27/11/2017
TShAO 1.0m	76:58:18	+43:03:26	2,723.5	16-22/11/2017
LOAO 1.0m	249:12:41	+32:26:32	2,776.0	11-13/11/2017
BOAO 1.8m	128:58:36	+36:09:53	1,143.0	01/12/2017

(SLT = Lulin Super Light Telescope, OWL = Optical Wide-field patrol, SOAO = Sobaeksan Optical Astronomy Observatory, CBNUO = ChungBuk National University Observatory, MAO = Maidanak Astronomical Observatory, TShAO = Tian Shan Astronomical Observatory, LOAO = Lemonsan Optical Astronomy Observatory, BOAO = Bohyunsan Optical Astronomy Observatory)

To get the information on pole orientation and 3D shape model, the LI (lightcurve inversion) method and SAGE algorithm were applied independently.

We obtained the 3D shape model of Phaethon based on the unique solution with a sidereal rotational period of 3.603957 hr and a spin direction of $308^\circ, -52^\circ$ (Fig. SC-B-7). As the lightcurve amplitude pointed out, overall, the asteroid looks like a spherical shape.

In addition, the convex model tells us that the asteroid can be classified as the “spinning-top” shape similar to Ryugu and Bennu, the target asteroids of sample-return missions from JAXA and NASA, respectively.

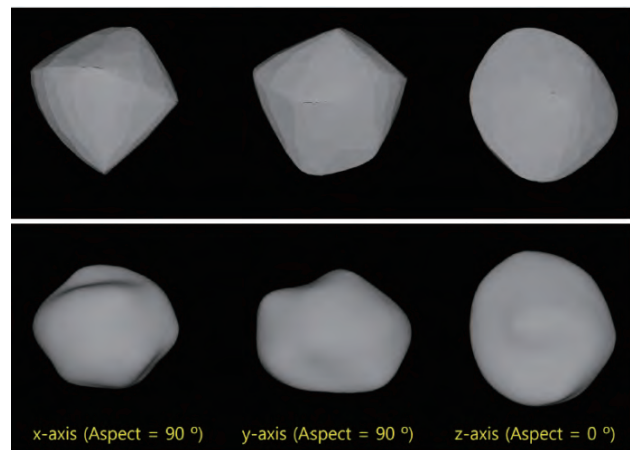


Fig. SC-B-7. 3D shape model of Phaethon obtained from LI method (top) and the SAGE algorithm (bottom). The three views in both shape models correspond to the views from the positive x, y, z axes, respectively (Kim et al. 2018).

References

- [1] Kim, M.-J., Lee, H.-J., Lee, S.-M., et al., (2018) Optical observations of NEA 3200 Phaethon (1983 TB) during the 2017 apparition. *Astronomy & Astrophysics* 619, A123.

Space Geodetic Infrastructures and Researches

Kyoung-Min Roh, Korea Astronomy and Space Science Institute

National Geographic Information Institute(NGII) and Korea Astronomy and Space Science Institute (KASI) have successfully cooperated to establish the Sejong geodetic fundamental site in which GNSS, VLBI, and SLR are collocated since 2015. With the growing need of real-time GNSS data for both geodetic and public sectors, a GNSS data sharing system was opened in 2016 as a real-time web service in which 174 GNSS sites nation-widely distributed are available.

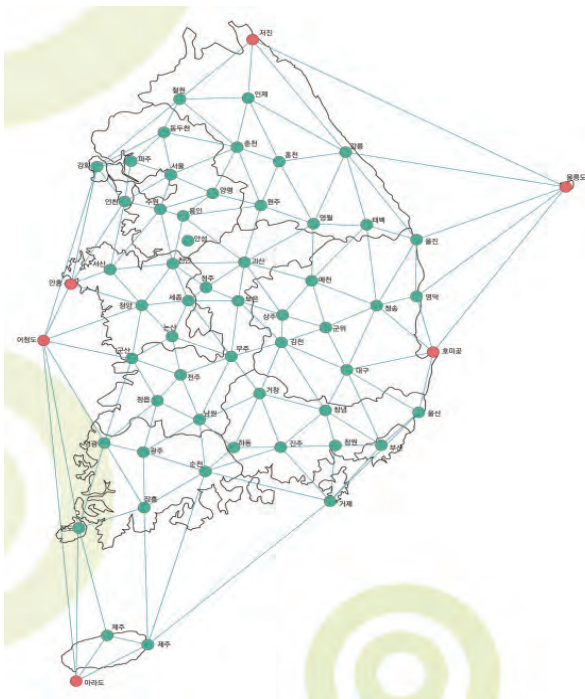


Fig. SC-B-8. Korea's GNSS Network (CORS)

KASI is also operating the global data center of International GNSS Service(IGS/GDC) that archives and provides GNSS data from the Asia-Oceania region. The KASI GDC also archives and shares all the IGS products from worldwide IGS stations and IGS analysis centers (<ftp://nfs.kasi.re.kr>, <http://gdc.kasi.re.kr>). In 2018, KASI extended GDC storage by adding another 32TB real-time backup disk to prevent from a disk failure.

KASI has been the GPS Radio Occultation (RO) data center for the Atmosphere Occultation and Precision Orbit Determination (AOPD) system onboard Korea Multi-Purpose Satellite (KOMPSAT)-5 since 2013.

This data service is conducted in collaboration with University Corporation for Atmospheric Research (UCAR), National Oceanic and Atmospheric Administration (NOAA), Korea Meteorological Administration (KMA), and Korea Aerospace Research Institute (KARI) since 2014. During the period, researches on natural hazards monitoring and Earth rotation modelling had been performed at KASI.

KOMPSAT-5 radio occultation products are now available to worldwide weather communities via Global Telecommunication System of the World Meteorological Organization (WMO) information system.

The Sejong SLR Station of KASI and the nearby VLBI and GNSS stations of the Space Geodetic Observation Center of NGII will contribute to determining the ITRF and EOPs as one of the GGOS site. Because each station utilizes different space geodetic techniques, their relative positions must be precisely determined to ensure the accuracy of the resulting reference frame. As shown in Fig. SC-B-9, each pillar around the Sejong SLR Station was designed to be solid from the deformation due to annual and daily temperature changes.



Fig. SC-B-9. Local tie survey pillar installation at Sejong GGOS Site

SC-C

The Upper Atmospheres of the Earth and Planets including Reference Atmospheres

Upper Atmospheric Research Activities

Ionospheric Observations from Space



Upper Atmospheric Research Activities

Geonhwa Jee, Korea Polar Research Institute

Young-Sil Kwak, Korea Astronomy and Space Science Institute

Jong-Yeon Yoon, Korea Space Weather Center

In recent years, South Korea has been developing various high-tech facilities, in particular, associated with advanced information technologies, one of the main engines of the South Korean economy and these become more vulnerable to the space weather events such as solar flares and coronal mass ejections. Reliable space weather information has thus become critical to the continued prosperity of the South Korean economy.

To meet this urgent demand, space weather research in South Korea has become a rapidly developing discipline. The government has taken an active role in space weather research and applications by monitoring the Sun, near-Earth space environments, and polar space environments, sponsoring robust national space science and meteorological programs as well as promoting efficient systems for the delivery of space weather information to the public.

In this report, we introduce the upper atmospheric research activities carried out by the related research institutes and government agencies in South Korea, which include the Korea Astronomy and Space Science Institute, the Korea Polar Research Institute, and the Korean Space Weather Center of Radio Research Agency.

Korea Astronomy and Space Science Institute (KASI)

Korea Astronomy and Space Science Institute (KASI) is creating excellent research results on the changes in the ionosphere/upper atmosphere through various ground- and satellite-based observational studies.

In order to study the irregularities of the mid-latitude ionospheric/upper atmospheric environment, all-sky cameras, VHF ionospheric radar, GPS scintillation monitor, and meteor radar have been operated.

The all-sky camera was installed at the Bohyeonsan Observatory (36.2°N, 128.9°E) in 2008 to study the ionosphere/upper atmospheric disturbances and waves over the Korean peninsula.

The VHF ionospheric radar was installed in Gyeryong city (36.18° N, 127.14° E) in 2009 in cooperation with the Air Force to observe and monitor the electron density irregularities of the E and F layers of the ionosphere in real time.

For real-time monitoring of ionosphere scintillation on a short time scale, a GPS ionosphere scintillation monitor was installed at the VHF Ionosphere Radar Observatory in 2016. In order to obtain information on the upper atmospheric wind speed and temperature of the E layer altitude to identify the cause of the electron density irregularities in the ionospheric E layer, a meteor radar has been operated at the VHF ionospheric radar site since 2017 (see Fig. SC-C-1).



Fig. SC-C-1. All-sky camera, VHF ionospheric radar, GPS scintillation monitor, and meteor radar (left to right)



Fig. SC-C-2. GPS scintillation monitor and all-sky camera in Antarctica

In order to study the high-latitude ionospheric/upper atmospheric irregular phenomenon, we installed a GPS scintillation monitor and an all-sky camera in Antarctic Jang Bogo Science Station in cooperation with Korea Polar Research Institute, in 2015 and 2016, respectively (Fig. SC-C-2).

Additionally, in 2015, we became affiliated with the European Incoherent Scatter Scientific Association (EISCAT), which is a powerful ground observation equipment capable of observing various physical components of the high-latitude ionosphere and upper atmosphere. We have the right to secure time and use observational data.

KASI is developing a low-Earth orbit space environment observation satellite consisting of four nano-satellites (<10 kg) and will launch it in 2021. By using these satellites, we can observe the temporal and spatial changes of the microstructure of the near-Earth space (ionosphere and magnetosphere) plasma simultaneously as well as to clarify the generation mechanism of the plasma structure with various scales.

Using a variety of high-resolution ground- and satellite-based observations and up-to-date models, we conducted research on the temporal and spatial characteristics and the source of the Earth's high-middle-low latitude ionosphere and upper atmospheric irregularity. The results were published in the high-level journal in the field such as *Journal of Geophysical Research*, *Geophysical Research Letters*, *Space Weather* and so on.

In recent years, the development and related studies of an ionosphere prediction model based on data assimilation and artificial intelligence have been conducted to predict the state of the ionosphere over the Korean Peninsula.

Korean Space Weather Center(KSWC)

The Korean Space Weather Center (KSWC) of the National Radio Research Agency (RRA) is a government agency which is the official source of space weather information. In early 2013, space weather was included in the national risk assessment process, and the official manual of space weather disaster management was adopted by the government. This manual describes the roles and missions of the organizations involved.

KSWC is the primary action agency of emergency measure against severe space weather condition. In addition, KSWC is a Regional Warning Center (RWC) of the International Space Environment Service Organization (ISES) and actively responds to space weather issues reported by international organizations such as the International Telecommunication Union (ITU) and the World Meteorological Organization (WMO).

KSWC operates a number of ground observation systems for space weather and also has satellite tracking facilities for receiving the telemetry from ACE, STEREO, and DSCOVR satellite (Fig. SC-C-3).

In addition, the ASSA model was developed to predict sunspot explosions and analyze changes in solar activity, which are also in NASA CCMC. The Safety during Aviation Flight Environment from radiation (SAFE) system provides estimates of radiation exposure on polar routes for airlines and crews.



Fig. SC-C-3. Observation Networks in KSWC

In particular, there are plans to build an advanced processing system using big data and Artificial Intelligence (AI) in 2021. Through the big data system, a large amount of space weather data will be collected, such as solar images and observations on solar wind, magnetic fields, and the ionosphere.

The system will automatically present relevant data to users who likely want to foster a high-quality research environment. AI is expected to improve the forecasting process and high accuracy space weather forecasts with supplement the information forecasters may miss.

If the space weather forecasting system with this new technology is built stably and has accurate space weather forecasting capability, KSWC become a reliable sharing system of efficient observational data. It has the potential to be an international role model in contributing to and developing the space weather field.

KSWC has been an active participant in international organizational discussions, sharing observation data as well as working to improve technology exchange and forecast accuracy between other countries. KSWC is working with Korea Astronomy & Space Science Institute (KASI) to establish a joint monitoring system for the ionosphere over the Korea-Japan-Taiwan area. Through this, KSWC will gradually expand exchanges for ionosphere research in Asia (Fig. SC-C-4).

Next, KSWC are developing an ionospheric prediction model over the Korean Peninsula. This model use the GPS-TEC, ionosonde data and COSMIC satellite data. The data assimilation process through the IDA4D model It generates the initial condition of ionosphere. In addition, this model uses the initial condition of neutral atmosphere calculated from TIE-GCM. Since 2020, KSWC use to this model for HF users and an ionospheric three-day forecast.

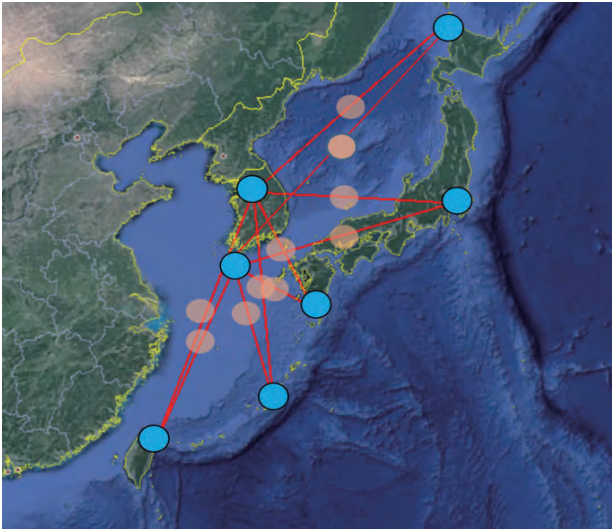


Fig. SC-C-4. Progress of Ionospheric joint observation East Asia(Korea-Japan-Taiwan). Blue point is Vertical site, Red site is oblique site on the sea

KSEC is also continue to play the role of the L1 satellite's Asia receiver and contribute to the preparation for global space weather risks. In addition to protecting the nation's assets threatened by space weather, KSWC plans to strengthen the international cooperation system so that Korea can be an equal partner in the global surveillance of space weather.

Korea Polar Research Institute (KOPRI)

Since Korean polar stations were established in Barton Peninsula (62° 13' S, 58° 47' W), King George Island, Antarctica in 1988 (King Sejong Station, Antarctica) and in Ny-Alesund (78° 55' N, 11° 56' E), Svalbard, Norway in 2002 (Dasan Station, the Arctic), the Korea Polar Research Institute (KOPRI) has been conducting a number of ground-based observations for the upper atmosphere and the near-Earth space environment including the ionosphere and thermosphere (IT), the mesosphere and lower thermosphere (MLT), and the magnetosphere in the northern and southern polar regions.

KOPRI has been operating Michelson interferometers both at Kiruna, Sweden, and at Dasan Station, mainly to monitor the neutral temperature in the polar MLT regions. But the observation at Dasan Station has been stopped a few years ago and we are looking for an alternative instrument to continue the observation.

For a similar purpose in the southern polar region, Spectral Airglow Temperature Imager (SATI) had been operating at King Sejong Station (KSS), Antarctica since 2002 until it stopped working in 2017. To continue the observation of

the MLT temperature at KSS, a mesospheric temperature mapper will be installed in 2021 to obtain a two-dimensional temperature map, which also allows us to observe the gravity waves in the MLT region.

Next, the meteor radar at KSS, installed in collaboration with Chungnam National University in 2007, observed the neutral winds and temperature in the MLT region. In 2008, All Sky Camera (ASC) was installed at the station to observe the atmospheric gravity wave in the upper atmosphere. In 2017, a Fabry-Perot Interferometer was installed in collaboration with High Altitude Observatory (HAO), National Center for Atmospheric Research (NCAR), USA to extend our observation of the neutral atmosphere from the MLT region to the thermosphere.

With the establishment of the second Korean Antarctic station (Jang Bogo Station: JBS) in Terra Nova Bay (74° 37' S, 164° 12' E), the ground-based observational activities at KOPRI were expanded to the near Earth's space environment in the polar region, including the ionosphere and thermosphere, the magnetosphere, and cosmic ray.

The new Antarctic station allows South Korean scientists to monitor the polar cap and the auroral region, depending on the magnetic activity or local time, in the southern hemisphere. At Jang Bogo Station (JBS), we initially installed Fabry-Perot Interferometer (FPI) in collaboration with HAO/NCAR in March 2014 and Vertical Incidence Pulsed Ionospheric Radar (VIPIR) in collaboration with the University of Colorado, Cooperative Institute for Research in Environmental Sciences (CIRES), USA in March 2015.

Simultaneous observations of the ionosphere (VIPIR) and thermosphere (FPI) will provide us with a unique opportunity to study the strong ionosphere-thermosphere coupling in the polar region, which is a fundamental physical process for transporting solar and magnetospheric energy into the upper atmosphere.

In addition to these instruments to observe the ionosphere and thermosphere, there are a number of ground instruments for the polar space environment, including a search coil magnetometer, GPS TEC/Scintillation monitor, neutron monitor, and three different types of All Sky Cameras at JBS.

In the Arctic, we expanded our observations to include the polar ionosphere and thermosphere in addition to the MLT region by installing a pair of FPI and GPS TEC/Scintillation monitor at Dasan Station and in Kiruna, Sweden. In 2016, we also joined European EISCAT's radar observation for the polar ionosphere. All these observations at KOPRI are summarized in Fig. SC-C-5 and C-6.

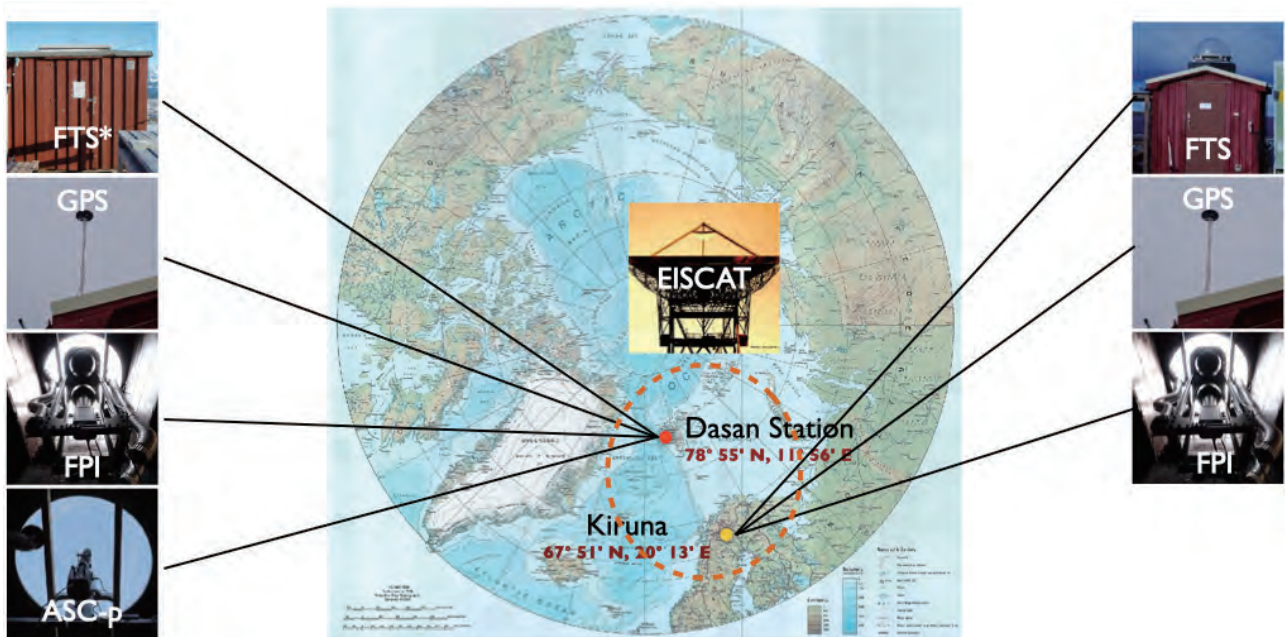


Fig. SC-C-5. Ground-based observation system for the upper atmosphere and near-Earth space environment in the northern polar region

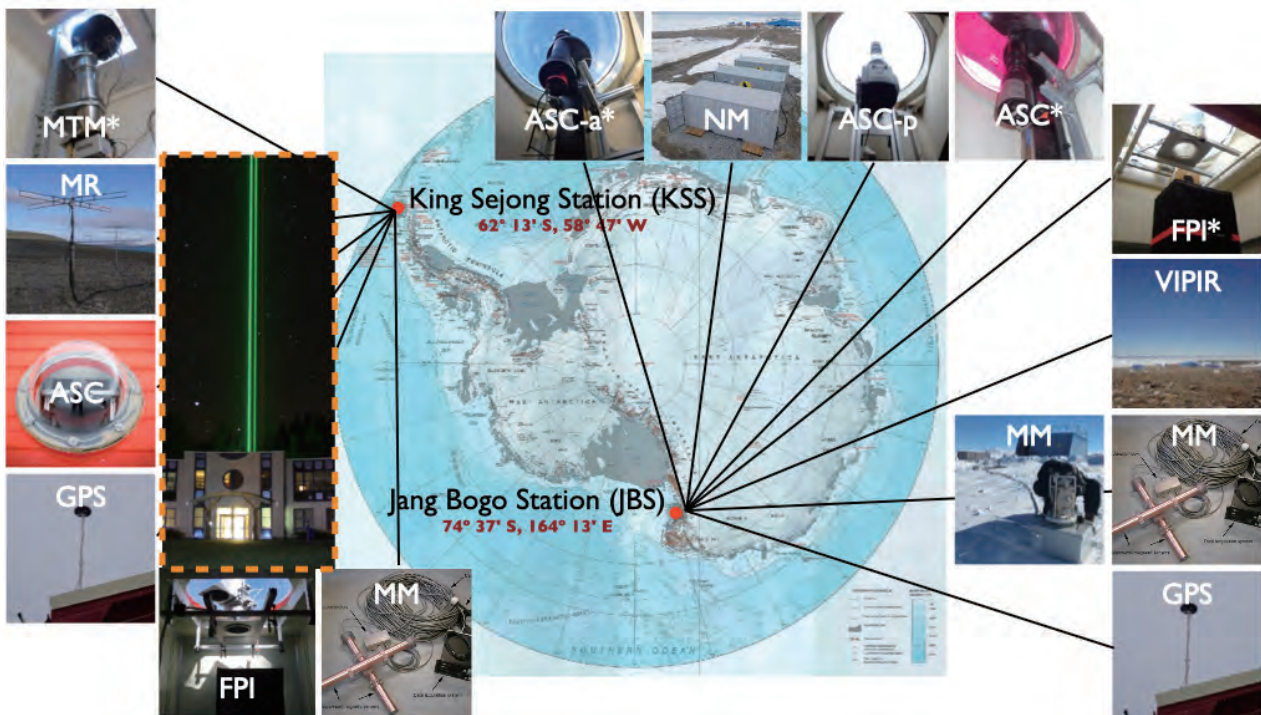


Fig. SC-C-6. Ground-based observation system for the upper atmosphere and near-Earth space environment in the southern polar region

Ionospheric Observations from Space

Kwang-Sun Ryu, Korea Advanced Institute of Science and Technology

History of Space Environment Observation by Satellites in Korea

The space activity in Korea was initiated by the KITSAT-1 ('92 launch) (Fig. SC-C-7).

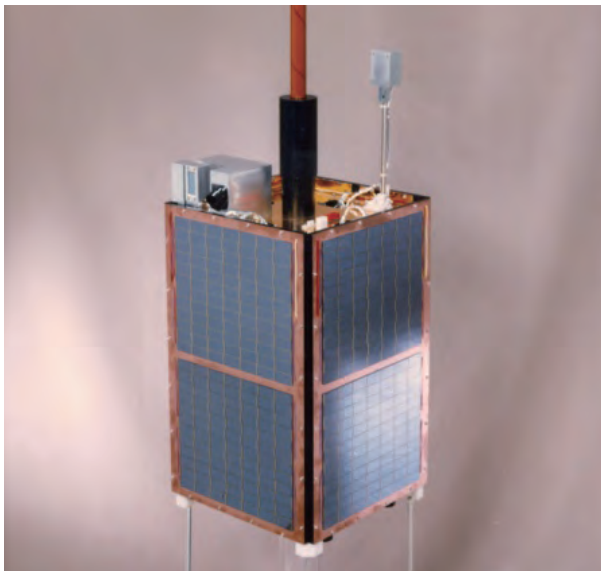


Fig. SC-C-7. Korea Institute of Technology Satellite-1 (KITSAT-1).

The satellites developed in Korea regarding the space environment focused on the low-orbit small satellites (such KITSAT-1, 2, 3, STSAT-1, 2, 3, KOMPSAT, and NEXTSAT-1).

The Chollian 2A, a geostationary satellite launched in 2018, has a Korean Space Environment Monitor (KSEM), a Korean-style space weather sensor comprised of a magnetometer, a satellite power detector, and a high-energy particle detector, which are being used in the space environment forecast business.

Recently, many cube satellites (CubeSat) developed for educational purposes carry space environment-related payloads but had have no indisputable success stories.

The constellated CubeSat mission is designed to study the microstructure of magnetosphere and ionosphere with four 6U-sized CubeSats named as SNIPE that are scheduled to be launched in 2021.

It is expected that more satellite constellations dedicated for the space environment and the ionospheric studies will follow in the near future (Table SC-C-1).

Table SC-C-1. Korean Space Science Missions to study ionosphere and magnetosphere.

I.D.	Instrument	Satellite	Launch	Developer	Objectives
1	Particle detector	KITSAT-1	1992	KAIST	Space Radiation
2	Electron detector	KITSAT-2	1993	KAIST	Electron Energy
3	Space Science Instruments	KITSAT-2	1999	KAIST	Ionosphere and High Energy Particles
4	Space Physics Sensors	KOMPSAT-1	1999	KAERI(KAIST)	Particle Detector, Langmuir Probe, Magnetometer
5	Space Physics Package	STSAT-1	2003	KAIST	Plasma density and Temperature
6	Langmuir Probe	NAROSAT	2013	KAIST	Electron Density
7	STEIN	CINEMA-1 KHUSAT-1,2	'12- '13	KHU, UC Berkeley Cooperation	Polar region electron, ion, and neutral particles (CubeSats)
8	ISSS	NEXTSAT-1	2018	KAIST	High energy particles and ionospheric plasma
9	KSEM	GK-2A (Geostationary)	2018	KHU	Magnetic field, spacecraft charge, and high energy particles
10	SNIPE	Cubesats(4)	2021 (plan)	KASI	Fine structure of the ionosphere and magnetosphere
11	LEO-DOS	NEXTSAT-2	2022 (plan)	KAIST(KASI)	Space Radiation Dose

STSAT-1, Optical and Particle Observations of Near-Earth Space

The Science and Technology Satellite-1 (STSAT-1) mission (launched in 2003), formerly known as Korea Advanced Institute of Science & Technology Satellite-4 (KAISTSat-4), aims to develop a high performance small satellite bus and high performance scientific payload design, research on space science, and develop advanced technology for future space missions.

STSAT-1 is a low-cost KAIST/SaTReC microsatellite technology demonstration mission funded by the Ministry of Science and Technology (MOST) of Korea, a follow-up mission in the KITSAT program.

The spacecraft (S/C) has a mass of 160 kg and S/C structure resembles a box of approximately 66 cm x 60 cm x 80 cm. It is three-axis stabilized and pointing requirements call for a pointing accuracy of 0.5°, an attitude knowledge of 5 arcmin, and a stability of about 5 arcmin/s. In addition, the S/C requires a complex set of attitude maneuverability in support of its mission objectives. The S/C features three solar panels, one fixed and two deployable, providing a power of 150 W. .

It has two scientific instruments called as FIMS and SPP.

FIMS (FUV Imaging Spectrograph) was developed in a cooperative project by KAIST, KAO (Korea Astronomy Observatory), and UCB/SSL (University of California at Berkeley/Space Sciences Laboratory). The objective of FIMS observations is to study the diffused hot interstellar matter in the Far Ultraviolet (FUV) spectrum.

The instrument allows for detailed mapping of the spatial distribution of the hot galactic plasmas and the determination of the physical states of hot interstellar matters as well as the detection of the various emission lines from the Earth's upper atmosphere. FIMS employs a dual bandpass (900-1175 Å and 1335-1750 Å), high spectral resolution (1.5 Å and 2.5 Å, respectively) imaging spectrograph with a 8° x 5' FOV (Field of View) and a 5 arcmin angular resolution (Fig. SC-C-8).

SPP (Space Physics Package), also referred to as PIP (Plasma In-situ Package), consists of four instruments: ElectroStatic Analyzer (ESA), Solid State Telescope (SST), Langmuir Probe (LP), Scientific Magnetometer (SMAG).

The science objectives of SPP are to provide a fast-sampling capability of high-energy magnetospheric plasma components and cold ionospheric plasmas, and to measure the Earth's magnetic fields.

The SPP's more specific objectives are to detect of directly penetrating solar wind plasmas and up-flowing, cold ionospheric electrons; to investigate of sub-km scale structures of the Earth's polar regions; and to compare of the in-situ measurements with the FIMS spectrographic images ($\Delta\lambda/\lambda$ of about 500) of the Earth's aurora in the far-ultraviolet ranges.

SST measures the high-energy components of auroral particles. It permits research on particle acceleration mechanisms in the magnetosphere. In addition, plasma fluxes are studied flowing in and out of the Earth's magnetosphere.

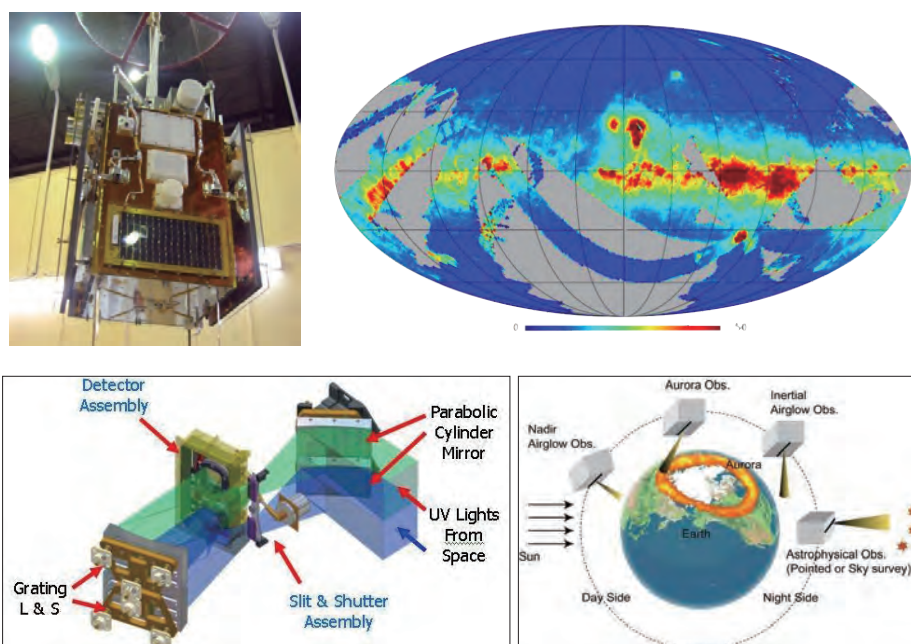


Figure SC-C-8. STSAT-1 and its main scientific payload FIMS.

NEXTSat-1, Observation of the Ionospheric Storm

The Next Generation Small Satellite-1 (NEXTsat-1), a 100 kg-class small satellite developed by Korea Advanced Institute of Science and Technology Satellite Technology Research Center (KAIST SaTReC), was launched on December 4, 2018 on the Falcon 9 from the Vandenberg Air Force launch site.

The NEXSAT-1 has a sun-synchronous orbit at an altitude of 575 km with the orbital inclination angle of 97.7 degrees. Its orbital speed is 7.57 km/s and the orbital period is 96.17 minutes.

Two scientific payloads are aboard the spacecraft in addition to seven core technology payloads: one is the Near-Infrared Imaging Spectrometer for Star formation history (NISS) and the other is the Instruments for the study of Stable/Storm-time Space (ISSS).

Normal operations of these two scientific instruments started in April 2019 after the spacecraft systems had been checked during the first one month and the scientific payloads had been calibrated during the next three months. Fig. SC-C-9 shows the NEXTsat-1 spacecraft with NISS and ISSS integrated and the ISSS instrument sets.

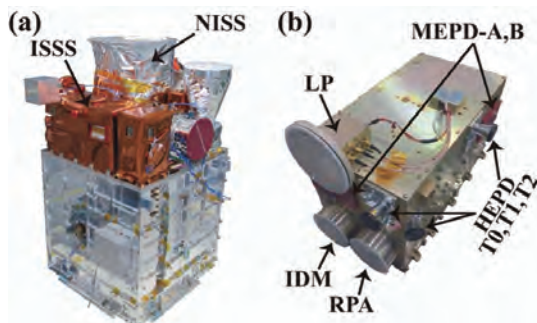


Fig. SC-C-9. The flight model of NISS and ISSS of NEXTSat-1 integrated to the spacecraft main body and (b) the flight model of ISSS

ISSS is a space science payload that consists of Space Radiation Detectors (SRDs) and Space Plasma Detectors (SPDs): SRDs measure energies and fluxes of precipitating medium and high energy particles from the terrestrial radiation belts and SPDs observe the disturbances in the topside ionosphere by measuring the plasma density and temperature.

SRDs are composed of the High Energy Particle Detector (HEPD) and the Medium Energy Particle Detector (MEPD). HEPD detects electrons in the energy range of ~350 keV to above ~2 MeV with time resolution of 32 Hz and pitch angle information with three telescopes that

have 0°, 45°, and 90° angles with respect to the local geomagnetic fields. HEPD can also detect high energy protons. MEPD measures electrons, ions, and neutral atoms of ~20 to ~400 keV with time resolution of 1 Hz and pitch angle information with two telescopes that have 0° and 90° angles with respect to the local geomagnetic fields.

SPDs are composed of a disk-type Langmuir Probe (LP) for electron density and temperature measurement, Retarding Potential Analyzer (RPA) for ion density/composition and temperature measurement, and Ion Drift Meter (IDM) for ion drift measurement. Time resolution of SPDs is 10 Hz.

Fig. SC-C-10 shows the nighttime electron density and temperature measured by the Space Plasma Detector on January 8, 2019 for the low latitude region as an example.

The density decreases with latitude at mid-latitudes, whereas the electron temperature varies from below 1,000 K to above 3,000 K and increases dramatically with latitude in the mid-latitude regions. Further, we can note the general anti-correlation between the density and the temperature.

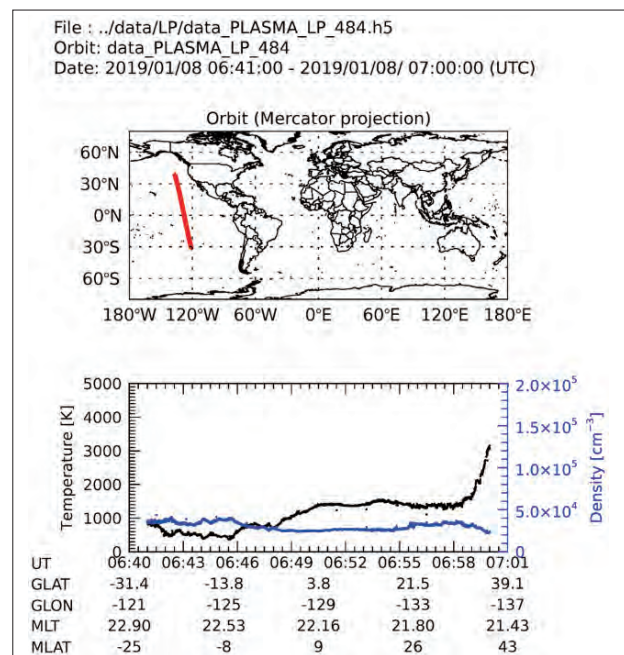


Fig. SC-C-10. Observation made by the Space Plasma Detector on January 8, 2019.

These observations can be compared with those made by the Detection of ElectroMagnetic Emissions Transmitted from Earthquake Regions (DEMETER) spacecraft at an altitude of ~710 km.

Fig. SC-C-11 shows the nighttime electron density and temperature made by DEMETER on January 6, 2007. Note that both spacecraft made observations in almost identical conditions in terms of the local time, day of year, and the solar activity.

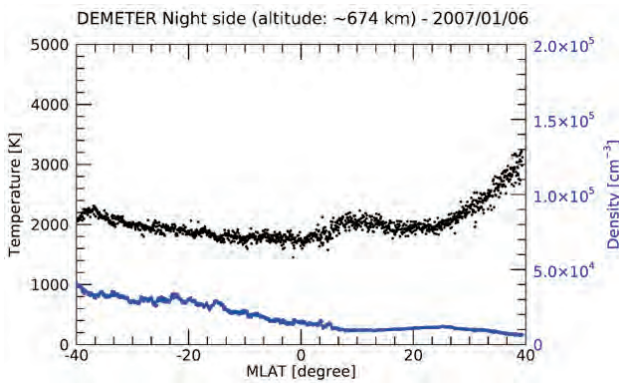


Fig. SC-C-11. The comparison with the observation made by the DEMETER spacecraft on January 6, 2007

We can clearly see the dramatic increase of electron temperature above 20 ° MLAT and the anti-correlation between the density and the temperature, as in the NEXTSat-1 observation. The DEMETER electron density is lower than the NEXTSat-1 electron density, whereas the DEMETER electron temperature is higher than the NEXTSat-1 electron temperature, which is reasonable because the DEMETER was operated at a higher altitude than the NEXTSat-1 by ~100 km.

Ground Experiments, Cradle for New Technologies for Ionospheric Observation in Space

The spatial limit of the in-situ measurement of the ionosphere can now be overcome through the constellation of small satellites. The innovative space access by CubeSats will provide even more frequent and dense measurements of the ionospheric plasma.

Since various countries and institutes are developing their own plasma instruments, it is essential to calibrate the plasma sensors before flight in a plasma chamber within which a plasma environment similar to the destined orbits is generated.

A space plasma chamber was built first in Korea within Satellite Technology Research Center (SaTReC), Korea Advanced Institute of Science and Technology (KAIST) for the purpose of calibration of plasma instruments and laboratory experiments to the various phenomena of the space plasma. To generate a stable plasma in a large vacuum chamber filled with nitrogen gas, a back-diffusion-

type plasma source was devised and installed in the door side of the vacuum chamber. A disk-type Langmuir probe was utilized to check the generation and characteristics of the plasma inside the chamber.

In this paper, the physical conditions of the generated plasma measured by the Langmuir probe are introduced and possible applications of the plasma chamber are discussed.

A schematic diagram of the plasma chamber and the plasma source is shown in Fig. SC-C-12. A vacuum chamber with a diameter of ~1.5 m equipped with a turbo pump was utilized in the experiments. Pure nitrogen gas is supplied into the chamber through the digital flow controller. The back-diffusion-type plasma source consists of cathode filaments at the front, a grid anode near the filaments, and a plate anode at the rear side.

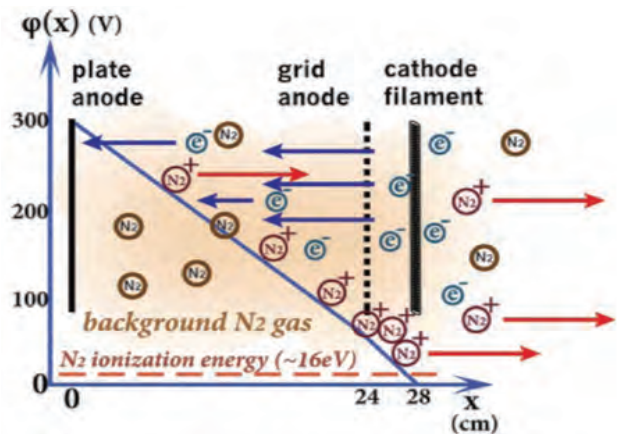


Fig. SC-C-12. Schematic drawing of the space plasma chamber and plasma source.

It was demonstrated that typical ionospheric conditions suggested in the literature can be reproduced in the plasma chamber by adjusting the electrode voltages of the back-diffusion-type plasma source.

It is important to investigate how space instruments behave under various plasma conditions. It is expected that the space plasma chamber can be used in various sounding rocket and satellite missions in the future.

In terms of space technology, the plasma chamber can be utilized in experiments on spacecraft charging and discharge, which are critical especially in the outer radiation belt where a geosynchronous orbit is passing through.

SC-D

Space Plasma in the Solar System, Including Planetary Magnetosphere

The Chromospheric Instrument Development Plans

Toward Next Generation Coronagraph: DICE, BITSE, and CODEX

Solar wind researches based on new space missions

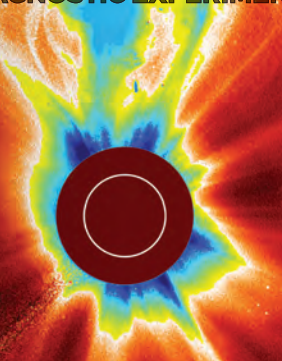
SNIFE Mission for Space Weather Research

Korean Space Environment Monitor (KSEM) on GK-2A



NEXT GENERATION SOLAR CORONAGRAPH

CORONAL DIAGNOSTIC EXPERIMENT



2017
DICE



2018-2019
BITSE



2020-2023
CODEX

KASI 한국천문연구원 <http://kswrc.kasi.re.kr/snipe>

Microbursts

ELECTRON MICROBURSTS

Plasmapause, Polar-cap patches, Plasmasphere, Plasma trough, Plasmapause, Plasmasphere

PLASMA TROUGHS AND POLAR-CAP PATCHES

Equatorial Plasma Bubbles

EQUATORIAL PLASMA BUBBLES / BLOBS / MSTIDS

Field-aligned currents, Pedersen currents, Pedersen currents, Hall currents

FIELD-ALIGNED CURRENTS

SNIFE

SMALL SCALE MAGNETOSPHERIC AND IONOSPHERIC PLASMA EXPERIMENTS

자기권/전리권 소규모 플라즈마 현상 관측을 위한 4기 나노위성군 (2020년 발사 예정)

The Chromospheric Instrument Development Plans

Heesu Yang and Juhyung Kang, Korea Astronomy and Space Science Institute

Dong-uk Song, National Astronomical Observatory of Japan, Japan

Kwangsu Ahn, Big Bear Solar Observatory, California, US

Introduction

Studying the solar chromosphere is important to understand the generation, transmission, and the release of the energy from the inner sun to outer space. The energy in the chromosphere is usually transferred by the waves or magnetic activities, and the energy is released and heat the plasma by magnetic reconnection. These solar activities are observed as Doppler shift or the brightening of the chromospheric atomic lines.

Therefore, it is necessary to capture the emission or the absorption of the spectral lines. The chromospheric activities can be observed by various instruments such as filtergrams, spectrograph, and spectropolarimeter.

On-Going Instrument Development for Chromospheric Observations

The Korean solar physics community has successfully finished several solar projects; the Solar Flare Telescope (SOFT) installed in Mt. Bohyun, the Fast Imaging Solar Spectrograph (FISS) in Big Bear Solar Observatory (BBSO), and the Korean Data Center (KDC) for the SDO at Korea Astronomy and Space Science Institute (KASI).



Fig. SC-D-1. (Current) Super-Eye schematic drawings

Currently, KASI is developing a 30 cm H α solar telescope for extremely harsh environments such as the polar base or space titled the Super-Eye Bridge . The primary purpose of the project is to advance the technology.

The Super-Eye team has been trying to improve the technology on the off-axis mirror design and manufacturing, low-order adaptive optics, the SiC mirror polishing aimed to use in space, and the mechanical design for extreme environments such as space or Antarctica. The Super-Eye is expected to be built and tested in 2021 (Fig. SC-D-1).

Plans of South Korea

Our community has conducted important studies on the chromosphere using the high-resolution observations and the solar chromospheric seismology.

We take the experience of developing the FISS as a foothold to set up missions for Wide-field Spectro-Imaging Solar Telescope, Post Solar Flare Telescope (PSOFT) and the Antarctica Solar Telescope (AST).

We plan to coordinate the missions with instruments which have related optical designs to expand the chromospheric research. The planned major projects in our community are as follows; 1) the high-spatial-resolution imaging spectrograph, 2) the meso-spatial resolution spectro-imaging telescope, and 3) Spectro-imaging solar telescope in space.

High-spatial resolution imaging spectrograph

We have collaborated with BBSO for over decades. The 1.6-meter Goode Solar Telescope (GST) at BBSO was once the world's largest solar telescope. Although the Daniel K. Inouye Solar Telescope (DKIST) now holds that record, the GST is still large enough to study the fine-scale objectives on the Sun.

In the near future, we will expand our research by upgrading the FISS. We have upgraded operating software

to increase the observing degree of freedom and to shorten the data cadence.

We have a plan to enhance the FISS to have a sharper image resolution by reconstructing the spectral data using the high-speed slit-jaw images in collaboration with the Max Plank Institute in 2021.

We also plan to add one or two more cameras in the FISS to study the chromospheric seismology of the multi-layer solar atmosphere. With these upgrades, three or four layers of the strong lines in the visible (VIS) and the near-infrared (NIR) can be observed simultaneously.

Table SC-D-1 shows the strong chromospheric lines in the VIS and NIR wavelength ranges that can be chosen for FISS. The table also includes a few near ultraviolet (NUV) lines in the solar low atmosphere.

Table SC-D-1. Solar low atmosphere spectral lines.

Spectral line [nm]	$1.22 \lambda/D$ [arc](D=30cm)	Formation height [km]
Si III 120.7	0.1	Close to TR [1]
He II 30.4	0.02	TR, 3300 [6]
Ly α 121.6	0.10	TR [1]
Mg II k 279.6	0.23	1300 [1]
Ca II K 393.3	0.33	1000 [1]
H β 486.1	0.4	1500, 1200 [5]
Fe I 543.4	0.46	400-650 [4], 280 [2]
Na D 589.0	0.49	200-600 [3], 684 [2]
H α 656.3	0.55	1500 [1]
Ca II 854.2	0.72	500 [3]
He 1083	0.91	2000 [7]

In the future, we can develop Integral Field Spectrograph (IFS) using an image slicer or a micro-lenslet to obtain the supra-spatial-temporal resolution data. This instrument will be beneficial to study the oscillations and variations in a period shorter than a few seconds. The micro-lenslet based IFS had been developed and used in the 2019 total solar eclipse by the KASI team.

Meso-spatial resolution spectro-imaging solar telescope

As the Sun being an extended and high flux light source, high-resolution imaging and spectroscopy are exclusive advantages. On top of them, polarimetry with high spatial and high sensitivity becomes a must-have in new instruments, because it deduces a lot of physical properties of local solar activities, either in active regions or quiet Sun.

The newer instrumentations are competitively seeking cutting-edge capability to grasp every detail of the Sun by

adopting new large telescopes. While this is definitely a new area to reach to answer some key questions about the Sun - the mechanism of coronal heating, fundamental magnetic flux size, or spatial frequency of magnetic reconnection - there is still room for new science by using a unique combination of the instruments with moderate specifications.

Thus, adding spectro-imaging polarimetric capability to mid-grade instruments can expand possibilities of new scientific findings. Building a seamless stratified atmospheric structure by using multiple instruments is a plus if a new instrument can fill any gaps in the capabilities of existing telescopes and instruments.

We still have a very limited supply of polarimetry of non-photospheric spectral lines, such as He I 1083 nm and Ca II 854.2 nm. Even with all these combined, if there is any need to fill more gaps for unknown physical properties or extend the capability limit of an instrument, newer techniques like deep learning could be a help.

KASI designs the PSOFT which is a 30 cm auto-observing solar telescope with an echelle spectrograph and adaptive optics. It will take over the optical layout of the Super-Eye and the FISS.

The FISS takes in the light to the slit using a linear motor to obtain the spectral information of the 2D imaging plane. However, the PSOFT uses a tip-tilt mirror for both the low-order atmospheric turbulence compensation and the scanning. This technique is challenging, but it can efficiently reduce the optical components.

To observe the Sun continuously without gaps, three telescopes will be installed in Korea, USA, and Europe, consequently. The PSOFT is selected as one of the main projects in KASI for the next seven years.

The PSOFT can take not only the intensity information, but also the polarimetry information by adding a polarization component in the beam path. The calibrating the polarization of the small telescopes is (relatively), which is easy by maximizing their geometrical symmetry. The PSOFT can measure the photospheric magnetic field from the Zeeman splitting. It might be possible that the PSOFT measures the chromospheric magnetic field by the Hanle effect of the ion lines. The Hanle effect is generated by the polarization reduction of the light by the magnetic field.

The photospheric or chromospheric spectral bands should be carefully selected after estimating the flux and noise capability. It is important to note that we have experiences in development of the polarimeter by participating in the NIRIS of the GST and the CLASP rocket mission.

The AST is in the process of designing a related concept with the PSOFT that will be set up with a larger aperture in a harsh environment. It is considered that the AST would play a role in one of the main instrumentations in the Korean Antarctic inland base camp, which is developed by the Korea Polar Research Institute (KOPRI) at Dome-C.

If the AST is built successfully, we can continuously receive solar chromospheric observation data for 24 hours in a few weeks for a year. The AST is now under evaluation of its feasibility. In this case, temperature control is critical among the factors such as optical lenses or cameras.

Table SC-D-2 lists the specification of the AST, PSOFT, and FISS. The main data output of the PSOFT and the AST is meso-spatial resolution (1 arcsec), high spectral resolution, high temporal cadence, and longer time-coverage spectral imaging data in the low solar atmospheric lines, such as H α , Ca II 854.2 nm, Na D I, etc.

Table SC-D-2. Specification of the AST, PSOFT, and FISS.

	AST	PSOFT	FISS
Aperture	40-50cm	30cm	1.6m
F/#	>10	>10	22
Resolving Power	200,000	200,000	140,000
Wv Coverage	1nm (multi-slit)	1nm (multi-slit)	0.8nm
Target	H α , Ca II, He II, etc	H α , Ca II, etc	H α , Ca II, Na D I, etc
Spatial-resolution	<1 asc	~1 asc	~0.3 asc
Adaptive Optics	Tip-tilt + Deformable Mirror	Tip-tilt	
Scanning Method	Tip-tilt mirror	Tip-tilt mirror	Linear Motor
Time cadence	11sec (multi slit)	11sec (multi slit)	16sec
# of Telescope	1 (Antarctica)	3 (Korea, BBSO, Europe)	1
FOV	450 by 450	900 by 900	40 by 16
Observing days per year	~30 days	365 days	21 days
Observing period	24 hours	~24 hours	6 hours
Camera	sCMOS	sCMOS	EMCCD

Though these high-spectral resolution data on the low atmospheric lines have been obtained through CRISP/SST, IMAX/SUNRISE, and FISS/BBSO, they are restricted to a tiny field-of-view and irregular observing cadence. The data expected from the PSOFT and AST is unique in that sense.

The data can be used not only in statistical studies on the chromospheric magnetic reconnection and the jets, but also in the space weather forecast because of its continuous observation.

We can make our own large aperture size telescope. We have to consider overseas sites because Korea's environment is too humid and turbulent for a telescope to be built into.

The Antarctic inland base mentioned above is attractive site for a large telescope. Accessing the site might be difficult, but it seems that the site would be proper to observe the Sun with stable atmospheric conditions. Therefore, a meter-class telescope may be installed in the base.

If it is successfully built, we can consider to install not only the imaging-spectrograph of VIS or NIR waveband, but also the imaging-spectropolarimetry of mid-infrared (MIR) waveband, which have not been explored as much on the ground due to the water vapor absorptions

Spectro-imaging solar telescope in Space

In the near future, we can install the imaging spectrograph in space. In this case, the technology developed by the Super-Eye project, such as light-weight SiC mirrors, or extreme environment compatible designs and controls, can be used.

The NUV wavelength range such as Si III 120.7, Ly α 121.6, or He II 30.4, is a beneficial complement to study the multi-layer Sun in collaboration with the ground-based observatories (See Table SC-D-1). The NUV range also has an advantage of its spatial resolution.

If circumstances allow, a relatively large aperture mirror could be considered. Because of its nature of high spatial resolution, getting more details of photospheric and chromospheric bands is still a strong advantage.

The imaging-spectropolarimeter is very competitive as seeing-free imaging under minimal noise. It will expand signal-to-noise ratio of chromospheric magnetic structures observed in the He 1083 nm and Ca II 854.2 nm lines. While stable long-term observation is realized in space, this spacecraft could serve as a powerful tool for monitoring active local events such as flares.

The satellite can be launched on the Sun-Earth L4 or L5 Lagrangian point. The L4 or L5 is a unique advantageous location for understanding not only the space weather forecast such as the CME propagations or solar wind variations, but also the 3-dimensional structures of the chromosphere.

References

- [1] J.E.Vernazza et al., Structure of the Solar Chromosphere. III. Models of the EUV Brightness Components of the Quiet Sun, *ApJ*, 45, 635
- [2] J., Chae, et al., Photospheric Origin of Three-minute Oscillations in a Sunspot, *ApJ*, 836, 18, 8
- [3] H. Utenbrock, Chromospheric Diagnostics, ASPCS, Vol 354, 2006
- [4] N. Bello Gonzalez et al., Acoustic Waves in the solar Atmosphere at High Spatial Resolution, *A&A*, 522, A31
- [5] Zhong-Quan Qui and Zhi Xu, Key Properties of Solar Chromospheric Line Formation Process, *CJAA*, Vol 2, 70
- [6] C.E. Alissandrakis, Measurement of the Height of the Chromospheric Network Emission from Solar Dynamics Observatory images, *Solphys*, 294, 11
- [7] E.H. Avrett, Formation of the Solar He 10830Å Line, *IAUS*, 154, 35

Toward Next Generation Coronagraph: DICE, BITSE, and CODEX

*Kyungsuk Cho, Yeon-Han Kim, and Seonghwan Choi, Korea Astronomy and Space Science Institute
Nat. Gopalswamy and Jeff Newmark, NASA/GSFC*

Introduction

The Sun is extremely dynamic and continuously influences the Earth. It has been known that energetic coronal mass ejections (CMEs) can cause disruption to communications, malfunctions of a navigation system, and radiation hazards to humans. So far, previous coronagraphs (e.g., Large Angle and Spectrometric Coronagraph: LASCO) have contributed to increasing our knowledge about solar corona by measuring only the electron density.

The missions toward the Next Generation Coronagraph (NGC) including Balloon-borne Investigation of the Temperature and Speed of Electrons in the Corona (BITSE) and Coronal Diagnostic Experiment (CODEX) are NASA-KASI joint collaborations funded by KASI and NASA. The missions are designed to archive a comprehensive data set to answer the question: what are the sources and acceleration mechanisms of the solar wind? In this overall project, NASA designs, builds, and qualifies the optical and mechanical assemblies of the coronagraph and provides engineering facilities and services as needed. KASI develops filter wheel, filters, main electronics, camera, and ground and ground/flight software (Cho et al. [1]).

DICE: Diagnostic Coronagraph Experiment

KASI coronagraph team built the eclipse observation system, DICE, for the total solar eclipse on August 21, 2017. The team observed the solar corona using the system at a site near Jackson Hole, Wyoming.

They obtained polarization data at four different wavelengths (393.9 and 402.5 nm for temperature, and 399.0 and 424.9 nm for speed) during the limited total eclipse time of about 140 seconds. KASI team successfully demonstrated the measurement technology. The team determined temperature distributions in the eastern limb and northern polar region, and found that temperatures are higher at the streamer and lower at the boundaries between the streamer and the coronal holes.

Since hot spots in the northern coronal hole were identified, the team is investigating the spots in detail to study their relationships with jets and flows in polar plumes. More detailed descriptions of the DICE instrument and observation can be found in Cho et al. [2].



Fig. SC-D-2. KASI team and instruments for 2017 eclipse expedition in Wyoming, USA.

BITSE: Balloon-borne Investigation of the Temperature and Speed of Electrons in the Corona

KASI and NASA joint team had developed BITSE for a scientific balloon experiment. BITSE is the first coronagraph observing from a stratospheric balloon at the blue end of the solar spectrum. Two minutes of observation of the total solar eclipse was extended more than 4 hours through the high-altitude experiment.

On 2019 September 18 (08:50 AM, MDT), BITSE was launched from Fort Sumner, New Mexico. It reached around 40 km in altitude after about 2.5 hours flight by the 39 million cubic feet balloon. BITSE observed the Sun for about five hours and landed at a location near Farmington, New Mexico. BITSE obtained about 4200 images in each bandpass filter.

Fig. SC-D-3 shows BITSE integrated to the gondola and the Wallops Arc Second Pointing (WASP) system at NASA's Wallops Flight Facility (WFF).

Two critical technologies of polarization camera and filters were demonstrated through the BITSE experiment. The polarization camera has uniqueness because it can directly collect polarized light without any extra mechanism. The traditional detector adopts rotating polarization wheels.

The second key component is the narrowband filters that block all wavelengths of visible light except for those in four spectral bands (393.5 and 405.0 nm for temperature, and 398.7 and 423.4 nm for speed) in the violet range.

BITSE demonstrated the technologies and obtain spectral polarization brightness images to determine the temperature, speed, and density in the corona. Through the BITSE, NASA-KASI coronagraph team achieved TRL 6 or higher in all technologies for NGC. Goplaswamy et al. [3] describe more details of the mission and report observational results.



Fig. SC-D-3. BITSE integration, launch, and observation at NASA's WFF.

CODEX: Coronal Diagnostic Experiment

The duration of the balloon mission was too short, and the background sky was still too bright to obtain all the data needed for achieving the scientific objectives.

The next step is to fly in space by utilizing the new coronagraph technology demonstrated by BITSE. By using the ISS platform and Azimuth/Elevation (Az/EI) Telescope Gimbal Mount, KASI-NASA coronagraph team is developing the next generation coronagraph on ISS, CODEX.

CODEX utilizes existing ISS infrastructure because ISS is a cost-effective platform for the new coronagraph. CODEX system consists of the coronagraph part and other components such as pointing system. Main parts of CODEX are aperture door, external occulter, straylight baffles, heat rejection mirror, filter wheel, polarization camera, and control electronics.

Fig. SC-D-4 presents mission phases and critical activities of CODEX from pre-launch to the end of the mission. It is expected to be launched in February 2023 and installed onto zenith-pointing location on ISS.

CODEX shall produce more than 1000 density images with less than 1-minute cadence per day, 16 temperature images per day. Images may be further averaged over more orbits for higher signal-to-noise ratio.

We are expecting that NGC will conduct simultaneous detection of electron density, temperature, and speed in the corona from 2023.

Conclusion and prospects

The BITSE KASI and NASA team formed a nucleus for the CODEX mission. NASA-KASI heliophysics working group is archiving their goals toward the NGC.

Flying CODEX on ISS serves as a pathfinder for an improved instrument to fly on the Lunar Orbiter Platform-Gateway or Earth-Sun L4 Space Weather mission as a future mission

References

- [1] K. S. Cho et al., Journal of Korean Astronomical Society 50, 139 (2017).
- [2] K.-S. Cho et al., Journal of Korean Astronomical Society 53, 87 (2020).
- [3] N. Gopalswamy et al., The Balloon-borne Investigation of Temperature and Speed of Electrons in the corona (BITSE): Mission description and preliminary results, Solar Physics 296, 15 (2021).

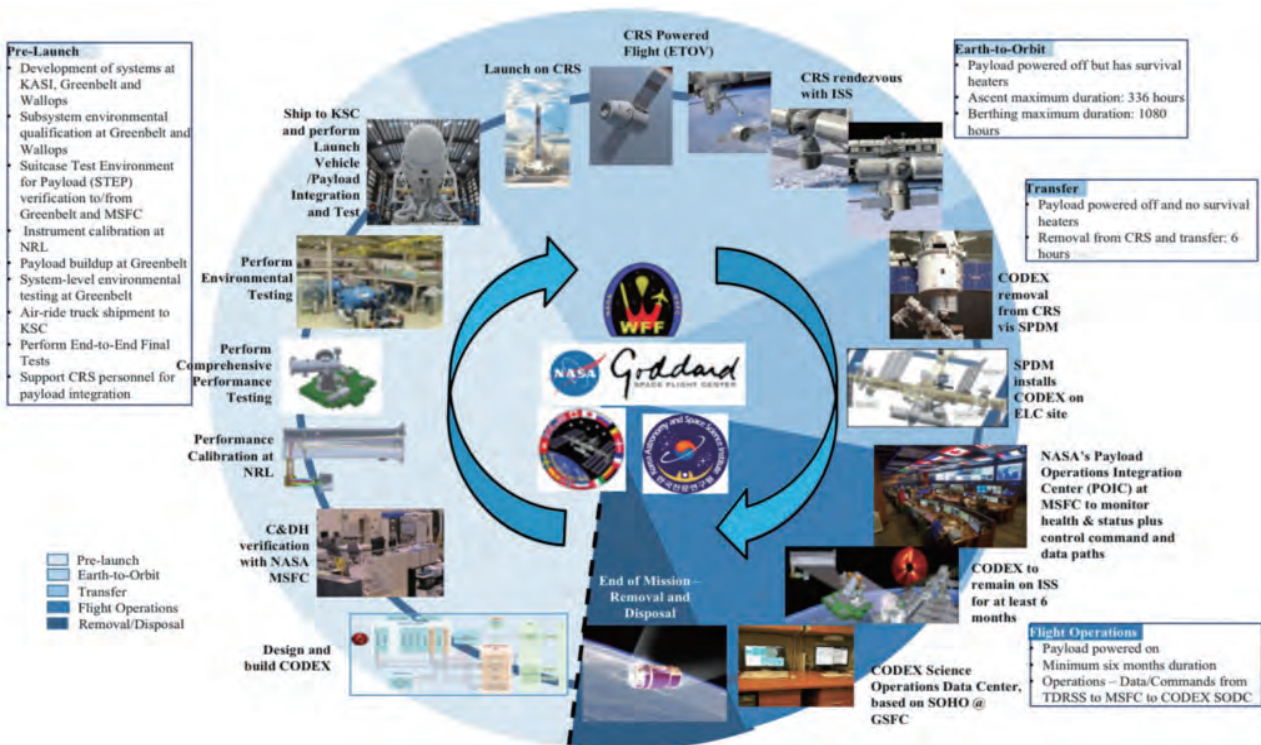


Fig. SC-D-4. CODEX mission phase and key activities, follows standard mission development and ISS practices.

Solar wind researches based on new space missions

Jungjoon Seough, Korea Astronomy and Space Science Institute

Peter H. Yoon, University of Maryland at College Park; Kyung Hee University

Introduction

The interplanetary medium is pervaded by the solar wind, a flow of magnetized plasma expanding supersonically from the upper atmosphere of the Sun.

In situ measurements of the inner heliosphere offer the best opportunity to study the fundamentals of plasma physics in that it allows us to test a viable theory of kinetic descriptions with the aid of simultaneous measurements of the particle distributions and electromagnetic fluctuations. In view of the currently operating inner heliosphere missions, NASA's Parker Solar Probe (PSP) and ESA's Solar Orbiter (SO) [1-2], it is timely to discuss the current status of solar wind research.

In this report, we will focus on a topic of fundamental importance for both kinetic and thermodynamic processes within the context of the expanding solar wind plasmas.

What controls the physical processes of the expanding solar wind?

Since the speed of the super-Alfvénic solar wind practically reaches a maximum constant value beyond a few tens of solar radii, a typical example of physical quantities describing the thermodynamic evolution of the solar wind might be the temperature of plasmas and their anisotropy.

Measurements in situ of solar wind proton temperature anisotropy have revealed that the adiabatic moments of the magnetized plasmas deviate significantly from the prediction of the double-adiabatic theory, implying that there may be other physical processes essentially acting on the expanding solar wind.

It is commonly believed that the thermodynamic property of the solar wind evolution results from a combination of physical processes, including the double-adiabatic expansion, the magnetic configuration, such as Parker spiral interplanetary magnetic field, Coulomb collisions,

turbulent heating, and kinetic plasma instabilities. Those are the intrinsically multi-scale physical processes that are simultaneously coupled to each other, resulting in a significant contribution to the overall energetics of the expanding solar wind through interplanetary space [3].

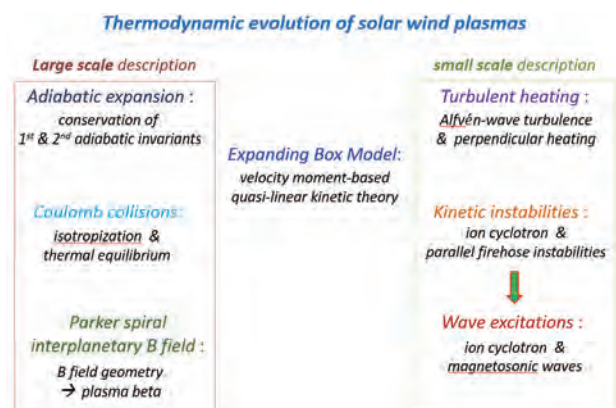


Fig. SC-D-5. A schematic diagram for the Expanding Box Model based on quasilinear kinetic theory. It includes various physical processes responsible for thermodynamic evolution of solar wind.

Recently, we try to address the fundamental question of how the intricate multi-scale coupling between global dynamics and local kinetic processes affects the thermodynamic properties of the solar wind. We therefore have been developing an Expanding Box Model (EBM) based upon quasilinear kinetic analysis that includes the above mentioned physical process (Fig. SC-D-5).

By incorporating the local kinetic processes, such as the heating by Alfvén-wave turbulence and micro-instabilities, into the large-scale description, we could describe how the solar wind temperature anisotropy evolves in interplanetary space and discuss the importance of the multi-scale nature of the solar wind.

Here, we report the recent progresses—not only observational results by the Parker Solar Probe but also theoretical efforts toward understanding observational features.

A role of Alfvén-wave turbulence: Heating of plasma

One of the interesting findings of the PSP's first perihelion encounter, is that the equatorial coronal hole can be a source of slow solar wind (SSW) [4]. These SSW contains Alfvénic fluctuations which could be the energy source of coronal heating and wind acceleration through the turbulent interaction between small-scale fluctuations and particles. In this regard, Alfvén wave energy cascades to the small scale near the local proton gyro-radius, eventually resulting in the cascade transitions to the Kinetic Alfvén Wave (KAW) [5].

The KAW is of great importance for the solar wind physics in that both the protons and electrons could be energized through the dissipations of KAWs. In this regard, the EBM of quasilinear analysis employs the analytic formulae of heating rates derived from the dissipation mechanisms of KAWs; 1) nonlinear stochastic heating for perpendicular proton heating and 2) Landau damping for both parallel proton and electron heating [5].

Numerous observation of ion-scale plasma waves in the innerheliosphere

The FIELDS instrument of the PSP has detected various plasma waves that may be driven by the micro-instabilities associated with the configuration of ion and electron velocity distribution functions [4].

It is interesting to note that the ion cyclotron waves, which are circularly polarized electromagnetic waves propagating quasi-parallel to the ambient magnetic field, are enhanced during the interval containing the Alfvénic fluctuations. This implies that the perpendicular proton heating by Alfvén-wave turbulence may result in by the excessive perpendicular proton temperature anisotropy, giving rise to the excitation of the kinetic ion cyclotron instability (Fig. SC-D-6).

The statistical study of ion scale wave measurements shows that these waves are frequently observed during the first perihelion encounter of the PSP [4].

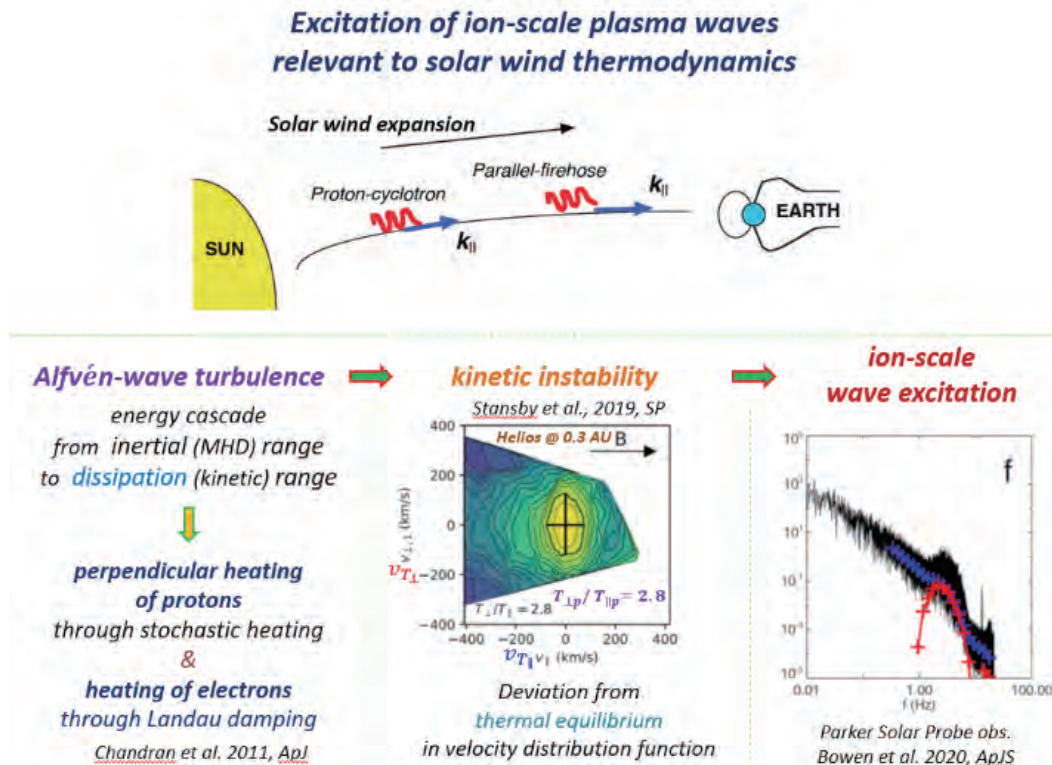


Fig. SC-D-6. A schematic processing for the excitation of the ion-scale waves relevant to thermodynamics of expanding solar wind.

A possible source of ion-scale waves: Kinetic instability driven by temperature anisotropy

Plasma kinetic instabilities could arise when the particle velocity distribution functions (VDFs) have non-thermal feature. In the solar wind, both protons and electrons frequently exhibit non-Maxwellian VDF such as temperature anisotropy and beams.

According to the particle measurements of the PSP, it turns out that the ion-scale waves are driven by the proton temperature anisotropy. Similarly, in situ measurements of the WIND spacecraft near 1 AU showed that the observed proton temperature anisotropy seems to be bounded by the marginal stability condition for anisotropy-driven instabilities, implying that the micro-instabilities may efficiently regulate the proton temperature anisotropy.

In the literature, linear Vlasov analysis has been frequently employed to examine the characteristics of kinetic instabilities, but it is not sufficient to understand physical processes, not only those like the excitation of ion-scale waves but also the evolution of those within the context of the expanding solar wind.

Example of theoretical results of EBM

Since there is no self-consistent theoretical model to consider both thermodynamics of protons and ion-scale wave, it is important to construct theoretical model that includes physical process responsible for the excitation of ion-scale plasma waves.

The EBM consists of the solver of linear kinetic dispersion relations and solves the self-consistent set of quasilinear kinetic equations for perpendicular and parallel temperature as well as the wave equation. Basically, the EBM contains various physical processes including the double-adiabatic expansion, the Parker spiral interplanetary magnetic field, Coulomb collisions, turbulent heating, and kinetic plasma instabilities.

Although we do not describe the details of EBM, it seems to nicely mimic the observational results during the first perihelion encounter of the PSP [5] (the vertical dotted lines for each panel in Fig. SC-D-7).

Here we assume the initial plasma parameters shown in the upper-left panel of Fig. SC-D-7 and the initial location of expanding solar wind as 20 solar radii. The upper-right panel shows the radial evolution of proton temperatures. It is shown that Alfvén-wave turbulence leads to the perpendicular proton heating. This increases the

proton temperature anisotropy, resulting in the excitation of ion cyclotron instability (Fig. SC-D-7).

The parallel proton temperature also increases due to the quasilinear relaxation of kinetic instability. The thermodynamic properties, such as proton temperatures and anisotropy, as well as the intensities of excited ion cyclotron waves seems to be within the observational range [5-6]. These theoretical results of EBM may help us to understand the observational features of not only the thermodynamic evolution of solar wind but also the wave excitation process.

Before we close, it should be noted that solar wind consists of multi-species, protons, electrons, and alpha particles. They also have different flow speeds that may give rise to the free-energy sources to excite small-scale plasma waves. For the future work, we shall consider that multiple sources of free energy may be important in understanding the multi-scale kinetic physics of solar wind.

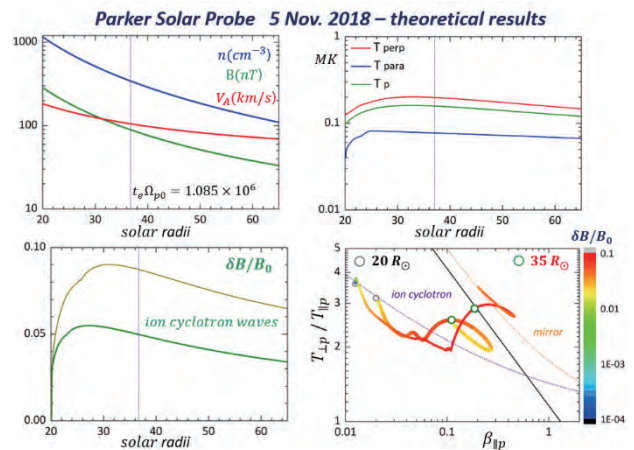


Fig. SC-D-7. Theoretical results of Expanding Box Model.

References

- [1] Fox N. J. et al., 2016, SSRv, 204, 7
- [2] Muller D. et al., 2013, Solar Physics, 258, 25
- [3] Verscharen D. et al., 2019, LRSP, 2019.
- [3] Bale S. D. et al., 2019, Nature, 576, 237
- [4] Chandran B. D. G. et al., 2011, ApJ, 743, 197
- [5] Bowen T. A. et al., 2020, ApJS, 246, 66
- [6] Huang J. et al., 2020, ApJS, 246, 70

SNIFE Mission for Space Weather Research

Jaejin Lee, Korea Astronomy and Space Science Institute

Introduction

Recent advances in small satellite technology are changing the scale of space missions opening up the possibility of using CubeSat-type platforms as a solution for low-cost constellation missions [Werner et al., 2018]. Particularly in the field of Astrophysics and Heliophysics, multi-point observation from CubeSat constellation has excellent potential to address many outstanding problems.

Small scale magNetospheric and Ionospheric Plasma Experiment (SNIFE) is a scientific mission consisting of four 6U CubeSats of ~ 10 kg under development by Korea Astronomy and Space Science Institute (KASI) for space weather research.

The observation of particles and waves causing space storms with a single satellite inherently suffers from space-time ambiguity. Recently, such ambiguity has often been resolved by multi-satellite observations such as CLUSTER, THEMIS, MMS, and SWARM missions; however, the inter-satellite distances of these satellites were generally vast (> 100 km).

The goal of the SNIFE mission is to measure the spatial and temporal variations of the micro-scale plasma structures on the topside ionosphere. For example, polar cap patches, field-aligned currents (FAC), radiation belt microbursts, and equatorial and mid-latitude plasma blobs and bubbles are the main observation targets of the SNIFE mission.

Scientific Instruments

Each SNIFE CubeSat carries the same scientific payloads, a Langmuir probe, a magnetometer, and a solid-state telescope (SST), which are the heritage from STSAT-1 [Lee et al., 2012].

The Langmuir probes are the instruments measuring ionospheric plasma densities and temperatures. The Langmuir probe produces electron density data every 0.1 s, and electron temperature every 1 s. Because the satellites move with supersonic speed, the spacecraft body generates different plasma environments in the backside track (wake). To reduce the effects caused by the wake, the probes are placed on the backside of the solar panel and deployed in orbit.

The SST consists of two Passivated Implanted Planar Silicon (PIPS) detectors whose active area is 50 mm^2 . The detectors measure the energetic electron flux of 100-400 keV with the 16 energy channels. Two collimators identify the incident direction of particles: one is perpendicular and the other is parallel to the geomagnetic field. In order to observe small scale electron precipitation phenomena on polar region, the SST has fast time resolution: 10 ms for burst mode and 100 ms for survey mode with the dead time of 10 μsec .

The flux gate magnetometers are aboard the SNIFE to measure the vector geomagnetic field in the range of $-60,000 - + 60,000$ nT with the 24-bit AD converter in fre-



Fig. SC-D-8. Mission Concept and Formation Flying of SNIFE

quency range of DC - 10 Hz.

The magnetic field data is used to identify field-aligned current variation associated with crossings of the auroral oval and transient current loops. To cancel the internal noise caused by electric currents in the bus system, two tri-axial sensors are installed. The noise level of the magnetometer is 30 pT/VHz at 1 Hz.

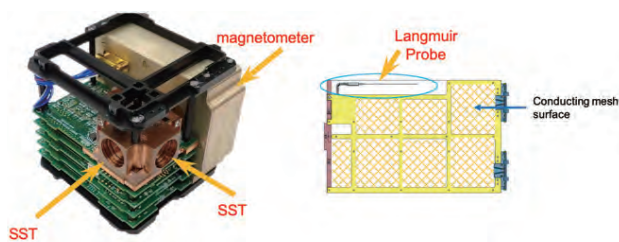


Fig. SC-D-9. Images of scientific instruments

Spacecraft

The SNIPE's 6U CubeSats have been developed with the cooperation of KASI and KARI (Korea Aerospace Research Institute). The spacecraft has two deployable solar panels and four body-mounted panels to produce electric power more than 44W. SNIPE is a 3-axis stabilized spacecraft consisting of three reaction wheels, magnetorquers, sun sensors, star trackers, MEMS Gyros, and magnetometers to achieve the capability of attitude control of the accuracy of less than 1 arc-degree.

The on-board computer utilizes the core Flight Software (cFS) and handles the command and data in addition to the guidance, navigation, and control processing with a high-speed micro dual processor.

The communication subsystem is a critical part of deciding CubeSat's success. For the low-speed but effective communication, UHF, and for the high-speed data download (~2Mbps), S-band uplink/downlink RF modules are installed on the bus system. In addition, the IRIDIUM communication module would make possible the real-time housekeeping data monitoring in addition to providing an opportunity to upload changes in operational modes when geomagnetic storms occur.

In the SNIPE mission, the key technology is the demonstration of formation flying. For the orbit maneuver, each spacecraft has a cold gas thruster that produces the total thrust of Δv 50 m/sec.

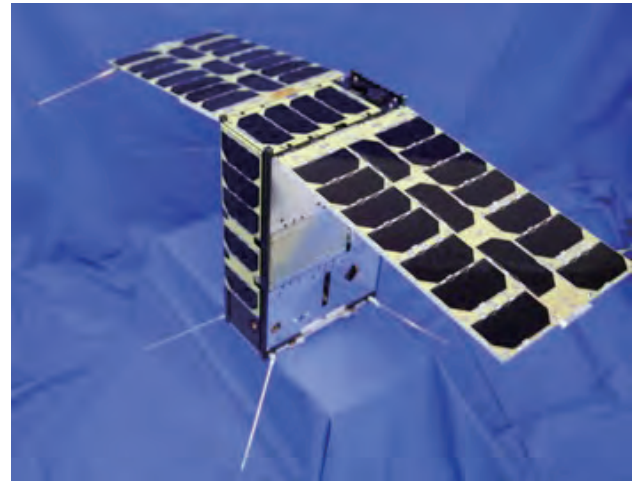


Fig. SC-D-10. Integrated SNIPE mission (Engineering and Qualification model)

Current Status

Work on SNIPE began in January 2017. Phase A (System Design) was completed by October 2017, Phase B (Critical Design) by November 2019. The mission is currently in Phase C (Integration), awaiting launch from Baikonur on a Russian Soyuz-2 rocket as a secondary payload to the primary Korean Compact Advanced Satellite (CAS500-2) mission. The SNIPE will be launched during the third (Q3) or fourth quarter (Q4) of CY 2021.

References

- [1] N. Werner et al., CAMELOT: Cubesats Applied for MEasuring and LOCALising Transients mission overview, 2018, in Space Telescopes and Instrumentation 2018: UI-traviolet to Gamma Ray, vol. 10699 of Society of Photo-Optical Instrumentation Engineers (SPIE) Conference Series, page 106992P.
- [2] J.J. Lee et al., Anisotropic pitch angle distribution of ~100 keV microburst electrons in the loss cone: measurements from STSAT-1, 2012, Annales Geophysicae 30, 1567.

Korean Space Environment Monitor (KSEM) on GK2A

EunSang Lee, Kyung Hee University

Introduction

The Korean space environment monitor (KSEM) is a suite of instruments to monitor space weather in the geostationary orbit onboard the Korean geosynchronous satellite Geo-KOMPSAT-2A (GK2A) (Fig. SC-D-11).

The primary mission of GK2A is to monitor the weather conditions over the Korean peninsula from the geostationary orbit. As the secondary mission it monitors space weather at the geostationary orbit, which provides important information for the safe operation of satellites around geostationary orbit. GK2A was successfully launched on 4 December 2018 and finally located at the longitude of 128.2° East.

KSEM consists of three Particle Detectors (PDs), a Charging Monitor (CM), and a set of magnetometers (SOSMAG). It has been developed by the group led by Prof. J. Seon at Kyung Hee University in collaboration with the Space Sciences Laboratory at UC Berkeley, Satrec Initiative Co., and ESTEC of European Space Agency.

Fig. SC-D-12 shows an example of the measurement of differential fluxes by the PD instrument on 11 May 2019. The Dst index for the day was in the range of $-21 < \text{Dst} < -51$ nT, which indicates that the magnetosphere was moderately disturbed.

The differential flux of energetic electrons with the energies above ~ 800 keV significantly increased after ~ 1400 UT for all PDs, which suggests the enhanced fluxes are almost isotropic.



Fig. SC-D-11. The GK2A satellite at the launch site showing the KSEM suite.

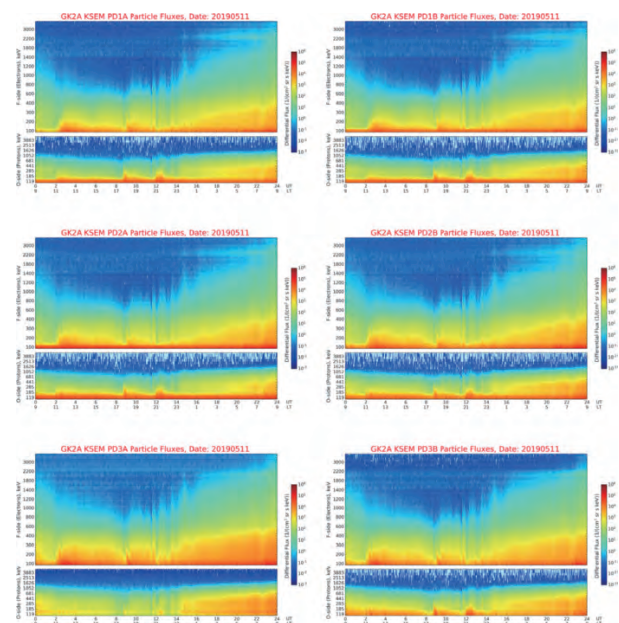


Fig. SC-D-12. Measurement of differential fluxes by the PD instrument on 11 May 2019.

Charging Monitor (CM)

The CM is a simple detector to measure an internal charging current caused by the penetration of energetic particles. It consists of an aluminum plate with the thickness of 1 mm and the diameter of 65 mm, which is covered by another 1-mm-thick aluminum plate. The cover plate can shield the electrons and ions with energies below ~ 0.6 MeV and ~ 13.8 MeV, respectively.

CM can measure the current density in the range of -3 – 3 pA/cm². Fig. SC-D-13 shows an example of the measurement by CM. The integral flux of the electrons with energies from 0.6 to 2 MeV measured by PD3 is also plotted for comparison. It shows that the charging current increases when the integral flux of electrons increases.

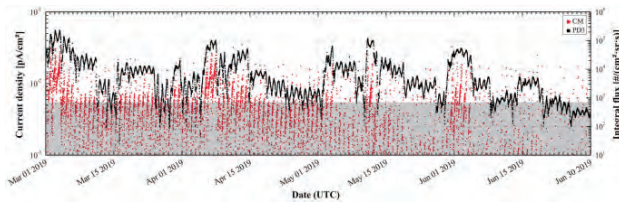


Fig. SC-D-13. Charging current density (red) measured by CM and the integral flux of the electrons in the energy range of 0.6 – 2 MeV measured by PD3 from 1 March 2019 to 30 June 2019. (From Woo et al. (2020)[1].)

Particle Detector (PD)

The PD instrument measures the fluxes of energetic electrons and ions in the geosynchronous orbit. It measures electrons with energies from ~ 100 keV to ~ 3.8 MeV by 48 energy channels and ions with energies from ~ 150 keV to ~ 2.2 MeV by 22 channels.

The energy resolution is much narrower than the previous and currently operating particle detectors in the other geosynchronous satellites. The PD instrument consists of three PD sensors looking at 6 directions (Fig. SC-D-14).

Each PD has two telescopes configured back-to-back (Fig. SC-D-15). The telescope uses foils and magnets to separate ions and electrons. The field of view of the telescope is 20° by 20°

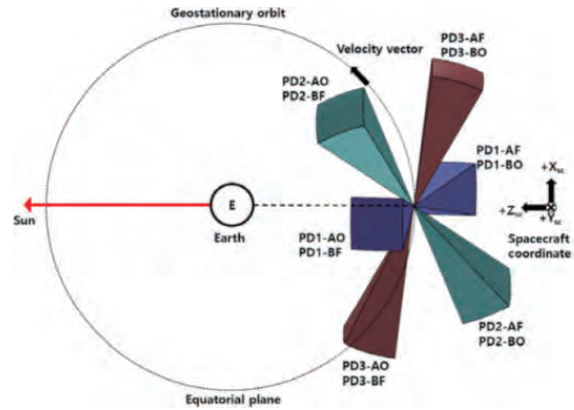


Fig. SC-D-14. Illustration of field of view of the PD instrument (From Fig. 4 of Seon et al. (2020)[2].)

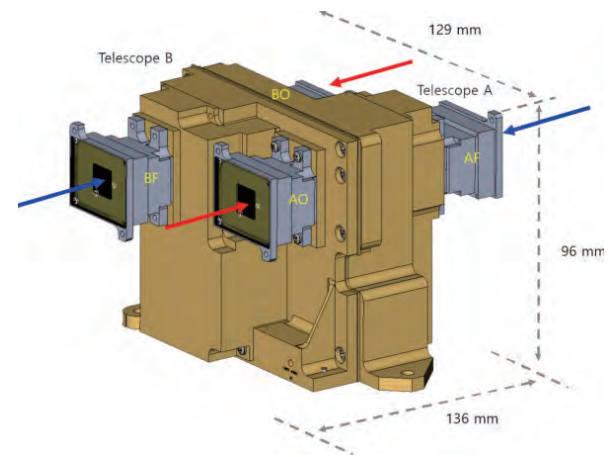


Fig. SC-D-15. Configuration and dimensions of PD (From Fig. 2 of Seon et al. (2020)[2].)

Set of Magnetometers (SOSMAG)

During the operation of a satellite, magnetic disturbances are generated and the measurement of the natural magnetic field needs a magnetic cleanliness program for the satellite. SOSMAG is a magnetometer designed to discriminate the magnetic disturbances by a satellite from the natural magnetic field using a set of magnetometers located at different positions [3].

SOSMAG consists of two fluxgate magnetometers mounted on a boom and two anisotropic magnetoresistive (AMR) magnetometers on the satellite body. Fig. SC-D-16 shows the configuration of SOSMAG.

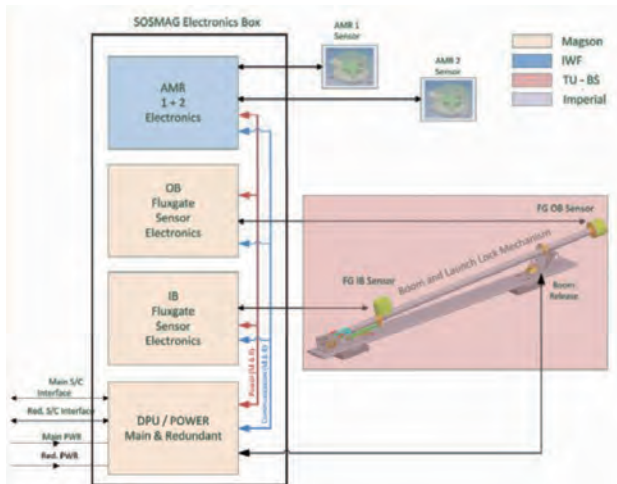


Fig. SC-D-16. The configuration of SOSMAG. From Fig. 1 of Auster et al. (2016)[3].

Fig. SC-D-17 shows an example of the measurement by SOSMAG from 5 May 2019 to 7 June 2019. The measurement from GOES-15 is also plotted for comparison. The longitudinal difference of the locations of GK2A and GOES-15 is reflected in the difference in the He and Hn components.

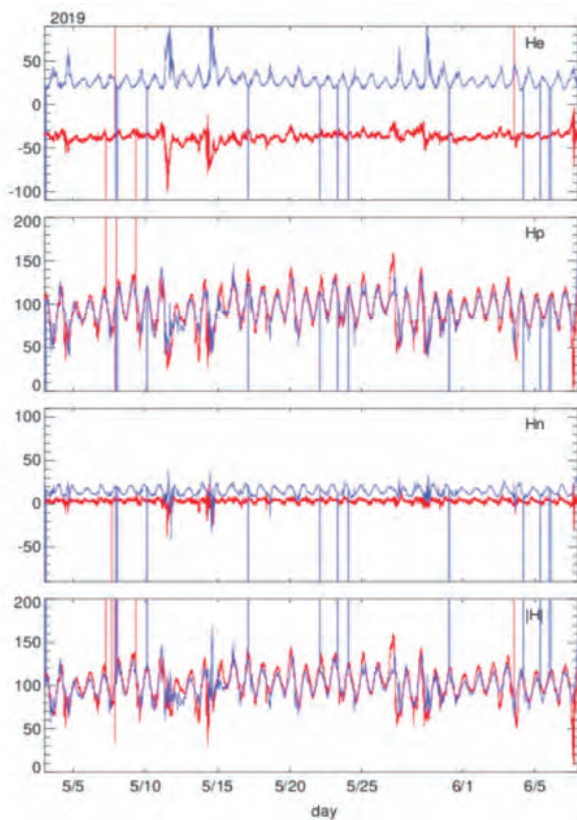
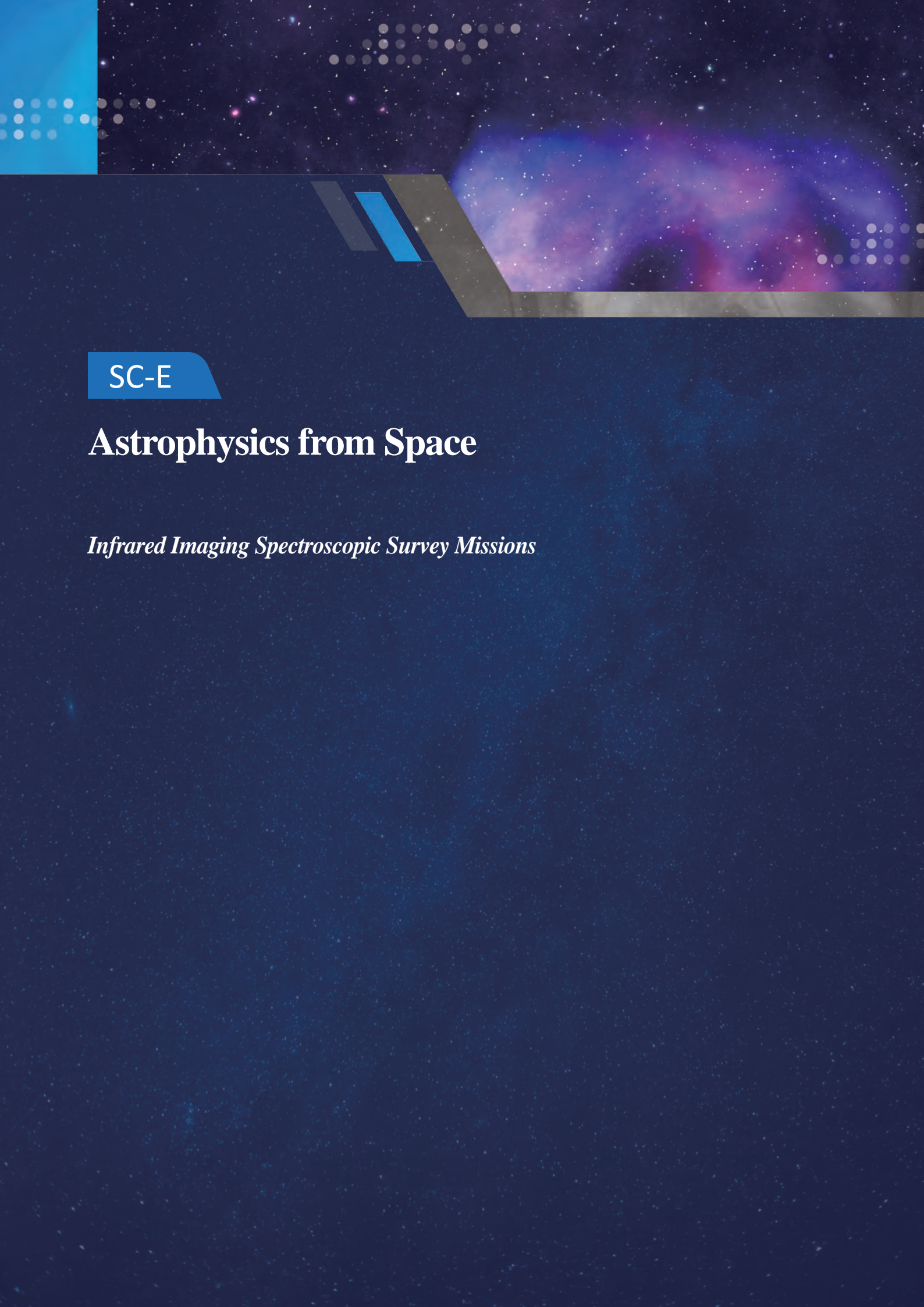


Fig. SC-D-17. Measurements of magnetic field by SOSMAG (red) and GOES-15 (blue) from 3 May 2019 to 7 June 2019. From top to bottom shown are He, Hp, Hn, and the magnitude in the EPN coordinate system.

References

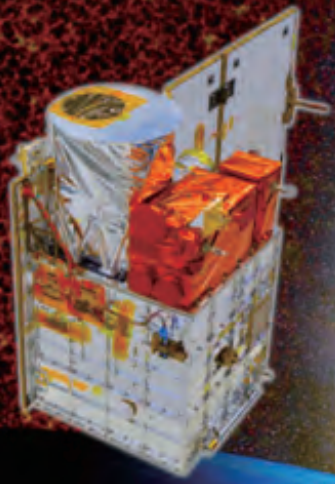
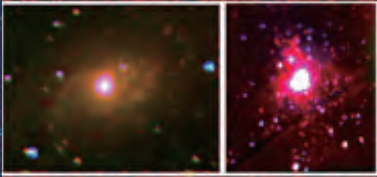
- [1] J. Woo et al., Charging Monitor Aboard the Geostationary Satellite GK2A at 128.2o E Longitude, 2020, *IEEE Trans. Nucl. Sci.*, 67, 740
- [2] J. Seon et al., Particle Detector (PD) Experiment of the Korea Space Environment Monitor (KSEM) Aboard Geostationary Satellite GK2A, 2020, *Space Sci. Rev.*, 216, 13
- [3] U. Auster et al., Space weather magnetometer set with automated AC spacecraft field corection for GEO-KOMPSAT-2A, 2016, *Proc. Of 2016 ESA Workshop on Aerospace EMC (ESA SP-738, May 2016)*



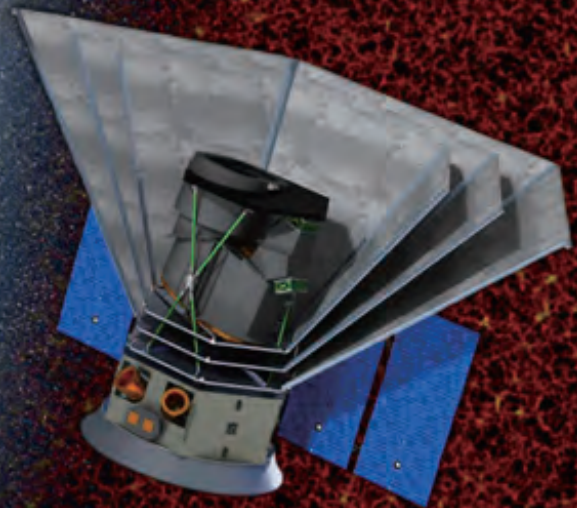
SC-E

Astrophysics from Space

Infrared Imaging Spectroscopic Survey Missions



NISS
onboard NEXTSat-1
(launched 2018 Dec.)



SPHEREx
(to be launched 2023)

Infrared Imaging Spectroscopic Survey Missions

Woong-Seob Jeong, Korea Astronomy and Space Science Institute

NISS onboard NEXTSat-1

KASI has been putting in effort to develop the infrared space instruments for the measurement of extragalactic background light (EBL) in the infrared. To address the origin of the large-scale fluctuation of EBL, KASI developed the Near-infrared Imaging Spectrometer for Star formation history (NISS) onboard NEXTSat-1.

The unique capability of near-infrared imaging spectroscopy (see Table SC-E-1 and Fig. SC-E-1) was optimized to study the scientific objectives, i.e., the origin of the fluctuation spectrum of EBL and the star formation in local Universe through the spectral mapping of astronomical objects (e.g., nearby galaxies, star-forming regions, galaxy cluster, deep fields).

Table SC-E-1. Specifications of NISS and SPHEREx

Parameter	NISS	SPHEREx
Field of View (deg)	2X2	3.5X11.3
Aperture (mm)	150	200
Spectral coverage (μm)	0.95-2.5	0.75-5.0
Spatial resolution (arcsec)	15	6
Spectral resolution ($\lambda/\Delta\lambda$)	20	41-135
Sensitivity (AB mag)	17	19

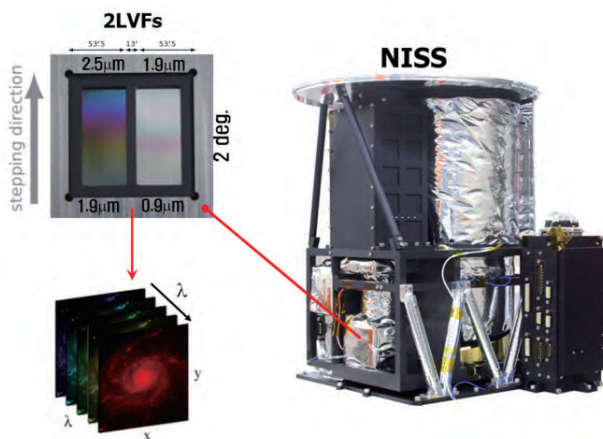


Fig. SC-E-1. Development of the LVBs on the focal plane (upper-left) and the NISS (right) and the expected output images from the NISS (lower-left).

System calibration was done by utilizing our constructed test facility. After the successful launch of the NISS (2018), the NISS had been in operation for the scientific observations by June 2019.

The NISS demonstrated the infrared imaging spectroscopy in space and performed the near IR imaging spectroscopic survey for star-forming regions, nearby galaxies, extragalactic deep fields, and so on (see Fig. SC-E-2). The performance of the infrared imaging spectroscopy was as good as the design specification.

SPHEREx

Based upon the heritage of the NISS, KASI has been collaborating for SPHEREx, the first all-sky infrared spectro-photometric surveyor as the NASA Medium Explorer (MIDEX) mission (PI institute: Caltech).

Compared with the NISS, the SPHEREx accommodates higher spectral/spatial resolution and a wider field of view to achieve the major three scientific themes such as the origin of our Universe, evolution of galaxies, and Galactic ice survey (see Table SC-E-1).

KASI, as its unique international partner, will contribute to the SPHEREx project in the development of the calibration facility and the scientific research.

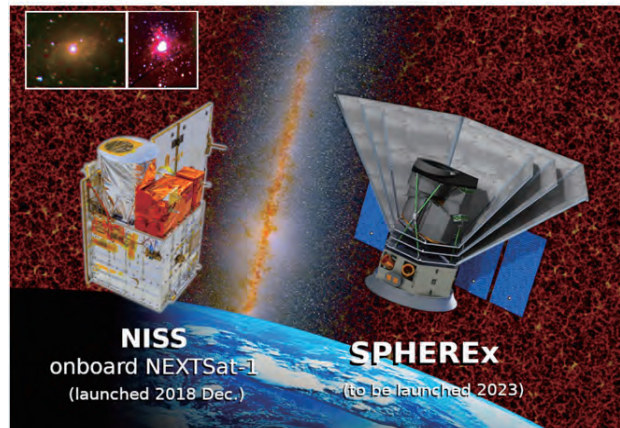


Fig. SC-E-2. Development of the NISS onboard NEXTSat-1 (left) and the first all-sky infrared spectro-photometric survey mission SPHEREx (right)

SC-F

Life Sciences as Related to Space

What the egg diversity of Antarctic tardigrades tells us

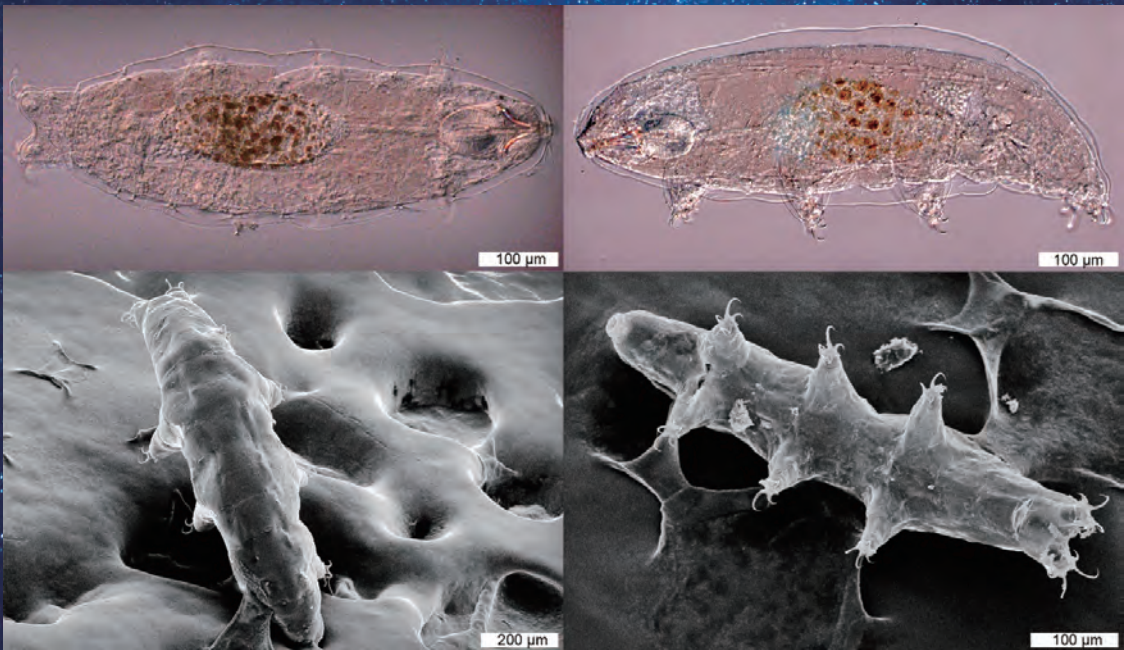
Genetics, development and physiology of animal models in altered gravity

Hormetic effects of hypergravity on the immune system and its mechanism

Impairment of cerebellar motor coordination and object recognition in the hypergravity-exposed rats



<*C. elegans*>



<*Dactylobiotus ovimutans* near the King Sejong Station>

What the egg diversity of Antarctic tardigrades tells us

Ji-Hoon Kihm, Sanghee Kim, and Tae-Yoon S. Park, Korea Polar Research Institute

Tardigrades, the animals which have a reputation for cryptobiosis

Phylum Tardigrada is a hydrophilous microscopic animal with four pairs of legs (Kinchin, 1994). Generally, the body length of tardigrades ranges from 50 μm to 800 μm , but marine heterotardigrades tend to be smaller than limno-terrestrial eutardigrades (Nelson et al., 2015).

Because tardigrades need water to survive, most eutardigrade species cease metabolism through dehydration of the body and enter the 'tun-state' when the environment becomes unfavorable. Cryptobiosis is the ability to adapt to various environmental stress.

Tardigrades show four types of cryptobiosis: anhydrobiosis (desiccation), cryobiosis (low temperature), anoxybiosis (low oxygen level), and osmobiosis (high or low salt concentration) (Guidetti et al., 2011). During tun-state using cryptobiosis, tardigrades use special molecules to protect their cells, e.g. trehalose, LEA (Late Embryogenesis abundant), HSP (Heat Shock Protein), CAHS (Cytoplasmic Abundant Heat Soluble), SAHS (Secretory Abundant Heat Soluble), and aquaporin proteins (Förster et al., 2009; Yamaguchi et al. 2012; Grohme et al., 2013; Guidetti et al., 2011, 2012; Wełnicz et al., 2011; Weronika & Kaczmarek, 2017).

Additionally, tardigrades can resist radiation in both active and tun-state (Horikawa et al., 2006; Hashimoto et al., 2016). Due to their tolerance abilities, tardigrades have attracted attention from astrobiologists, and have been involved in several space experiments.

The representative space mission was FOTON M-3 mission which had three tardigrade related projects: TARSE (Tardigrade Resistance to Space Effects), TARDIS (Tardigrada In Space), and RoTaRad (Rotifers, Tardigrades, and Radiation). Through these projects, tardigrades showed potential to survive at space environment.

Antarctica is one of the most extremely harsh regions on Earth, which has only ca. 0.44 % ice-free lands (Brooks et al., 2019). Although liquid water is an essential pre-

requisite for tardigrades, Antarctic freshwater is frozen throughout the year, except for a brief summer season.

Due to cryptobiosis, tardigrades have been adapted to water-lacking environments and become one of the dominant invertebrate groups on the terrestrial ecosystem of Antarctica (Convey & McInnes, 2005; Adams et al., 2006; Sohlenius & Boström, 2008).

An Antarctic tardigrade species which shows the intraspecific variation in egg morphology

The genus *Dactylobiotus* (Shuster, 1980) is one of the four representative limnic taxa. Nonetheless, two *Dactylobiotus* species have been reported from King George Island (KGI), Antarctica, i.e. *D. ambiguus* (Murray, 1907) and *D. ovimutans* (Dastych, 1984; Kihm et al., 2020).

We collected *Dactylobiotus ovimutans* (Fig. SC-F-1.) near the King Sejong Station, KGI, Antarctica, from benthic sediment of Lake Boeckella. From the sediment sample, eight adult tardigrades were extracted and cultured in the laboratory. Through the culture system, we found intraspecific variation in eggshell morphology of *D. ovimutans* (Fig. SC-F-2.).

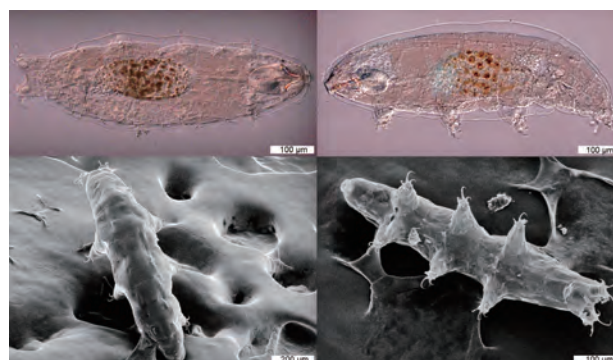


Fig. SC-F-1. *Dactylobiotus ovimutans* near the King Sejong Station

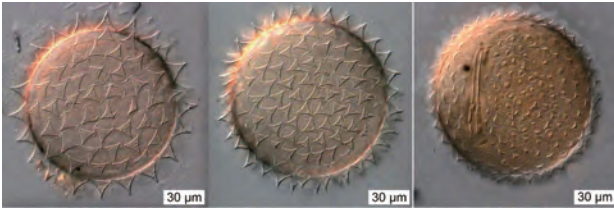


Fig. SC-F-2. An intraspecific variation in eggshell morphology of *D. ovimutans*

While there was no significant difference in egg diameter, the egg processes differed in size and morphology. Number of processes on the circumference varies from 20 to 37 and the size of the processes varies in both height and base width. Some eggs show uninflated processes throughout the whole egg or part of them (Fig. SC-F-3.).

Such intraspecific variation in eggshell morphology was also documented in several limno-terrestrial species. The cause of the variation in eggshell morphology remains elusive. Dormancy, seasonality, and various oviposition sites have been suggested as the cause of morphological variation in tardigrade eggs.

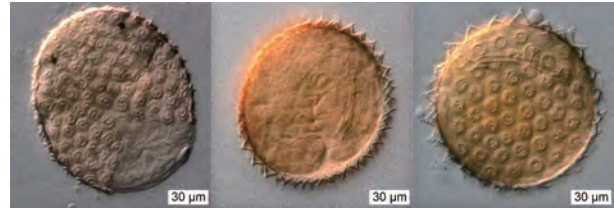


Fig. SC-F-3. Uninflated processes throughout the whole egg or part of them

However, because *D. ovimutans* was cultured in the stable laboratory condition, these possibilities are excluded. The only possibility that cannot be ruled out is a differential gene expression. The intraspecific variation in egg morphology may also reflect a superb ability of tardigrades to endure in various harsh environments in Antarctica.



KOPRI's King Sejong Station at Antarctica

Lithic niches acting as reservoirs of microbial life in a high Arctic polar desert

Yong-Hoe Choe, Mincheol Kim, and Yoo Kyung Lee, Korea Polar Research Institute

Lithic niche and astrobiology

Polar regions have extremely low temperatures, dry atmosphere, strong ultra violet radiation, low nutrient availability and long periods without sunlight.

Microorganisms living in these environments may find a sheltered habitat in rocks to protect themselves from environmental stresses (Walker and Pace 2007). Thus, rock-inhabiting microbes are a major focus of many investigations of life in harsh environments or studies with astrobiological implications (Wierzbos et al. 2013; De los Rios et al. 2005). In this study, we examined the community structure of bacteria and fungi inhabiting different types of rock collected from four sites in Svalbard.

The main objectives of this study were (1) to investigate the major members of the bacterial and fungal communities colonizing the lithic environments in this cold

and dry region and (2) to investigate whether microbes that are the same as or closely related to those in this environment can also be found in other environments by searching databases for taxa from other studies.

Lithic microbial communities in a high Arctic polar desert

We collected different types of rocks such as sandstone, limestone, granite, basalt, and travertine from Svalbard. SEM of the rock samples clearly showed microbial structures (Fig. SC-F-4). A total of 34 bacterial phyla were identified, of which nine phyla were present in all types of rock isolated in this study (Fig. SC-F-5a).

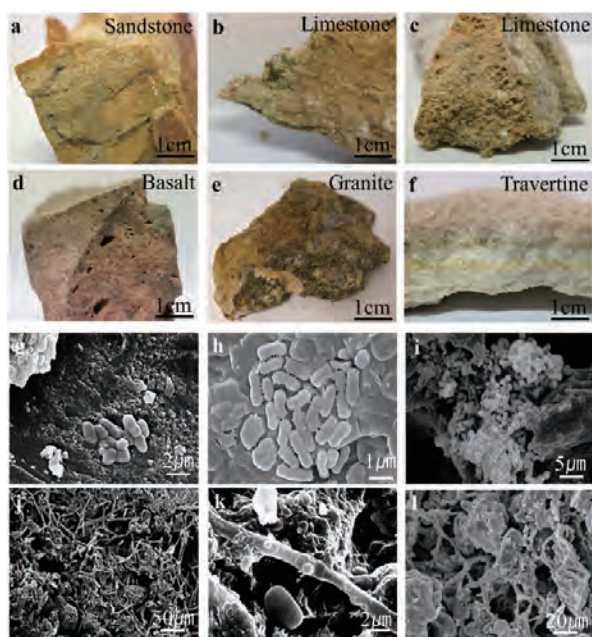


Fig. SC-F-4. Fractured rocks and SEM images of endolithic microorganisms. (a–f) Pictures showing fractured rock samples. SEM images showing bacterial aggregates on fractured basalt (g), granite (h) and travertine (i). SEM images showing fungal hyphae on fractured sandstone (j) and limestone (k and l).

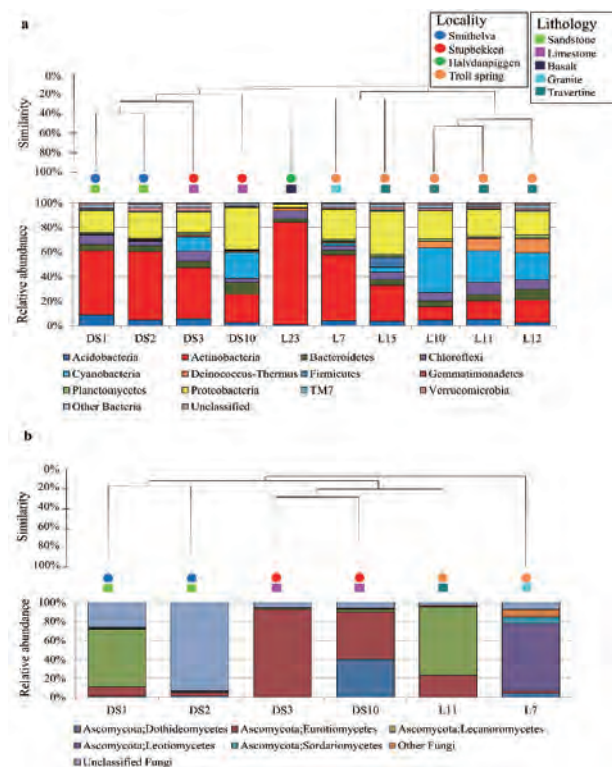


Fig. SC-F-5. Clustering pattern of rock samples based on bacterial phylum composition (a) and fungal class composition (b). The dendrogram at the top was generated using the Bray-Curtis dissimilarity of bacterial phylum abundance between samples (a) and fungal class abundance between samples (b)

Actinobacteria was the most abundant phylum (38.6% on average) across the entire sample set, followed by Proteobacteria (21.8%), Cyanobacteria (12.6%), Chloroflexi (6.3%), Bacteroidetes (5.5%), and Acidobacteria (4.4%). Four fungal phyla were present across all samples (Figure 2b). Ascomycota was the most abundant phylum (96.0% on average) across the entire sample set. At the class level, fungal communities were dominated by four fungal classes: Eurotiomycetes (30.0% on average),

Lecanoromycetes (23.0%), Leotiomycetes (12.1%), and Dothideomycetes (8.1%).

We also investigated whether bacterial and fungal OTUs found in this environment also occurred in other environments. Bacterial major OTUs obtained in this study were highly affiliated (97.0%–98.7% DNA sequence similarity) to strains that originated from soil or rocks with an Arctic or Antarctic origin (Table SC-F-1.).

Table SC-F-1. Phylogenetic affiliation and isolation source of dominant bacterial operational taxonomic units (OTUs) obtained from rock samples

Locality	Lithology	OTUa	Similarity (%) ^b	Taxonomyc	Isolation source
Smithelva	Sandstone	DS1_05	98.4	<i>Nocardioideaceae</i>	Antarctic Dry Valley, mineral soils
		DS1_11	98.4	<i>Blastocatella</i>	Antarctic Dry Valley, mineral soils
		DS1_18	97.5	<i>Sphingomonas</i>	Antarctic Miers Valley, quartz rocks
Smithelva	Sandstone	DS2_04	97.5	<i>Acetobacteraceae</i>	Mont Blanc, snow with Saharan dust
		DS2_05	98.2	<i>Nocardioideaceae</i>	Antarctic King George Island, soil
		DS2_26	98.2	<i>Acetobacteraceae</i>	Antarctic, soil
Stupbekken	Limestone	DS3_19	98.7	<i>Loriellopsis</i>	Antarctic Dry Valleys, quartz rocks
		DS3_15	97.5	<i>Sphingomonas</i>	Antarctic Dry Valleys, rock
		DS3_28	97.7	<i>Ilumatobacter</i>	Negev desert, soil
Stupbekken	Limestone	DS10_03	97.7	<i>Chroococcidiopsis</i>	Arctic Svalbard Troll spring, rock
		DS10_04	97.0	<i>Acetobacteraceae</i>	Arctic Ny-Ålesund, glacier moraine
		DS10_15	98.1	<i>Sphingomonas</i>	Switzerland, central Alps, white rock
Troll spring	Granite	L7_10	97.9	<i>Pseudarthrobacter</i>	Dry desert, soil crust
		L7_44	97.3	<i>Nocardioides</i>	Arctic Northeast Greenland, soil
		L7_13	97.5	<i>Arthrobacter</i>	Antarctic Dry Valley, rock
Halvdanpiggen	Basalt	L23_13	97.7	<i>Arthrobacter</i>	Antarctic Victoria Land, stone
		L23_17	97.7	<i>Nocardioideaceae</i>	Norway, cold desert, rhizosphere soil
		L23_07	98.2	<i>Frankiales</i>	Atacama desert 6000 m, mineral soil
Troll spring	Travertine	L10_01	97.0	<i>Chroococcidiopsis</i>	Arctic Svalbard Troll spring, rock
		L10_16	97.5	<i>Pseudanabaenaceae</i>	Arctic Svalbard Troll spring, rock
		L10_02	97.4	<i>Truepera</i>	Antarctic Dry Valleys, soil
Troll spring	Travertine	L11_02	97.4	<i>Truepera</i>	Antarctic Dry Valleys, soil
		L11_06	97.5	<i>Leptolyngbya</i>	Antarctic microbial mat
		L11_01	96.8	<i>Chroococcidiopsis</i>	Arctic Svalbard Troll spring, rock
Troll spring	Travertine	L12_02	97.4	<i>Truepera</i>	Antarctic Dry Valleys, soil
		L12_08	97.9	<i>Chroococcidiopsis</i>	Norway, cold desert, rhizosphere soil
		L12_01	97.0	<i>Chroococcidiopsis</i>	Arctic Svalbard Troll Spring, rock
Troll spring	Travertine	L15_14	97.5	<i>Brevundimonas</i>	Argentina, Lake Naheul Huapi, rock
		L15_23	97.8	<i>Sporosarcina</i>	Arctic permafrost wetland acidic soil
		L15_09	98.4	<i>Sphingosinicella</i>	Norway, cold desert, rhizosphere soil

A similar trend was also found in fungi. Although fungal major OTUs showed relatively lower levels of DNA sequence similarity (93.2%–98.8%) to the sequences of the closest relatives in the database, most affiliated sequences originated from soil, rock and lichen in the Arctic and Antarctica (Table SC-F-2.).

Table SC-F-2. Phylogenetic affiliation and isolation source of dominant fungal operational taxonomic units (OTUs) obtained from rock samples

Locality	Lithology	OTUa	Similarity (%) ^b	Isolation source
Smithelva	Sandstone	DS1_04	97.6	Sweden, lichen
		DS1_05	98.8	Norway, lichen
		DS1_06	97.3	California, semiaquatic rock
Smithelva	Sandstone	DS2_02	95.7	Canadian High Arctic, soil
		DS2_10	97.3	Canadian High Arctic, soil
		DS2_31	99.6	Canadian High Arctic, soil
Stupbekken	Limestone	DS3_01	98.2	Iceland, rock
		DS3_08	97.3	Canadian High Arctic, soil
		DS3_12	93.2	Iceland
Stupbekken	Limestone	DS10_01	99.4	Canadian High Arctic, soil
		DS10_03	93.5	Alaska Howe Island, soil
		DS10_20	95.7	Antarctic King George Island, lichen
Troll spring	Travertine	L7_14	99.1	Canadian High Arctic, soil
		L7_27	99.1	Canadian High Arctic, soil
		L7_42	97.9	Alaska Franklin Bluffs, soil
Troll spring	Travertine	L11_07	97.6	Romania, lichen
		L11_01	98.5	Canadian High Arctic, soil
		L11_10	98.8	Canadian High Arctic, soil

Taken together, the ability of rock-inhabiting microbes to survive in varied environments depends on key features such as oligotrophy, resistance to various stresses, and diversity of growth forms.

In conclusion, this study examined the microbial composition and diversity of lithic communities inhabiting different rock types in Svalbard. Lithic communities in this region were dominated by stress-tolerant members of bacteria and fungi, and major microbial lineages were closely related to those frequently found in other cold and arid environments.

These findings expand our knowledge of what communities dominate various rock types and what microorganisms are common in the cold desert. Furthermore, understanding lithic microbial ecosystems of polar regions will allow us to better predict the potential distribution of biota on lithic habitats of extraterrestrial environments.

References

- [1] Choe YH, Kim M, Woo J. et al. 2018. FEMS Microbiol Ecol. 94:fiy070
- [2] De los Rios A, Sancho LG, Grube M. et al. 2005. New Phytol. 165:181–9
- [3] Walker JJ and Pace NR. 2007. Appl Environ Microbiol. 73:3497–504
- [4] Wierzos J, Davila AF, Artieda O. et al. 2013. Icarus. 224:334–46



KOPRIS's JangBogo Station at Antarctic

Genetics, development and physiology of animal models in altered gravity

Jin Lee, Yonsei University

Background

Organisms and biological systems constantly adapt to and evolve with their changing environments. However, earth's gravity is a static environmental parameter that remains unchanged through time. Thus, biological processes on earth are not adapted to conditions of space gravity or high gravity.

Studying the effects of gravity on health and basic biology is a challenge due to the difficulty in altering gravity force, but a clearer understanding of how microgravity and hypergravity can alter the body will be necessary as space travel and habitation become more frequent in the near future.

True microgravity conditions can be only experienced in spaceflight. Observations of astronauts, as well as biological experiments during spaceflight have shown that muscle and bone mass decrease in microgravity conditions (Fitts et al, 2001; Vandenburg et al, 1999). In human twin studies, long-term space habitation resulted in specific gene expression changes that in some cases appear to be permanent (Garret-Bakelman et al, 2019). However, a deeper understanding of how genetics, development and physiology is affected by gravity requires rigorous testing that cannot occur in humans.

The nematode *Caenorhabditis elegans* has been a valuable tool to study the effects of altered gravity at the genetic level. Studies of *C. elegans* in space have verified that microgravity lowers the expression of muscle development transcription factors to decrease muscle development (Higashibata et al, 2006), alters TGF- β expression to decrease growth of body length (Higashibata et al, 2006) and alters fat-related genes and results in decreased accumulation of fat (Harada et al, 2016).

100G hypergravity treatment in *C. elegans* does not alter overall muscle integrity but causes nuclear accumulation of the DAF-16 FOXO transcription factor, a conserved stress-response protein (Kim et al, 2007). In addition, worms exposed to hypergravity for 12 hours in liquid cul-

ture had slightly delayed adaptive locomotory responses after treatment (Saldanha et al, 2016).

In this study, we are using *C. elegans* to elucidate the effects of hypergravity, simulated microgravity and space microgravity on neuron development and immune function at the genetic level. We have shown that the development of motor neurons is hindered by high gravity due to compression of tissues blocking migration pathways. We have also shown that the proper development of the delicate dendritic endings of touch-sensing neurons are affected by high gravity. We are currently investigating the effects that space microgravity has on neuron development via experiments aboard the International Space Station. Finally, preliminary experiments have shown that microgravity can decrease *C. elegans* immune function and increase bacterial infection rates.

Hypergravity hinders proper neuron development by compressing rigid tissue layers in the nematode *C. elegans*

To study the effect of hypergravity on *C. elegans* biology, we used a tabletop centrifuge to create a gravity force and designed a small worm cultivation tube from a 1.5 cm centrifuge tube filled with agar and seeded with OP50 *E. coli* bacteria on top, the food of the nematode. To visualize the DD/VD motor neurons, we used a *C. elegans* transgenic strain that expresses GFP under the control of the *unc-25* gene promoter.

Eggs containing developing embryos were placed in the cultivation tube, and either spun in the centrifuge to induce a high gravity force of 100G or placed in a 20C incubator as a 1G gravity control. At 1G, most of the animals showed normal DD/VD commissural projections that reached the dorsal nerve cord. However, in animals exposed to 100G hypergravity for 60 h, defective axonal projections could be seen more frequently. Axonal defects occurred at a frequency of $1.5\% \pm 0.36$. In 100G, defects occurred at a rate of $5.1\% \pm 0.17$, an over three-fold increase compared to 1G (Fig. SC-F-6).

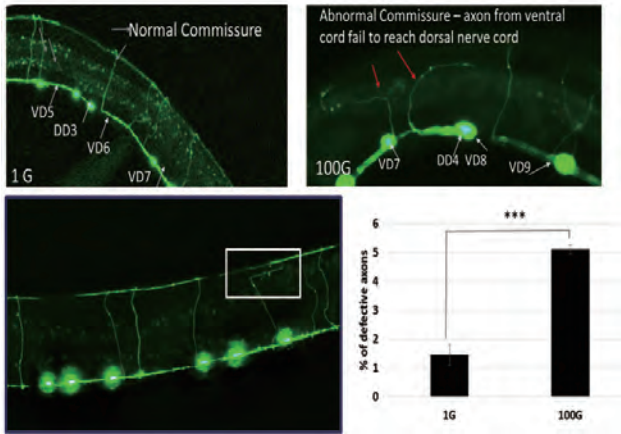


Fig. SC-F-6. Hypergravity induces axon defects in motor neuron development in *C. elegans*.

To understand the mechanism of how gravity force is affecting motor neuron axon development, we performed a candidate genetic screen and looked for mutants that would suppress the hypergravity-induced axon defects (HIAD). We found that neuronal factors surprisingly did not alter HIAD. Instead, mutants of proteins that were localized to the muscle, epidermis and ECM suppressed HIAD (Fig. SC-F-7).

These proteins, including UNC-70 spectrin, SMA-1 spectrin, UNC-54 myosin, VAB-10 spectraplaklin, VAB-19 kank, UNC-52 perlecan, and ROL-6 collagen, were important in forming a hemidesmosomal structure called the fibrous organelle that holds the muscle, epidermal, and cuticular tissue layers together. We surmised that hypergravity may compress these rigid tissue layers together hindering proper motor neuron axon migration, but loss of fibrous organelle proteins loosens the rigid structure of the tissues restoring normal axon migration and development (Fig. SC-F-7).

We are also investigating the effect of space microgravity in motor neuron development after sending *C. elegans* to space aboard the International Space Station in collaboration with the University of Exeter and the European Space Agency.

Publications from this project:

Kalichamy, S. S., Lee, T. Y., Yoon, K. H. & Lee, J. I. Hypergravity hinders axonal development of motor neurons in *Caenorhabditis elegans*. *PeerJ* 4, e2666, doi:10.7717/peerj.2666 (2016).

Kalichamy, S.S, Alcantara A.A., Kim B.S., Park J, Yoon K.H. & Lee, J.I. Muscle and epidermal contributions of the structural protein β -spectrin promote hypergravity-induced motor neuron axon defects in *C. elegans*. *Sci Rep*, revision submitted (2020)

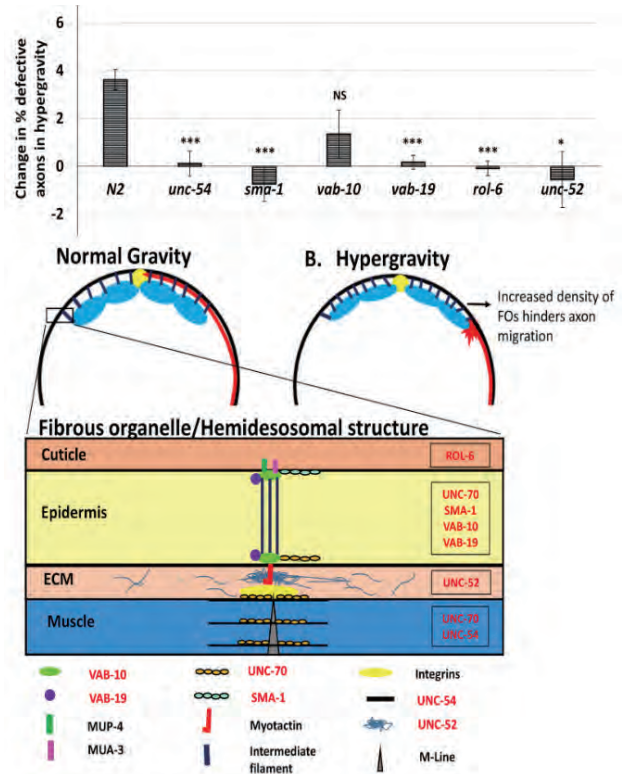


Fig. SC-F-7. Genetic analysis of hypergravity-induced axon defects.

Hypergravity alters the development of dendrites of *C. elegans* touch sensory neurons

In addition to investigating the effect of gravity of motor neuron axon development, we are currently studying hypergravity's effect on the dendrite development of the *C. elegans* touch sensory neurons. The PVD touch sensory neurons provide an elaborate dendritic structure that requires proper developmental signaling and cellular interactions during development.

We find that 100G hypergravity can hinder the proper development of the PVD neuron quaternary dendrite structure (Fig. SC-F-8.), and these defects are dependent on the expression of UNC-52 perlecan protein in the ECM.

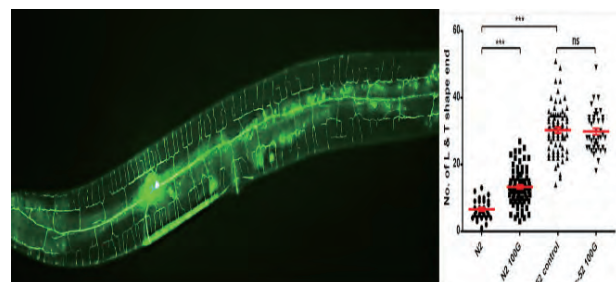


Fig. SC-F-8. Hypergravity induces defects in the development of quaternary dendrite structures of the PVD touch neuron.

Increased bacterial infection in simulated microgravity

The effect of microgravity on the immune system is not fully known. We are testing *C. elegans* innate immunity in different gravity conditions. In normal conditions, *C. elegans* is not susceptible to infection of the bacteria *Enterobacter cloacae*. However, in immune-compromised *dbl-1* mutants, *E. cloacae* robustly colonizes the intestine of *C. elegans*.

We successfully cultured *C. elegans* in a 3D clinostat using a technique developed by our collaborators in the Japanese Aerospace Exploration Agency (JAXA). We found that, unlike in normal 1G gravity culture, worms cultured in simulated clinostat microgravity showed increased *Enterobacter cloacae* bacterial infection in their intestine (Fig. SC-F-9.), indicating that *C. elegans* in microgravity conditions may have a compromised immune system. We are currently conducting genetic experiments to elucidate the mechanism of how microgravity alters the worm innate immune system.



Fig. SC-F-9. Simulated microgravity increases bacterial infection of *C. elegans* intestine.

References

- [1] Fitts, R. H., Riley, D. R. & Widrick, J. J. Functional and structural adaptations of skeletal muscle to microgravity. *J Exp Biol* 204, 3201-3208 (2001).
- [2] Vandenburg, H., Chromiak, J., Shansky, J., Del Totto, M. & Lemaire, J. Space travel directly induces skeletal muscle atrophy. *FASEB J* 13, 1031-1038 (1999).
- [3] Garrett-Bakelman, F. E. et al. The NASA Twins Study: A multidimensional analysis of a year-long human spaceflight. *Science* 364, doi:10.1126/science.aau8650 (2019).
- [4] Higashibata, A. et al. Decreased expression of myogenic transcription factors and myosin heavy chains in *Caenorhabditis elegans* muscles developed during spaceflight. *J Exp Biol* 209, 3209-3218, doi:10.1242/jeb.02365 (2006).
- [5] Higashibata, A. et al. Microgravity elicits reproducible alterations in cytoskeletal and metabolic gene and protein expression in space-flown *Caenorhabditis elegans*. *NPJ Microgravity* 2, 15022, doi:10.1038/npjmgrav.2015.22 (2016).
- [6] Harada, S. et al. Fluid dynamics alter *Caenorhabditis elegans* body length via TGF-beta/DBL-1 neuromuscular signaling. *NPJ Microgravity* 2, 16006, doi:10.1038/npjmgrav.2016.6 (2016).
- [7] Kim, N. et al. Gravity force transduced by the MEC-4/MEC-10 DEG/ENaC channel modulates DAF-16/FoxO activity in *Caenorhabditis elegans*. *Genetics* 177, 835-845, doi:10.1534/genetics.107.076901 (2007).
- [8] Saldanha, J. N., Pandey, S. & Powell-Coffman, J. A. The effects of short-term hypergravity on *Caenorhabditis elegans*. *Life Sci Space Res (Amst)* 10, 38-46, doi:10.1016/j.lssr.2016.06.003 (2016).

Hormetic effects of hypergravity on the immune system and its mechanism

Young Hyo Kim, Inha University, School of Medicine

Gravity of an excessively large magnitude can adversely affect the human body and even lead to death. However, it has recently been discovered that moderate hypergravity can act in a direction that is beneficial to the human body. For example, there is a study showing that when a fly was exposed to a hypergravity of 3 to 5 G for two weeks continuously, its lifespan was extended compared to that of a fly living under normogravity.

However, the effect of chronic hypergravity on allergic diseases such as allergic asthma and rhinitis has not been studied. Therefore, we tried to study the effect of chronic hypergravity on the course of allergic disease by first inducing allergic asthma in experimental animals, and simultaneously exposing chronic hypergravity for four weeks.

We divided forty BALB/c mice as group A (control group, n = 10), who were sensitized and challenged with physiologic saline, group B (asthma group, n = 10) challenged with ovalbumin (OVA) through intraperitoneal and intranasal route to induce allergic asthma, and groups C (asthma/rotatory control group, n = 10) and D (asthma/hypergravity group, n = 10), who were exposed to 4 weeks of normogravity (1G) or chronic hypergravity (5G) during induction of asthma.

Group D showed significantly lower serum total IgE concentration than Groups B and C and significantly lower number of inflammatory cells (eosinophils, neutrophils, and lymphocytes) in the bronchoalveolar lavage (BAL) fluid by exposure to chronic hypergravity (Fig. SC-F-10).

As a result of real-time PCR, Bcl-2 and heme oxygenase-1 gene expressions were significantly decreased in Group D, whereas Bax and EC-SOD gene expressions were increased.

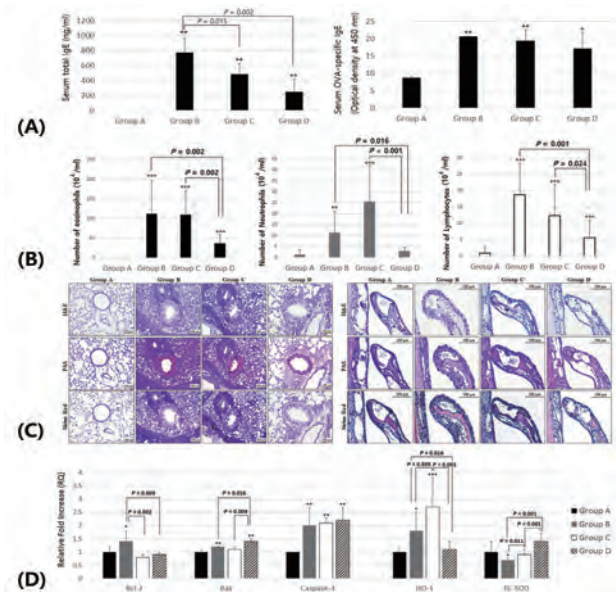


Fig. SC-F-10. (A) Serum total and ovalbumin (OVA)-specific IgE. (B) The number of eosinophils, neutrophils, and lymphocytes in the bronchoalveolar lavage fluid. (C) Histologic findings of the pulmonary parenchyma (left) and nasal turbinate (right). (D) Real-time PCR. Group A is the control group, group B is the asthma group, group C is asthma/rotatory control group, and group D is asthma/hypergravity group. * * Significant difference from group A, $p < 0.01$; * * * significant difference from group A, $p < 0.001$ (Kruskal-Wallis and Mann-Whitney U tests).

To find out the mechanism of this phenomenon in more detail, we conducted in vitro study. We repeatedly exposed RPMI2650 cells to intermittent hypergravity (10G for 20 minutes and rest period for 20 minutes) and then measured transepithelial electrical resistance (TEER), and performed immunostaining, and RT-PCR.

As a result, TEER was significantly decreased by hypergravity exposure, and changes in the intracellular cytoskeletal structure were observed in immunostaining. In addition, expression of genes such as CLDN-1 and OCLN was significantly increased.

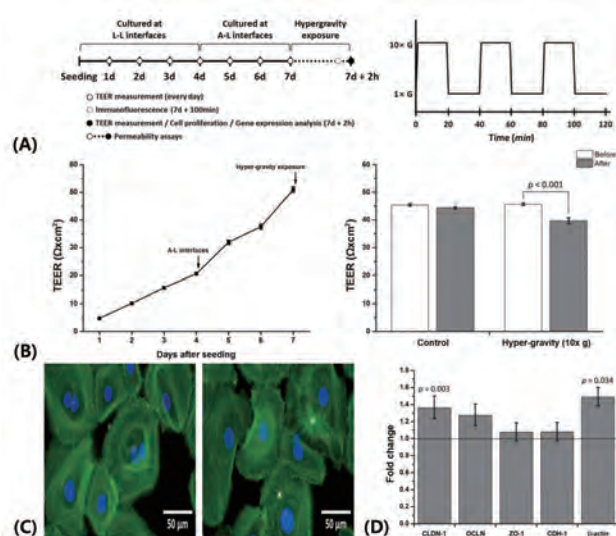


Fig. SC-F-11. (A) Protocol for hypergravity in vitro study. (B) Trans-epithelial electrical resistance (TEER). (C) Immunostaining before (left) and after (right) exposure to intermittent hypergravity. (D) RT-PCR.

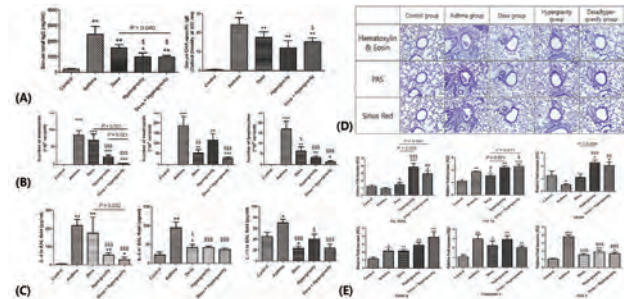
We also tried to find out how potent the anti-allergic effect of the hypergravity was, compared to that of medication (such as dexamethasone), and whether there was an additive effect when the medication and hypergravity were administered together.

Therefore, we divided another 40 BALB/c mice into five groups: Control group (only saline administered intraperitoneally and intranasally), Asthma group (administered intraperitoneal and intranasal OVA to induce asthma), Dexa group (Dexamethasone (0.75 mg/kg) was administered while inducing asthma), Hypergravity group (exposed to hypergravity of 5G continuously for 30 days while inducing asthma), and Dexa/Hypergravity group (hypergravity and dexamethasone were administered together).

As a result, the Dexa/hypergravity combined treatment group showed a more significant reduction in serum total IgE than the mono-treatment groups (dexamethasone or hypergravity), and the number of inflammatory cells such as eosinophil in the BAL fluid was significantly reduced.

Also, the concentration of IL-4 in the BAL fluid was significantly reduced, and histological findings were also improved in the combined treatment group compared to the mono-treatment groups.

As a result of real-time PCR, gene expressions such as EC-SOD, Hif-1a, and VEGF were significantly up-regulated in the combined treatment group compared to the mono-treatment groups.



In conclusion, for the first time, we found that gravity stimulation of an appropriate size has a therapeutic effect on allergic diseases, and this effect is comparable to drugs, and when co-administered with drugs, it exhibits an additive effect.

References

- [1] Jang TY, Jung AY, Kim YH. Hormetic Effect of Chronic Hypergravity in a Mouse Model of Allergic Asthma and Rhinitis. *Sci Rep.* 2016 Jun 2;6:27260. doi: 10.1038/srep27260.
- [2] Kim D, Kim YH, Kwon S. Enhanced nasal drug delivery efficiency by increasing mechanical loading using hypergravity. *Sci Rep.* 2018 Jan 9;8(1):168. doi: 10.1038/s41598-017-18561-x.
- [3] Jang TY, Jung AY, Kwon S, Kim YH. Hypergravity enhances the therapeutic effect of dexamethasone in allergic asthma and rhinitis animal model. *PLoS One* 2018 May 17;13(5):e0197594. doi: 10.1371/journal.pone.0197594.eCollection 2018.

Impairment of cerebellar motor coordination and object recognition in the hypergravity-exposed rats

Kyu-Sung Kim, Inha University, School of Medicine
Sunggu Yang, Incheon National University

The cerebellum coordinates voluntary movements to gain smooth and balanced motor activity. It remains unknown how gravity is associated with cerebellum-dependent behaviors and cerebellar Purkinje cell's activities.

To investigate the relationship between gravity and Purkinje cell's physiology, we measured AMPA-mediated fast currents and mGluR1-mediated slow currents of Purkinje cells along with cerebellum-dependent behaviors such as footprint and irregular ladder under a hypergravity condition.

We found abnormal animal behaviors in the footprint and irregular ladder test in response to hypergravity which are correlated with decreased AMPA/mGluR1-mediated currents of Purkinje cells. These results indicate that gravity could regulate the activity of Purkinje cells, thereby modulating cerebellum-dependent motor outputs.

The gravity is necessary for living organisms to operate various biological events including hippocampus-related functions of learning and memory. Until now, it remains inconclusive how altered gravity is associated with hippocampal functions.

We demonstrate the effects of hypergravity on hippocampus-related functions using an animal behavior and electrophysiology with our hypergravity animal model. The hypergravity group showed impaired synaptic efficacy and long-term potentiation in CA1 neurons of the hippocampus along with poor performance of novel object cognitive function.

Animals exposed to hypergravity undergo a deleterious effect of muscle function and show a higher anxiety level. In the genetic level, the gene expression pattern under different gravity conditions is sporadic and inconclusive. Hypergravity increases the expression of several hippocampus-related genes such as proSAAS, Neuroblastoma ras oncogene, Thymosin beta-10, Inhibin beta E, Ngfi-A binding protein 2, and Syndet, while microgravity decreases genes as phosphatidyl-ethanolamine binding

protein and Pgam 1 protein.

Interestingly, hypergravity in rats severely affects cerebellar function, leading to the dysfunction of motor coordination, which is accompanied by the decreased number of Purkinje cells, cerebellar mass, and cerebellar proteins such as GFAP and synaptophysin.

Here, we investigated Purkinje cell's intrinsic properties and mGluR1- and AMPAR-mediated currents associated with motor coordination. Moreover we also investigated a certain relationship between gravity and the hippocampal synaptic mechanisms underlying a cognitive function.

An animal (Sprague Dawley rats)-containing large centrifuge was used for generating a hypergravity condition of $4 \times G$ (Fig. SC-F-12A). Hypergravity exposure process is continued twenty-three hours a day with one hour resting for 4 weeks (Fig. SC-F-12B). The behavior tests followed by electrophysiology were conducted right after hypergravity exposure (Fig. SC-F-12B).

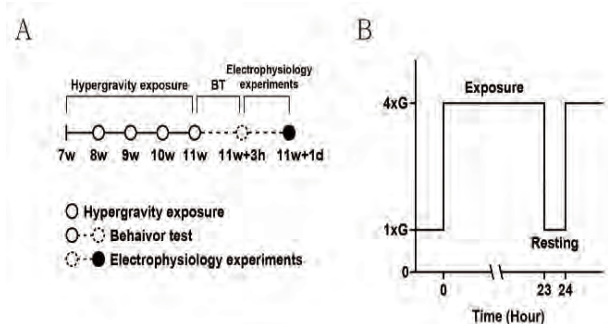


Fig. SC-F-12. The schematic of hypergravity exposure.

(A) Experimental schematic for the hypergravity induction. SD rats are exposed under hypergravity for 4 weeks. Right after that, behavior and electrophysiology experiments are performed. (B) 24h timetable for hypergravity exposure. 23h' hypergravity exposure followed by an hour rest period.

To see whether hypergravity affects motor coordination, we examined a footprint test and an irregular ladder, which are known to be indicators of how animals coordinate motor behavior. When rats walked on a glass plate, the distance between front paw and hind paw of their footprints was measured (Fig. SC-F-13A). Footprints of the hypergravity group had a smaller distance than those of the control group. The slip number of the hypergravity group was larger than that of the control group (Fig. SC-F-13B).

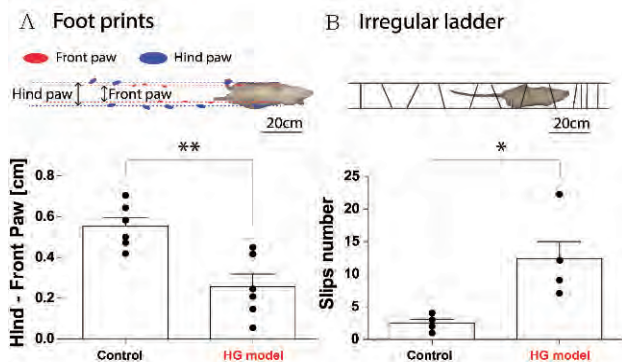


Fig. SC-F-13. Behavior tests under hypergravity.

(A) Footprints test. The image shows rats walking on a glass plate. Dotted lines depict foot prints of front (red) and hind (blue) paws. Distance differences between front and hind paws are measured in both control and hypergravity rats. (B) The image shows rats walking on a ladder which is Inclined (30~40°) and irregular. Slipping numbers are counted on the irregular ladder. (all data are normalized as unpaired t-test. ** $P < 0.005$. * $P < 0.05$.)

Next, we wondered whether hypergravity-induced impairment of motor coordination has a certain relationship with the intrinsic membrane properties of Purkinje cells. For this, we measured cells' resting membrane potential (RMP), input resistance (M Ω), depolarizing sec (mv), and firing frequency (ms), which are indicators of static membrane property of quiescent cells, signal holding capability, hyperpolarized-induced rebound action of signals, and intrinsic firing behavior. We found there were no differences between control and hypergravity groups in resting membrane potential (Fig. SC-F-14).

We examined mGluR1-mediated slow (I_{slow}) and AMPAR-mediated fast current (I_{fast}) current by stimulating parallel fiber. There was the significant reduction of I_{slow} amplitude in hypergravity rats over various intensity (Fig. SC-F-15A)

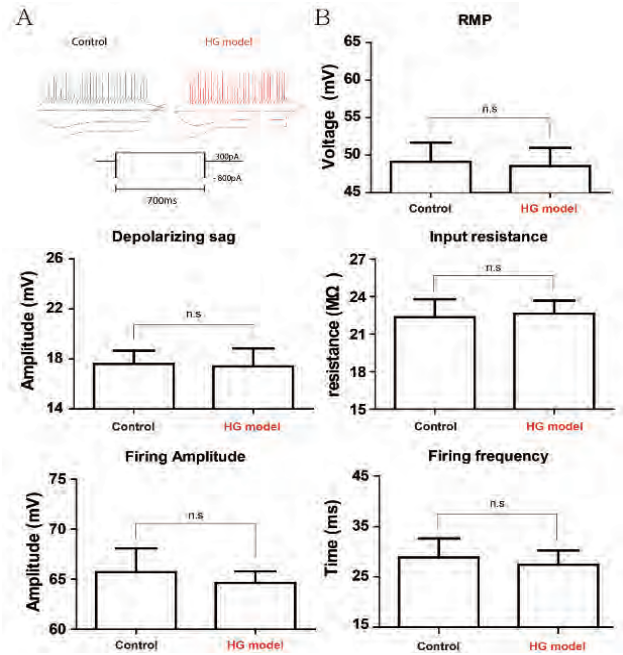


Fig. SC-F-14. The Purkinje cell's intrinsic property under hypergravity (A) Responses to long depolarizing and hyperpolarizing currents (700 ms) from -800pA to 300pA have a firing pattern and hyperpolarization-activated current (I_h)-mediated depolarization sag, respectively. (B) The intrinsic properties in resting membrane potential (RMP), Input resistance, depolarizing sag, Firing Amplitude and Firing frequency. There are no differences in the intrinsic properties. n.s., not significant.

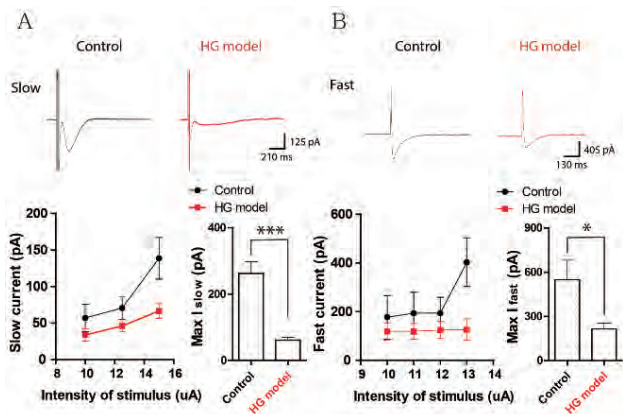


Fig. SC-F-15. Decreased I_{slow} and I_{fast} in a hypergravity condition (A) Burst stimulation of Parallel fibers produces mGluR1-mediated slow currents (under voltage-clamp mode; resting membrane potential, -65mv). Slow currents (upon various intensities) and Max I_{slow} are reduced under hypergravity (** $P < 0.005$, ANOVA test). (B) Single stimulation of Parallel fibers produces AMPAR-mediated fast currents. The fast currents (upon various intensities) and Max I_{fast} are reduced under hypergravity (* $P < 0.05$, ANOVA test). *** $p < 0.001$. * $p < 0.05$.

In order to examine whether HG affects synaptic events in the hippocampus CA1 network, we tested synaptic transmission of CA1 pyramidal cells in response to SC stimulation.

A significant deficit of synaptic transmission was observed in the HG group when it is compared to that in the 1G group. Next, to test whether the response difference is attributed to altered function of NMDARs, NMDAR responses were measured. We found that the HG group had significant reduction in NMDAR responses.

In conclusion, the Purkinje cell's activity will be decreased as an adaptation mechanism during long-term exposure of hypergravity. As the other possible mechanism, when gravity was shifted from hyper-condition to hypo-condition right after 4G, the activity of Purkinje cells might be reversed.

Long-term gravity shifts can cause the impairment of electrophysiological property in hippocampus and behavior in NOR tasks, and it could be due to a defect of post-synaptic receptors.

References

- [1] Noh W, Lee M, Kim HJ, Kim KS, Yang S. Hypergravity induced disruption of cerebellar motor coordination. *Sci Rep.* 2020 Mar 10;10(1):4452. Doi: 10.1038/s41598-020-61453-w.
- [2] Lee J, Jang D, Jeong H, Kim KS, Yang S. Impairment of Synaptic Plasticity and Novel Object Recognition in the Hypergravity – Exposed Rats. *Sci Rep.* In press

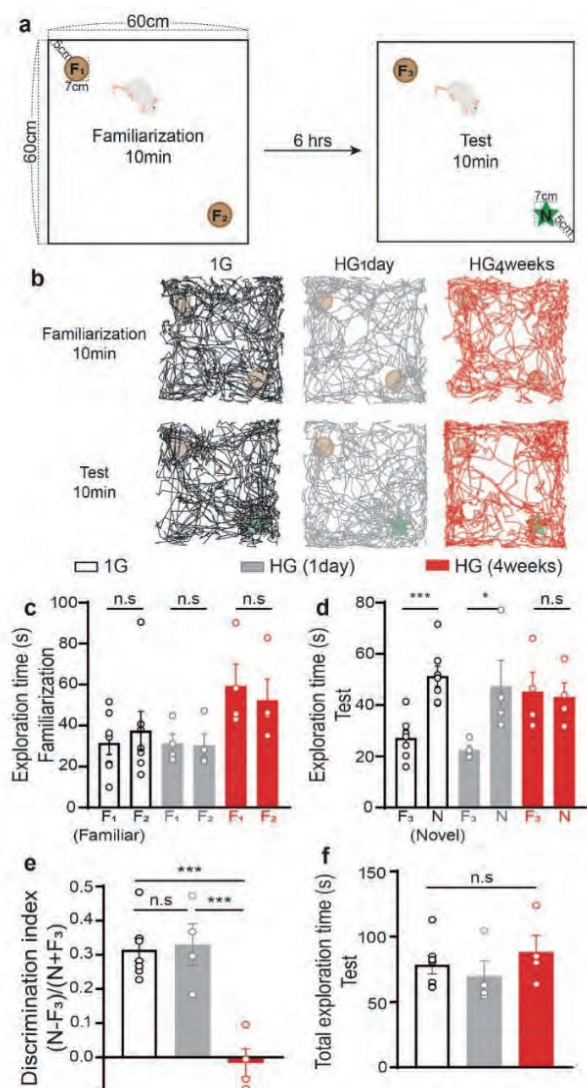


Fig. SC-F-16. Novel object recognition (NOR) test with 1G and HG rats. (a) The scheme of arena and the position of objects. (b) Representative traces of 1G, HG(1day) and HG(4weeks) for each phase (familiarization and test). (c) Exploration times for each object during familiarization phase. (d) HG(4weeks) group had no preference on both F3 and N objects during test phase. (e) Discrimination indexes are plotted as a function of the 1G and HG groups. HG(4weeks) impairs the discrimination of novel objects. (f) Total exploration time does not show any differences between the groups.

SC-G

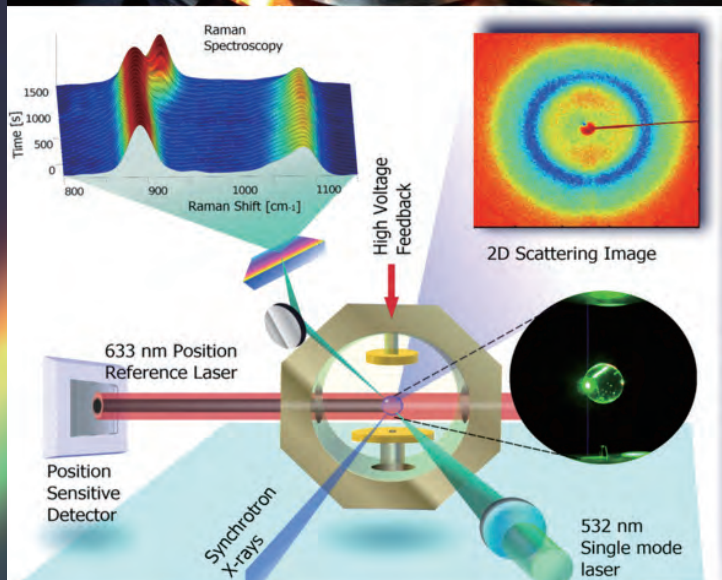
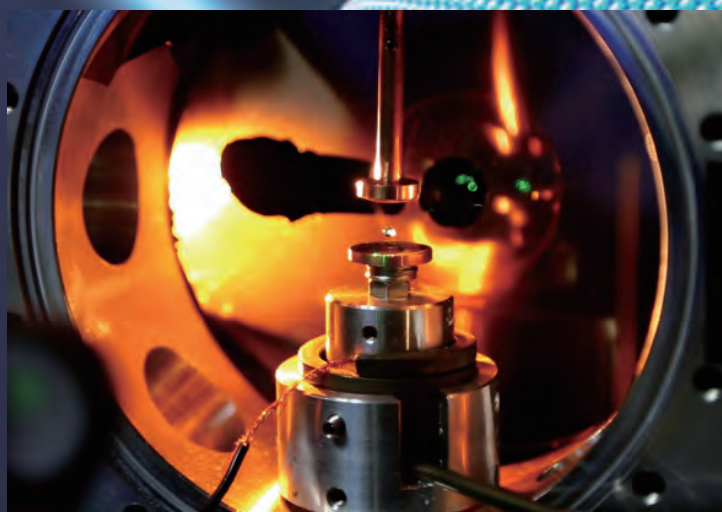
Materials Science in Space

Levitation Technology for Ground Based Experiments

Vol. 16 • No. 11 • March 19 • 2020

www.small-journal.com

NANO · MICRO small



WILEY-VCH

Levitation Technology for Ground Based Experiments

Geun Woo Lee, Sooheyong Lee, and Yong Chan Cho, Korea Research Institute of Standards and Science
Joonho Lee, Korea University
Wonseung Cho, Inha University

Ultra-high temperature and Low temperature electrostatic levitation (ESL) devices

Geun Woo Lee's group in Korea Research Institute of Standards and Science (KRISS) has developed electrostatic levitation (ESL) devices for materials study at both ultra-high temperature and low temperature. This is a good test-bed for space-sciences that can be conducted in international space station.

Under high vacuum condition, KRISS has successfully melted refractory materials over 3000 K and continued its research on thermophysical properties, such as melting temperatures, density, viscosity, surface tension, thermal expansion, and so on.

Moreover, KRISS has modified the high temperature ESL to investigate highly supersaturated aqueous solutions and found a new phenomenon which is called multiple pathways of crystallization under extreme supersaturation with aqueous KH₂PO₄ solution. This provides a new insight for non-classical nucleation theory for large communities, e.g., physics and chemistry, materials sciences, food, cosmetics, biology, and so on.



Fig. SC-G-1. Low temperature ESL device (top in left), combination of synchrotron X-ray and Raman scattering devices (bottom in left), and levitation of colloids (right).

Both technical developments in ESL are now expanding to combine to scattering techniques such as Synchrotron X-ray and in-situ micro-Raman scattering devices. This will give a comprehensive understanding how thermophysical properties and structures are related to each other in metals, alloys, aqueous solutions, and colloidal liquids.

Structure Analysis of CaO-SiO₂-Al₂O₃ Melts

In Korea University, Joonho Lee's group has studied the structure of aluminosilicate melts, which is affected by the degree of polymerization, the fitting of cations, and the nature of the network modifiers present in the melts.

Density measurements of the levitated melts by using the aerodynamic levitation method, and the structure analysis with Raman spectroscopy were carried out. Structural modification results in the changes of density and thermal expansion coefficient.

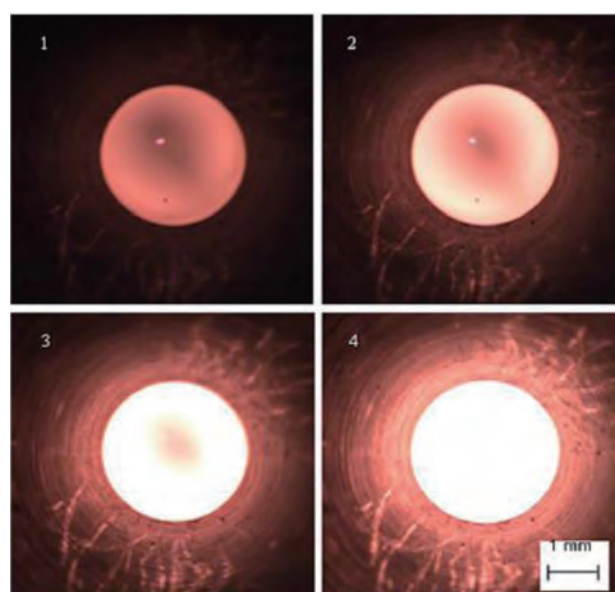


Fig. SC-G-2. Typical sample images of a slag drop in the aerodynamic levitation facility ((1) 1773 K, (2) 1873 K, (3) 1973 K, and (4) 2073 K). [1]

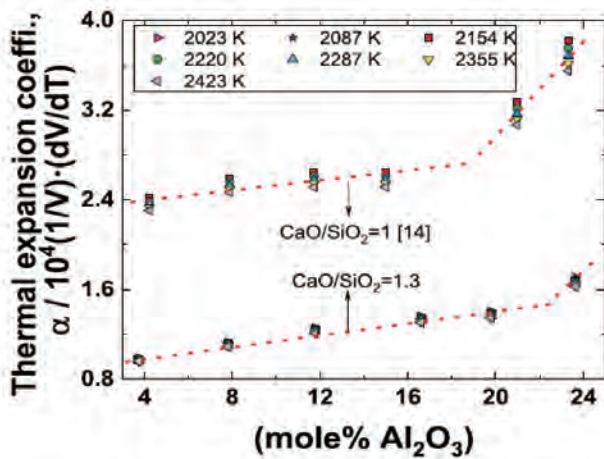


Fig. SC-G-3. Thermal expansion coefficients of CaO-SiO₂-Al₂O₃ slags as a function of Al₂O₃ concentration for CaO/SiO₂=1.3 and 1. [2]

Solidification study by aerodynamic levitation

In Inha University, Wonseung Cho's group has studied BaTiO₃ by using aerodynamic levitation. The solidified BaTiO₃ shows compositional shift by heat treatment with Ti or TiO₂ rich compositions.

The effect of heat treatment on the microstructure of BaTiO₃ shows ~400 nm BaTiO₂ grains which is understood by the formation of Ba₆Ti₁₇O₄₀ by atomic diffusion.

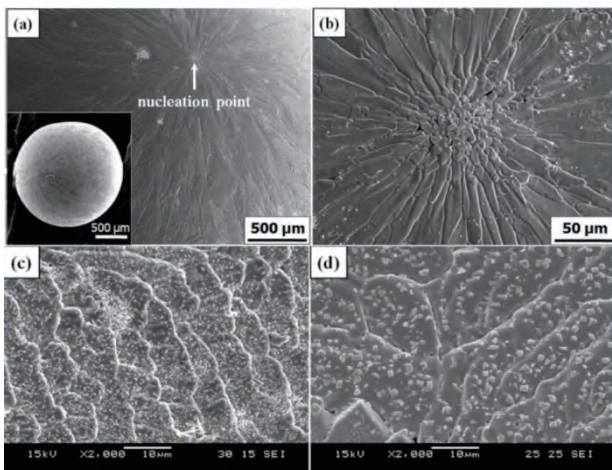


Fig. SC-G-4. SEM images of (a) surface of as-levitated BaTiO₃ sample and (b) nucleation point at surface, (c) microstructure after heat treatment at 1000 °C-1 h, and (d) at 1000 °C-12 h (surface).

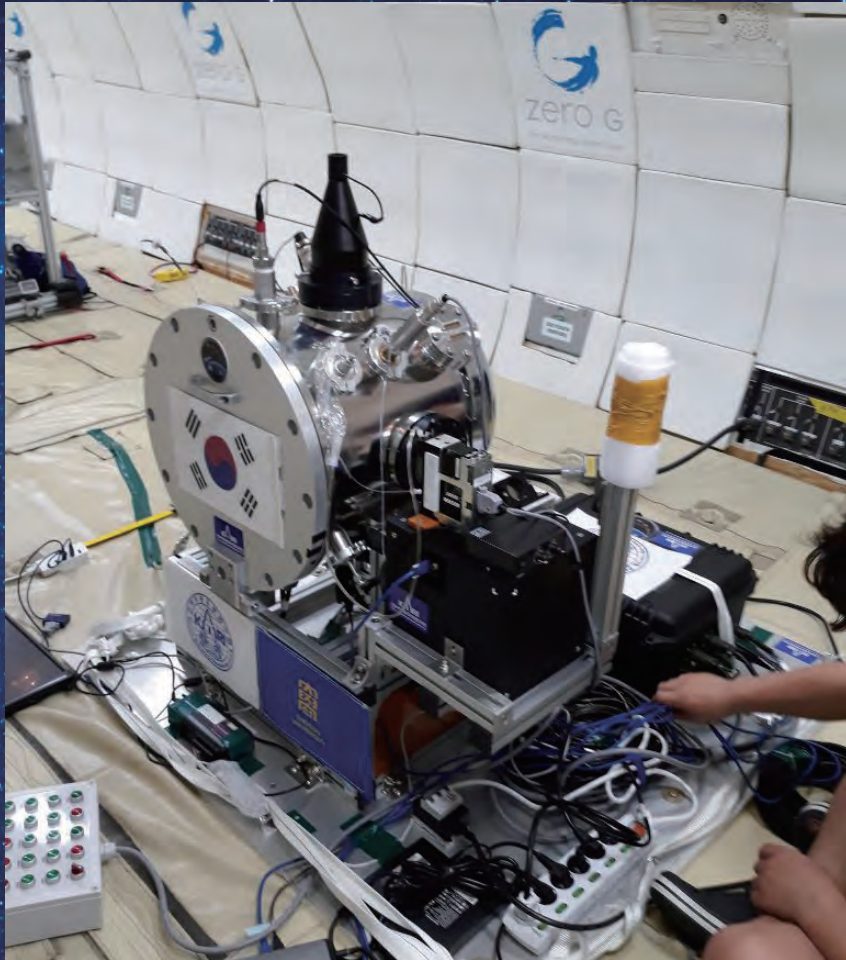
References

- [1] S Jeon, YC Cho, YI Kim, YH Lee, S Lee, GW Lee, *Metals* 10 (6), 760, 2020.
- [2] S Ganorkar, YH Lee, S Lee, Y Chan Cho, T Ishikawa, GW Lee, *AIP Advances* 10 (4), 045114, 2020
- [3] H Hwang, YC Cho, S Lee, TM Choi, SH Kim, GW Lee, *Small* 16 (11), 1907478, 2020
- [4] S Ganorkar, S Lee, YH Lee, T Ishikawa, GW Lee, *Physical Review Materials* 2 (11), 115606, 20205.
- [5] S Lee, W Jo, YC Cho, HH Lee, GW Lee, *Review of Scientific Instruments* 88 (5), 055101, 2020
- [6] GW Lee, YC Cho, B Lee, KF Kelton, *Physical Review B* 95 (5), 054202, 2020
- [7] S Lee, HS Wi, W Jo, YC Cho, HH Lee, SY Jeong, YI Kim, GW Lee, *Proceedings of the National Academy of Sciences* 113 (48), 13618-13623, 2020
- [8] S Jeon, DH Kang, YH Lee, S Lee, GW Lee, *The Journal of chemical physics* 145 (17), 174504
- [9] R. Rajavaram, et al., *Metall. Mater. Trans. B* 48 (2017) 1595–1601.
- [10] R. Rajavaram, et al., *Ceramics International* 45 (2019) 19409–19414.
- [11] Y. Kang et al., *Journal of Molecular Liquids* 319 (2020) 114294.
- [12] Chi-hoon Lee, et.al., *Journal of Ceramic Processing Research*. Vol. 17, No. 2, pp. 97~102 (2016)

SC-H

Fundamental Physics in Space

Combustion Science and Fire Safety Research for Manned Space Exploration



<Combustion Experiment Chamber mounted on a Parabolic Flight Aircraft>



<Flight Model of the KMSL nanosatellite>

Combustion Science and Fire Safety Research for Manned Space Exploration

Seul-Hyun Park, Chosun University

Joo-Hee Lee, Hae-Dong Kim, and Gi-Hyuk Choi, Korea Aerospace Research Institutew

Background

Catastrophic events related to fires can result in the loss of crew members during manned space flights. It has been reported that several fire or overheat events on orbit were identified as critical risks to the crew members. Therefore, the fire risk assessment in a spacecraft environment is one of the important research topics in fire safety engineering.

Korea Aerospace Research Institute (KARI) has considered two areas as major parts of space experiments and conducted researches on related experimental fields. One area is biotechnology related to manned space exploration and the other part is combustion science in fundamental physics.

The field of biotechnology is aimed at supporting human's safe space exploration under microgravity environment in the future, and combustion experiments are also aimed at understanding the combustion characteristics and preventing fire problems in manned space exploration. As part of KARI's major research projects, KARI has developed a combustion experimental system for understanding combustion characteristics with Chosun University.

In this part, combustion and fire research activities in Korea to expand the knowledge base for fire risk assessment in the spacecraft and microgravity environment will be described.

Parabolic flight experiments

During manned space exploration to Mars, crew members are inevitably exposed to different gravity environments. In the present study, the flame spread characteristics were investigated from the perspective of fire safety for manned space module.

To this end, a flame spread over thermally-thin optical fiber was experimentally investigated in a quiescent envi-

ronment. An optical fiber with a thin combustible (polyethylene) layer was used as solid fuel.

Noting that changes in the gravitational field are essential during the manned space exploration to Mars, the effects of changes in the gravitational field on flame spread were investigated using a series of parabolic flight campaigns provided by Zero G company. Parabolic flights provide approximately 20 second periods of reduced gravity ranging from Mars gravity to Microgravity (Fig. SC-H-1).



(a) Combustion chamber and auxiliary devices (KARI & Chosun University)



(b) Boeing 727-200F for parabolic flight operated by Zero G cooperation

Fig. SC-H-1. Parabolic flight experiments for fire safety research.

The experimental results clearly show that the flame spread rate was much faster in the microgravity environment compared to that in Mars' gravity environment followed by Earth's gravity environment (Fig. SC-H-2). These experimental findings provide important foundational understanding of the influence of gravity on the flame spread over thermally-thin combustibles that has not been studied previously.

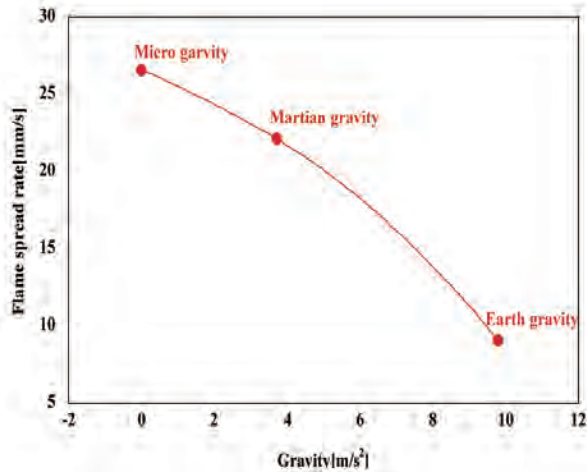
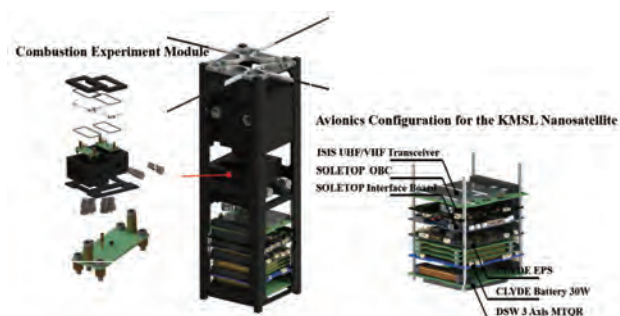


Fig. SC-H-2. Measured flame spread rate for different gravitational fields.

A nanosatellite as an ideal platform to study the fire safety for human spaceflight

This study investigates the feasibility of nanosatellite (which was named as “Korea Microgravity Science Laboratory, KMSL”) as a scientific platform to investigate the fire safety in space.

The KMSL mission is designed and implemented to perform a series of flame spread experiments in microgravity inherently created during its on-orbit operation. The KMSL was selected as the final recipient satellite through a national CUBESAT competition in 2017 and has been funded by Korea Aerospace Research Institution (KARI) for implementation and fabrication.



(a) Structural overview of the KMSL nanosatellite



(b) Flight Model of the KMSL nanosatellite

Fig. SC-H-3. Overview for the KMSL nanosatellite

The KMSL nanosatellite is a 3U-sized CubeSat that includes a combustion scientific payload (Combustion Experiment Module, CEM) for flame spread experiments in microgravity (Fig. SC-H-3).

This payload is perfectly sealed and plays a role of miniature science laboratory that enables to conduct a series of the scientific experiments at a designed atmospheric environment during on-orbit operation. The objectives of combustion experiments are to visualize a sequence of flame ignition, spread, and extinction for given atmospheric environments in microgravity.

The KMSL nanosatellite is tentatively scheduled to launch on a Soyuz rocket in January 2021.

References

- [1] J.H. Lee, Y.K. Kim, J.W. Lee, et al, Core Technology Development for Countermeasure & Utilization of Space Environments, Research Report of KARI (2018).
- [2] S.H. Park, W.S. Nam, T.K. Hong et al, Research on Droplet Combustion Experiment for Space Experiment, Research Report of Chosun University (2018).

COSPAR 2020

Secretariat of the Korean National Committee for COSPAR

Korea Astronomy and Space Science Institute
776, Daedeok-Daero, Yuseong-Gu, Daejeon, 34055, South Korea